Solid State Physics
in Electronics and Telecommunications
Volume 2

Volume 1 : Semiconductors. Part 1

Volume 2 : Semiconductors. Part 2

Volume 3 : Magnetic and Optical Properties. Part 1

Volume 4 : Magnetic and Optical Properties. Part 2

International Union of Pure and Applied Physics

Solid State Physics

in Electronics and Telecommunications

Proceedings of an International Conference
held in Brussels, June 2–7, 1958

CHECKED

Edited by

M. DÉSIRANT
Société Belge de Physique
Loverval
Belgium

J. L. MICHIELS
Laboratoire de Recherches
Physiques, Charleroi
Belgium

Volume 2

SEMICONDUCTORS. PART 2

1960
ACADEMIC PRESS · LONDON · NEW YORK

ACADEMIC PRESS INC (LONDON) LTD
17 OLD QUEEN STREET
LONDON, S W 1

U S Edition, Published by
ACADEMIC PRESS INC
111 FIFTH AVENUE
NEW YORK 3, NEW YORK

Copyright ©, 1960 by Academic Press Inc (London) Ltd

MBM LIBRARY

PV 87
15713
C21
KD

Library of Congress Catalog Card Number 59 12032

Printed in Great Britain by The Whitefriars Press Ltd
London and Tonbridge

FOREWORD

ONE of the major themes envisaged from the outset for the 1958 Brussels International Exhibition was to review scientific progress and its contribution to the welfare of Mankind. Accordingly, Group 38, the Postal and Telecommunications Group of the Exhibition, which included eminent representatives of the Universities, Government Departments and Industry under the able and energetic chairmanship of Mr. L. Ros, Inspector-General of the " Régie des Télégraphes et Téléphones ", decided that one of the best ways of furthering this object was to bring together scientific workers from many countries by holding an International Conference on a subject within the field of interest of the Group.

The choice of subject, " Solid State Physics in Electronics and Telecommunications ", was felt to be particularly appropriate in view of the extraordinarily rapid progress which has occurred in recent years in this field, and of the wealth of new practical devices which have been developed as a result. In addition, 1958 was the tenth anniversary of the discovery of transistor action by Drs. Shockley, Bardeen and Brattain, a discovery which can, in a certain sense, be said to have marked the beginning of this period of rapid evolution and for which a Nobel Prize was awarded to the discoverers. The importance of the Conference was recognized by the decision of His Majesty King Baudouin to accord it His Patronage, and by the consent of His Majesty King Leopold to accept the Presidency of the " Comité d'Honneur ". Furthermore, the International Union of Pure and Applied Physics agreed to sponsor the Conference.

The suitability of the choice of subject was rendered immediately evident by the response of scientists and engineers working in the field to the invitation to participate. Not only did Drs. Shockley, Bardeen and Brattain, as well as a number of other outstanding personalities, honour the Conference with their presence, but there were also some 800 active participants coming from twenty-three countries and, in all, 250 papers were presented.

With regard to the contents of the papers, we feel that they can be left to speak for themselves. Dr. Shockley, in the opening address, reviews the more important points raised by the authors which renders superfluous any further comment here.

The Conference was held on the premises of the University of Brussels, to whom thanks are due for according the necessary facilities. It is also a pleasure to recognize our indebtedness to the Minister of Economic Affairs for a grant which covered a major part of the cost of the Conference, and to the Belgian Physical Society for secretarial and other assistance in its organization.

We must also extend our special thanks to the Academic Press for undertaking the extremely arduous task of publishing the Proceedings of the Conference. Since a major object in this publication was speed, no attempt has been made to standardize notations and so on, the papers having been prepared according to the customs prevailing in the country of origin.

J. L. MICHIELS.
M. DÉSIRANT.

Contributors to Volume 2

G. F. Alfrey, *Electron Physics Department, University of Birmingham, Warwickshire.*

H. Beneking, *Dozentur für Transistortechnik, Technische Hochschule, Aachen, Germany.*

H. Benel, *Laboratoire du Magnétisme et de Physique du Corps Solide, Bellevue (Seine-et-Oise), France.*

K. W. Böer, *II. Physikalisches Institut der Humboldt-Universität, Berlin, Germany.*

J. B. Brauer, *Rome Air Development Center, Griffiss Air Force Base, New York.*

R. H. Bube, *R.C.A. Laboratories, Princeton, New Jersey.*

H. Carl, *Allgemeine Elektricitäts-Gesellschaft Forschungs-Institut, Frankfurt (Main), Germany.*

R. P. Chasmar, *Metropolitan-Vickers Electrical Co. Ltd., Manchester, Lancashire.*

F. A. Clemens, *Bell Telephone Manufacturing Co., Antwerp, Belgium.*

E. Cohen, *Metropolitan-Vickers Electrical Co. Ltd., Manchester, Lancashire.*

I. D. Colson, *Research Laboratories, The General Electric Company Ltd., Wembley, Middlesex.*

I. Cooke, *Electron Physics Department, University of Birmingham, Warwickshire.*

A. J. Cote, Jr., *Applied Physics Laboratory, The Johns Hopkins University, Silver Spring, Maryland.*

J. Della Riccia, *Compagnie Générale de T.S.F., Paris, France.*

Z. Dragoun, *Technische Hochschule, Brno, Czechoslovakia.*

P. Duclos, *Laboratoire du Magnétisme et de Physique du Corps Solide, Bellevue (Seine-et-Oise), France.*

J. M. Early, *Bell Telephone Laboratories Inc., Murray Hill, New Jersey.*

J. A. Evans, *Department of Physics, University of Nottingham, Nottinghamshire.*

H. P. R. Frederikse, *National Bureau of Standards, Washington, D.C.*

G. Freedman, *Semiconductor Division, Raytheon Manufacturing Company, Newton, Massachusetts.*

O. Garreta, *Compagnie Générale de T.S.F., Paris, France.*

J. Gibbons, *Shockley Semiconductor Laboratory, Beckman Instruments Inc., Mountain View, California.*

J. M. Gilles, *European Research Associates S.A., Uccle-Bruxelles, Belgium.*

D. W. Goodwin, *Royal Radar Establishment, Great Malvern, Worcestershire.*

P. Gosar, *Laboratoire du Magnétisme et de Physique du Corps Solide, Bellevue (Seine-et-Oise), France.*

L. C. Greene, *Aeronautical Research Laboratory, Wright Air Development Center, Air Research and Development Command U.S.A.F., Wright-Patterson Air Force Base, Ohio.*

R. Gremmelmaier, *Siemens-Schuckertwerke A.G., Erlangen, Germany.*

J. Grosvalet, *Compagnie Générale de T.S.F., Paris, France*
H. Guennoc, *Compagnie Générale de T.S.F., Paris, France*
R. A. Hanel, *U.S. Army Signal Research and Development Laboratory, Fort Monmouth, New Jersey*
W. Hartel, *Siemens Schuckertwerke A.G., Nuremberg, Germany*
R. M. Henry, *Departement Semiconducteurs, Compagnie Française Thomson-Houston, Paris, France*
C. Hilsum, *Services Electronics Research Laboratory, Baldock, Hertfordshire*
H. Hofbauer, *Battelle Memorial Institute, Division Internationale, Geneva, Switzerland*
W. R. Hosler, *National Bureau of Standards, Washington, D.C.*
T. Ichimiya, *Electrical Communication Laboratory, Nippon Telegraph and Telephone Public Corporation, Tokyo, Japan*
O. Jakits, *Brown Boveri & Cie., Baden, Switzerland*
Y. Kamiya, *Electrical Communication Laboratory, Nippon Telegraph and Telephone Public Corporation, Tokyo, Japan*
S. Kanai, *Electrical Communication Laboratory, Nippon Telegraph and Telephone Public Corporation, Tokyo, Japan*
P. Kaufmann, *Semiconductor Division, Raytheon Manufacturing Company, Newton, Massachusetts*
R. D. Knott, *Research Laboratories, The General Electric Company Ltd., Wembley, Middlesex*
G. Kohl, *Allgemeine Elektricitats Gesellschaft, Forschungsinstitut, Frankfurt (Main), Germany*
F. Kover, *Laboratoire du Magnétisme et de Physique du Corps Solide, Bellevue (Seine et Oise), France*
C. Lanza, *Research Division, Raytheon Manufacturing Company, Waltham, Massachusetts*
J. W. Lathrop, *Diamond Ordnance Fuze Laboratories, Washington, D.C.*
W. D. Lawson, *Royal Radar Establishment, Great Malvern, Worcestershire*
J. Lecorguillier, *Compagnie Française Thomson Houston, Paris, France*
J. Luscher, *Battelle Memorial Institute, Division Internationale, Geneva, Switzerland*
A. L. McWhorter, *Massachusetts Institute of Technology, Lincoln Laboratory, Lexington, Massachusetts*
D. E. Mason, *Ferranti Ltd., Wythenshawe, Manchester, Lancashire*
T. Masumi, *Department of Applied Physics, University of Tokyo, Japan*
M. Matyaš, *Institut fur Technische Physik, Tschechoslowakische Akademie der Wissenschaften, Prague, Czechoslovakia*
A. W. Matz, *Hivac Ltd., South Ruislip, Middlesex*
W. J. Merz, *Laboratories R.C.A. Ltd., Zurich, Switzerland*
G. C. Messenger, *Philco Corporation, Philadelphia, Pennsylvania*
O. Mikami, *Electrical Communication Laboratory, Nippon Telegraph and Telephone Public Corparation, Tokyo, Japan*
K. Mizuma, *Electrical Communication Laboratory, Nippon Telegraph and Telephone Public Corporation, Tokyo, Japon*
T. S. Moss, *Ministry of Supply, Royal Aircraft Establishment, Radio Department, Farnborough, Hampshire*
J. R. Nall, *Diamond Ordnance Fuze Laboratories, Washington, D.C.*
S. Nielsen, *Royal Radar Establishment, Great Malvern, Worcestershire*

T. Niimi, *Electrical Communication Laboratory, Nippon Telegraph and Telephone Public Corporation, Tokyo, Japan.*

E. Nitsche, *Siemens-Schuckertwerke A.G., Berlin-Siemensstadt, Germany.*

J. B. Oakes, *Applied Physics Laboratory, The Johns Hopkins University, Silver Spring, Maryland.*

K. Ono, *Electrical Communication Laboratory, Nippon Telegraph and Telephone Public Corporation, Tokyo, Japan.*

C. Paparoditis, *Laboratorie du Magnétisme de Physique du Corps Solide, Bellevue (Seine-et-Oise), France.*

J. E. Parrott, *Research Laboratory, Associated Electrical Industries, Aldermaston, Berkshire.*

A. W. Penn, *Research Laboratory, Associated Electrical Industries, Aldermaston, Berkshire.*

M. B. Prince, *Hoffman Electronics Corporation, Semiconductor Division, Evanston, Illinois.*

R. Pucel, *Research Division, Raytheon Manufacturing Company, Waltham, Massachusetts.*

E. H. Putley, *Royal Radar Establishment, Great Malvern, Worcestershire.*

A. Quilliet, *Laboratoire du Magnétisme et de Physique du Corps Solide, Bellevue (Seine-et-Oise), France.*

H. L. Rath, *Allgemeine Elektricitäts-Gesellschaft Forschungs-Institut, Frankfurt (Main), Germany.*

R. H. Rediker, *Massachusetts Institute of Technology, Lincoln Laboratory, Lexington, Massachusetts.*

A. J. Regeffe, *Lignes Télégraphiques et Téléphoniques, Paris, France.*

D. C. Reynolds, *Aeronautical Research Laboratory, Wright Air Development Center, Air Research and Development Command, U.S.A.F., Wright-Patterson Air Force Base, Ohio.*

D. H. Roberts, *Plessey Co. Ltd., Caswell Research Laboratories, Towcester, Northamptonshire.*

M. Rodot, *Laboratoire du Magnétisme et de Physique du Corps Solide, Bellevue (Seine-et-Oise), France.*

H. Rodot, *Laboratoire du Magnétisme et de Physique du Corps Solide, Bellevue (Seine-et-Oise), France.*

H. Salow, *Fernmeldetechnisches Zentralamt, Darmstadt, Germany.*

B. Salzberg, *Airborne Instruments Laboratory, Cutler-Hammer, Inc., Mineola, N.Y.*

A. Sato, *Electrical Communication Laboratory, Nippon Telegraph and Telephone Public Corporation, Tokyo, Japan.*

G. Seidler, *Allgemeine Elektricitäts-Gesellschaft, Röhren- und Gleichrichterfabrik, Belecke (Möhne), Germany.*

W. Shockley, *Shockley Semiconductor Laboratory, Beckman Instruments Inc., Mountain View, California.*

K. Šmirous, *Institut für Technische Physik, Tschechoslowakische Akademie der Wissenschaften, Prague, Czechoslovakia.*

B. A. Smith, *Department of Physics, University of Nottingham, Nottinghamshire.*

S. D. Smith, *Ministry of Supply, Royal Aircraft Establishment Radio Department, Farnborough, Hampshire.*

F SPITZER, *Standard Elektrik, Lorenz A G Bauelementewerk SAF, Nuremberg, Germany*

R A STAMPFL, *U S Army Signal Research and Development Laboratory, Fort Monmouth, New Jersey*

H STATZ, *Research Division, Raytheon Manufacturing Company, Waltham, Massachusetts*

W STEINHAUSER, *Standard Elektrik, Lorenz A G Bauelementewerk SAF, Nuremberg, Germany*

M J O STRUTT, *Department of Advanced Electrical Engineering, Swiss Federal Institute of Technology, Zurich, Switzerland*

Y SUGE, *Department of Applied Physics, University of Tokyo, Japan*

S TANAKA, *Department of Applied Physics, University of Tokyo, Japan*

D. F TAYLOR *Ferranti Ltd , Wythenshawe, Manchester, Lancashire*

K N R TAYLOR, *Electron Physics Department, University of Birmingham, Warwickshire*

S TESZNER *Centre National d'Études des Télécommunications, Issy les-Moulineaux (Seine), France*

C G THORNTON, *Philco Corporation, Philadelphia, Pennsylvania*

T TOMINAGA, *Electrical Communication Laboratory, Nippon Telegraph and Telephone Public Corporation, Tokyo, Japan*

A UHLIR, JR *Bell Telephone Laboratories Inc , Murray Hill, New Jersey*

J L VAN CAKENBERGHE *European Research Associates S A , Uccle Bruxelles, Belgium*

N VAN DONG, *Commissariat a l'Énergie Nucléaire, Centre d'Etudes Nucléaire de Saclay Gif sur-Yvette (Seine et Oise), France*

J P VASSEUR, *Laboratoire a la Compagnie Générale de T S F Paris, France*

W. VON MUNCH, *Fernmeldetechnisches Zentralamt, Darmstadt Germany*

K WALK, *Institut fur Schwachstromtechnik der Technischen Hochschule, Vienna, Austria*

H WEISS, *Siemens Schuckertwerke A G , Erlangen Germany*

H WELKER, *Siemens Schuckertwerke A G , Erlangen, Germany*

C S WIGGINS, *Electron Physics Department, University of Birmingham, Warwickshire*

M WOLF, *Hoffmann Electronics Corporation, Semiconductor Division, Evanston Illinois*

J WOODS, *Research Laboratories The General Electric Company Ltd Wembley Middlesex*

J C WOOLLEY, *Department of Physics University of Nottingham Nottinghamshire*

D A WRIGHT, *Research Laboratories The General Electric Company Ltd , Wembley, Middlesex*

A S YOUNG, *Royal Radar Establishment Great Malvern Worcestershire*

M R P. YOUNG, *Research Laboratories, The General Electric Company Ltd , Wembley Middlesex*

R ZABEL, *Siemens Schuckertwerke A G , Berlin Siemensstadt, Germany*

Contents of Volume 2

	PAGE
Foreword	v
Contributors to Volume 2	vii
Contents of Volume 1	xv

Semiconductor Compounds

Préparation et Propriétés des Couches Minces d'Antimoniure d'Indium. By C. Paparoditis	639
Physik der III-V-Halbleiter. By H. Welker	645
Magnetoresistive Effects in Indium Antimonide and Indium Arsenide. By H. P. R. Frederikse and W. R. Hosler	651
Galvanomagnetic Effects in Indium Arsenide and their Applications. By R. P. Chasmar and E. Cohen	659
Infra-Red Faraday Effect due to Conduction Electrons in Indium Antimonide. By S. D. Smith and T. S. Moss	671
L'Effet Magnétothermoélectrique dans l'Antimoniure d'Indium. By M. Rodot	680
Sur les Propriétés de Semi-Conducteurs Utilisables comme Thermo-éléments. By H. Rodot and H. Benel	692
Bismuth Telluride and its Thermoelectric Applications. By D. A. Wright	699
Modern Applications of Hall Effect in Semiconductor Compounds. By M. J. O. Strutt	706
Eigenschaften und Anwendungen der Hallgeneratoren. By W. Hartel	723
The Properties and Applications of *p*-type InSb. By C. Hilsum	733
Strahlungsnachweis mit III-V-Verbindungen. By R. Gremmelmaier	741
Electroluminescence at Grain Boundaries in Gallium Phosphide. By G. F. Alfrey and C. S. Wiggins	747
Some Observations on the Electrical Properties of Indium Antimonide at Low Temperatures. By E. H. Putley	751
Photoconductive Effects in Indium Antimonide. By D. W. Goodwin	759
Sur les Propriétés Électriques et Optiques de l'Antimoniure d'Aluminium. By F. Kover	768
Über die Eigenschaften der Halbleitenden Systeme an der Basis der Verbindungen von $A^{II}B^{V}$-typ. By K. Śmirous	779
Préparation d'Élements Spectrographiquement Purs entrant dans les Composés Semi-Conducteurs. By P. Duclos	784
III-V-Verbindungen als Heißleiter. By H. Weiß	794
Solid Solution in Zinc Blende Type Semiconductors. By J. C. Woolley, B. A. Smith and J. A. Evans	802
Some Photoelectric Properties on ZnS Single Crystals. By W. J. Merz	811

PAGE

Some Experiments on Zinc Sulphide Crystals By G F Alfrey, I Cooke and K N R Taylor 816
Photoconductivity in Lead Selenide By D H Roberts 819
Correlation of Semiconductivity Photoconductivity and Luminescence in Group II–Group VI Materials By R H Bube 825
Preparation and Properties of HgTe and Mixed Crystals of HgTe CdTe By W D Lawson S Nielsen and A S Young 830
The Preparation and Properties of Some Telluride Semiconductors By J E Parrott and A W Penn 836
Effect of Impurity Doping upon the Electrical Properties of Cadmium Telluride By T Ichimiya T Niimi K Mizuma O Mikami Y Kamiya and K Ono 845
Über die Magnetische Susceptibilität einiger Halbleitender Selenide und Telluride By M Matyas 854
Growth and Properties of Cadmium Sulfide Crystals By D C Reynolds and L C Greene 859
Magneto Resistance Effect in Cadmium Sulphide By Y Suge S Tanaka and T Masumi 872
Electron Traps in Photoconducting Cadmium Sulphide Crystals By J Woods and D A Wright 880
Zum Elektrischen Leitungsvorgang von CdS bei Hohen Elektrischen Feldern By K W Boer 889
Croissance des Cristaux dans les Couches Minces de Sulfure de Cadmium Obtenues par Sublimation sous Vide By J M Gilles and J Van Cakenberghe 900

SEMICONDUCTOR APPLICATIONS

An Earth Satellite Instrumentation for Cloud Measurement By R A Hanel and R A Stampfl 907
Future Applications of Solid State Devices in U S Air Force Ground Electronic Equipment By J B Brauer 913
Die Ausnutzung spezifischer Halbleitereigenschaften beim Entwurf der Voll Transistorrechenmaschine *Mailufterl* By K Walk 924
Low Temperature Semiconducting Computing Elements By R H Rediker and A L McWhorter 939
Matrix Methods in High Frequency Transistor Circuit Design By A J Cote Jr and J B Oakes 946
The Application of Semiconductors in Automatic Telephone Switching Systems of the Bell Telephone Manufacturing Co By F A Clemens 960

SEMICONDUCTOR DEVICES

Effets Selfiques dans les Diodes Polarisées dans le Sens Direct By J P Vasseur 970
The Technique of Bulk Diffusion and its Relation to other Transistor Making Techniques By P Kaufmann and G Freedman 977
The Fabrication and Packaging of Semiconductor Devices by Photo lithographic Techniques By J R Nall and J W Lathrop 987

Zur Theorie von *pn*-Dioden und Transistoren, bei denen die äusseren Anschlüsse den Grenzschichten räumlich nahe sind. By H. Beneking 994

A One-Dimensional Transistor Model Based Strictly on the Space-Charge Neutrality Approximation. By A. W. Matz 1000

Theory of Transient Build-Up in Avalanche Transistors. By W. Shockley and J. Gibbons 1024

Triode NPNP au Silicium à Impédance Négative Variable. By R. M. Henry 1036

A Four-Terminal Junction Transistor with Controllable Negative Output Resistance. By J. Lüscher and H. Hofbauer . . . 1042

Transistoren für Höhere Leistungen. By G. Köhl and K. H. Ginsbach 1047

Power Transistor Design for High Current Operation. By R. D. Knott, M. R. P. Young and I. D. Colson 1053

Ein Transistor mit Thyratroncharacteristik und seine Anwendungen. By W. von Münch and H. Salow 1062

Structure de Transistor à Effet de Champ et Transistor Analogue. By O. Garreta, J. Grosvalet, J. Della Riccia and H. Guennoc . 1076

Le Tecnetron, Nouveau Dispositif Semi-Conducteur. By S. Teszner 1086

Improved Design for Microwave Mixer Diodes. By G. C. Messenger 1100

Semiconductor Diodes for Low-Noise Microwave Amplification. By A. Uhlir, Jr. 1110

Structure-Determined Gain-Band Product of Junction Triode Transistors. By J. M. Early 1114

Physical Design Concepts for Ultra-High Frequency Graded-Base Transistors. By C. G. Thornton 1122

High-Frequency Semiconductor Devices Utilizing Injection of Carriers into Space-Charge Regions. By H. Statz, R. Pucel and C. Lanza 1136

Mélangeurs Symétriques à Large Bande Fonctionnant autour de 8·6 mm. By A. J. Regeffe 1153

Sur la Résistance de la Couche Superficielle dans les Cellules Photovoltaïques au Silicium. By P. Gosar and A. Quilliet . . . 1161

New Developments in Reverse Breakdown Silicon Diodes. By M. B. Prince 1172

Some Properties and Applications of Reverse-Biased Junction Diodes. By B. Salzberg 1178

New Developments in Silicon Photovoltaic Devices and their Application to Electronics. By M. Wolf and M. B. Prince 1180

Utilisation des Semi-Conducteurs comme Convertisseurs d'Énergie Nucléaire en Énergie Électrique. By N. Van Dong 1197

The Electrical Characteristics of Silicon Alloy Diodes. By D. E. Mason and D. F. Taylor 1205

A Double Base Diode with Hook Mechanism. By T. Ichimiya, T. Niimi, A. Sato, T. Tominaga and S. Kanai 1211

Photoduodiode—der Neue Typ eines Halbleiterphotoelementes. By Z. Dragoun 1216

Semiconductor Power Rectifiers

PAGE

Temperaturmessungen an Silizium Gleichrichtern By F Spitzer and W Steinhauser . 1222

Messverfahren zur Bestimmung der Grenzleistung von Ge und Si Starkstrom Gleichrichtern By H Carl H L Rath and G Seidler 1227

Entwicklung und Herstellung einer Siliziumgleichrichter Baureihe von 0 5 bis 600 Amp By E Nitsche 1237

Über die Anwendung von Siliziumzellen in Gleichrichtergeraten und Grossanlagen By R Zabel 1248

Über das Thermische Verhalten von Halbleiter Leistungsdioden By O Jakits 1258

Règles d Emploi des Cellules de Puissance au Germanium et au Silicium By J Lecorguilher 1263

Contents of Volume 1

Preparations of Semiconductors and Applied Problems

Continuous Multistage Purification of Silicon Tetraiodide by Zone-Melting. By G. H. Moates
The Preparation of Transistor-Grade Silicon. By B. Rubin
Recent Advances in the Preparation of Semiconducting Materials. By W. G. Pfann
Growing Single Crystals with Constant Resistivity by Floating Crucible Technique. By J. Goorissen. F. Karstensen and B. Okkerse
The Effects of Seed Rotation on Silicon Crystals. By A. J. Goss and R. E. Adlington
The Contamination of Silicon by the Crucible. By S. E. Bradshaw
Leerstellen und Doppelleerstellen in Germanium. By A. Seeger
Anisotropy of Carrier Transport in Semiconductor Bicrystals. By H. F. Mataré
Electrical and Photoelectrical Properties of Grain Boundary Layers. By O. Weinreich, H. F. Mataré and B. Reed
The Influence of Grain Boundaries on the Diffusion of Minority Carriers. By T. Figielski and L. Sosnowski
Localisation des Dislocations dans le Silicium et le Germanium par Microscopie Infra-Rouge. By O. Deutschbein and M. Bernard
Sur l'Interprétation Comparée de quelques Méthodes de mise en évidence de Dislocations dans les Cristaux de Germanium et de Silicium. By J. Burgeat
The Assessment of High Purity Silicon. By N. R. Howard
High Resistivity *n*-Type Silicon Crystals Grown from Fused Quartz Crucibles. By P. Ransom
Impuretés Électriquement Actives dans le Silicium. By J. P. Suchet
The Formation of Thin Films of Germanium by the Disproportionation of Germanium Di-Iodide. By R. C. Newman and J. Wakefield
Diminution du Nombre de Dislocations Introduit dans un Monocristal lors de sa Croissance de la Phase Liquide. By M. François
Réalisation de Plusieurs Jonctions dans un Semiconducteur par Cristallisation Accélérée à partir d'un Germe. By B. Dreyfus-Alain
Über die Auflösung von Germanium in Indium in Abhängigkeit von der Kristallgüte. By H. G. Plust, B. Seraphin and E. Weisshaar

Properties of Semiconductors

Determination of the Minority Carriers Lifetime in Semiconductors. By Z. Bodó
Microwave Methods of Measuring Mobility in Semiconductors. By H. M. Barlow and J. Brown
Dielectric Constant Measurements in Germanium and Silicon at Radio Frequencies as a Function of Temperature and Pressure. By M. Cardona, W. Paul and H. Brooks

Über die Impulsmaßige Aufnahme von Kennlinienfeldern von Halbleiterelementen mit Zweikoordinaten Kompensationsschreibern By A Stumpe
Experimentelle Bestimmung der Effektiven Masse der Ladungstrager in Halbleitern aus Messungen der Magnetischen Suszeptibilitat By D Geist
A Comparison of Drift Mobility Carrier Lifetime and Hall Effect Measurements on *p* type Silicon By F W G Rose, E L Heasell and F Paton
Mechanical Damping of Germanium and Silicon containing Impurity Oxygen By P D Southgate
Phénomenes de Compensation dans les Monocristaux de Silicium By G Dumas and C Georges
Interactions between Li and O in Si By E M Pell
Absorption de la Lumiere par des Charges Liberées par Effet Photoelectrique dans le Germanium By F Desvignes
Ultrarotabsorption Freier Photoelektrisch Erzeugter Ladungstrager in Halbleitern By F R Kessler
Recombinaison Radiative des Porteurs Libres avec des Porteurs Lies a des Centres d Impuretés By C Benoit à la Guillaume and O Parodi
Étude des Centres de Recombinaison Type Cuivre dans les Jonctions de Germanium *p n* By M Bernard
The Formation of Etch Pots and of Silicon Carbide on Silicon Surfaces at High Temperatures By R C Newman and J Wakefield

Solid State Theory

Cinétique de l Annihilation des Excitons By M Balkanski and J P Guiraud
Band Dynamics and Zener Effect By G H Wannier
On the Theoretical Variation of Electron Mobility with Applied Electric Field in Semiconductors By R Stratton
Theory of Electron Transport Processes in Solids By J M Richardson
Field Effect at High Frequency By F Berz
Static Space Charge Distributions By J R Macdonald
La Jonction *p n* Abrupte dans le Cas Statique By Ph Passau and M Van Styvendael
On the Nature of Electrical Conduction in Germanium at Low Temperatures Non Equilibrium Bulk and Contact Phenomena By S H Koenig
A Note on the Adiabatic Approximation in Solids By A Haug and G Sauermann
Statistical Problems in Semiconductors—II By P T Landsberg
Zur Deutung der Strahlungslosen Rekombination an Eindimensionalen Gitterfehlstellen in Halbleitern By W Schultz

Effects of Intense Electric Fields in Semiconductors

Électrons Chauds dans les Semi Conducteurs By J Bok
Quelques Propriétés de Diodes Silicium a Jonction Alliee de Structure Hémisphérique By J Grosvalet
Multiplication of Electrons and Holes in *p-n* Junctions By B M Wul and A P Shotov
Propriétes Non Linéaires des Semi Conducteurs et en Particulier du Carbure de Silicium By R Goffaux

Properties of Heavily-Doped Germanium and Narrow *p-n* Junctions. By L. Esaki
High Forward Current Flow in Junction Diodes. By A. K. Jonscher
Reverse Current Jumps in *p-n* Junction Silicon Diodes. By R. Mutabžija

NOISE IN SEMICONDUCTORS

Current Fluctuations in PbS Cells. By J. Blok and F. M. Klaassen
Properties of l/f Noise in Semiconductors. By J. J. Brophy
Noise Spectra and Current Growth in *p-n* Junctions in Moist Atmospheres. By J. E. Pallett and B. Meltzer
l/f Noise in Germanium Diodes. By T. B. Watkins

SURFACE PHENOMENA

Elektrische Eigenschaften von Inversionsschichten an Halbleiteroberflächen. By E. Groschwitz
Recent Advances in the Understanding of Semiconductor Surface Properties. By H. Statz and G. A. deMars
The Role of Surface States in Lead Sulfide Photoconductors. By R. L. Petritz and H. E. Sorrows
Some Structure and Adsorption Characteristics of Clean Surfaces of Germanium and Silicon. By H. E. Farnsworth, R. E. Schlier and J. A. Dillon, Jr.
Gas Adsorption on Germanium Surfaces. By M. J. Sparnaay
The Electrochemistry of the Germanium-Electrolyte Interface. By M. Green
The Influence of the Ambient Atmosphere on the Surface Recombination on Silicon. By H. U. Harten
Surface States in a One-Dimensional Crystal Model. By E. Aerts

Préparation et Propriétés des Couches Minces d'Antimoniure d'Indium

C. PAPARODITIS

Laboratoire du Magnétisme et de Physique du Corps Solide. Bellevue (Seine-et-Oise)

1. Introduction

Les couches minces sont le plus souvent un assemblage de cristallites de faible dimension. A l'opposé du monocristal massif dont on sait le rôle dans le développement récent des semi-conducteurs, les couches minces constituent en général un cas extrême d'état polycristallin. D'autre part le contrôle de la pureté. lorsqu'il s'agit de composés en couche mince, est rendu difficile par la faible quantité de matière mise en jeu ; le grand rapport de la surface au volume de la couche favorise enfin l'occlusion de gaz.

Malgré ces difficultés, les couches minces semi-conductrices ont reçu déjà des applications : par exemple, les cellules photoconductrices au PbS. On sait d'ailleurs que l'état polycristallin affecte peu certaines propriétés, comme l'effet Hall et le pouvoir thermoélectrique. Dans bien des cas la couche mince peut se présenter comme une forme commode d'étude d'un semi-conducteur.

Le présent travail sur l'antimoniure d'indium a pour but de montrer qu'on peut préparer des couches minces semi-conductrices intermétalliques présentant les caractéristiques essentielles du composé massif et se prêtant à des applications pratiques intéressantes.

Des études sur ces couches minces ont déjà été effectuées par Lark-Horovitz et Dietrich,[1] Presnov et Sironov,[2] Kurov,[3] Kurov et Pinsker,[4] J. Launay et A. Colombani,[5] C. Paparoditis.[6]

2. Préparation des Couches Minces de InSb

(a) L'évaporation

Les couches sont préparées par évaporation thermique dans le vide d'une pompe à diffusion. Le matériau de départ est de l'antimoniure d'indium de type n contenant $5 \cdot 10^{14}$: électrons par cm^3.

On évapore toute la substance du creuset (en tantale), sans interposer d'écran à aucun moment. Le support, en mica ou en verre, est pourvu des électrodes nécessaires pour faire les mesures de la tension de Hall et de la résistivité par une méthode indépendante des contacts (Fig. 1). La température du support est 20° C.

L'épaisseur de la couche est mesurée par pesée ou par la méthode interférentielle de Tolansky. L'épaisseur des couches étudiées varie entre 200 et 5600 Å.

(b) Traitement thermique

La couche ainsi obtenue est métallique. Son coefficient de Hall est

pratiquement nul, sa resistance est faible et presente un coefficient de température positif, elle evolue dans le temps comme l'indique la Fig 2, typique d'une couche metallique granulaire

SUPPORTS

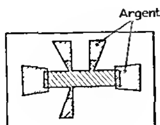

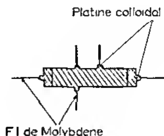

MICA VERRE ou MOLYBDENE

Fig 1

Les proprietes semi conductrices n'apparaissent qu'avec le recuit Ce traitement thermique est opere à des temperatures comprises entre 0 et 400° C pour certains echantillons dans une atmosphere d'argon, pour d'autres dans le vide

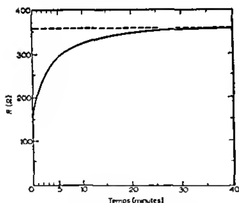

Fig 2

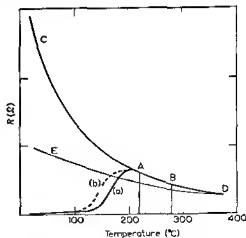

Fig 3

3 Propriétés des Couches Minces de InSb

(a) Évolution de la résistance au cours du recuit

Au cours du recuit la resistance de la couche évolue comme le montre la Fig 3 À partir de 100° C elle augmente fortement, d'autant plus que le traitement est plus lent (la courbe (a) est obtenue pour un chauffage rapide, la courbe (b) pour un chauffage lent) Elle atteint un maximum vers 200° C (point A) La branche OA de cette courbe est irréversible une couche ayant atteint le point A, decrit au refroidissement la branche AC qui

représente le diagramme résistance-température d'un semi-conducteur. Entre 200 et 250° C, la courbe n'évolue plus (la branche BAC est réversible). Au dessus de 280° C la couche évolue à nouveau, le coefficient de température de la résistance, quoique toujours négatif, devient plus faible (courbe DE).

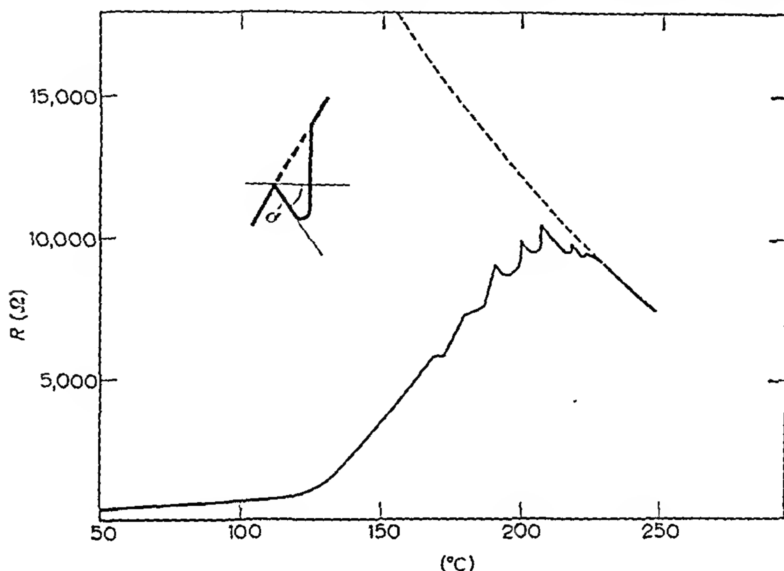

Fig. 4.

Le même processus apparaît sur le diagramme de la Fig. 4 qui est celui d'un chauffage par bonds : à chaque bond on observe successivement une branche réversible (r) caractérisant le coefficient de température de la couche au stade d'évolution atteint et une branche irréversible (i) représentant l'évolution de la courbe causée par le traitement thermique.

(B) PROPRIÉTÉS ÉLECTRIQUES DES COUCHES EN FONCTION DE LA TEMPÉRATURE DU RECUIT

La Fig. 5 montre la résistivité ρ et le coefficient de Hall R_H, mesurés là a température ambiante, pour diverses couches d'épaisseur 700 à 780 A traitées à différentes températures. Les couches traitées entre 200 et 250° C ont la résistivité et le coefficient de Hall les plus élevés :

$$\rho \; 7 \cdot 10^{-1} \, \Omega \text{ cm} \quad R_H - 80 \text{ cm}^3/\text{clb}$$

On peut comparer ces valeurs à celles du matériau massif intrinsèque qui a servi à l'évaporation :

$$\rho = 7 \cdot 10^{-3} \, \Omega \text{ cm} \quad R_H = -400 \text{ cm}^3/\text{clb}$$

Trois couches évaporées sur sel gemme et traitées à 100, 250 et 350° C ont été examinées aux rayons X ; la première et la troisième montraient simultanément les raies de InSb, In et Sb ; la deuxième ne présentait que les raies de InSb.

Il résulte de ces mesures que :

(1) Au cours de l'évaporation, il y a dissociation partielle du composé en ses éléments, avec condensation d'une couche à caractère métallique.

(2) Le recuit favori e la diffu ion donc la recombinaison chimique des elements dissocies, pour une temperature de recuit de 150 a 350° C on obtient une couche semi conductrice pour 250° C la couche obtenue a la resistivite et le coefficient de Hall les plus eleves

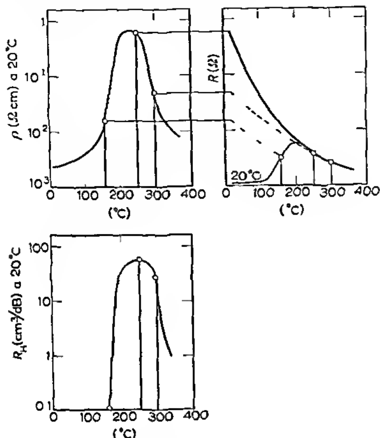

Fig 5

L evaporation jusqu a epuisement du materiau du creuset est necessaire pour obtenir ce resultat

(3) Le chauffage au dessus de 350° C dissocie a nouveau une partie des molecules InSb et détruit partiellement la couche

L effet Hall des couches minces de InSb traitees a 250° C est applicable a la *mesure des champs magnetiques tres faibles* Ainsi une *couche d epaisseur* 200 Å de resistance 500 $k\Omega$ parcourue par un courant de 0 5 mA permet d obtenir une tension de Hall de 200 μV/gauss

(c) MOBILITE ET STRUCTURE GRANULAIRE

Les meilleures valeurs de $\mu_H = R_H/\rho$ sont de 400 cm²/V S On peut en deduire le libre parcours moyen $l = (3\mu_H/4e)\sqrt{2\pi m_n kT}$ (k = constante de Boltzmann e = charge de l electron T = temperature absolue m_n = mas e efficace = 0 013 m_n) On obtient $l = 32$Å

Ces valeurs de μ_H et de l sont tres inferieures a celles du compose massif Cela est en rapport avec la structure cristalline extremement fine Des

couches évaporées sur du sel gemme et recuites à 280° C ont été examinées au microscope électronique, toutes les précautions ayant été prises pour réduire au minimum l'action du faisceau électronique. Nous avons observé une structure microcristalline, la taille moyenne des cristallites étant de 400 Å environ.

(D) VARIATION DE ρ ET R_H EN FONCTION DE LA TEMPÉRATURE

La Fig. 6 indique la variation de ρ et R_H en fonction de $1/T$ pour trois échantillons recuits à 250° C, d'épaisseur 1200, 2500 et 5600 Å respectivement.

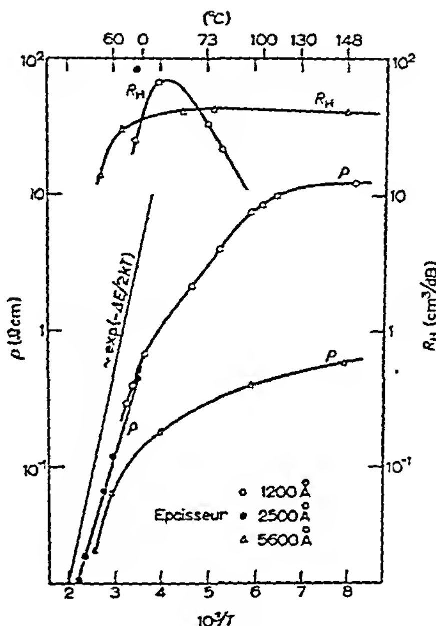

Fig. 6.

Pour la couche de 2500 Å, le coefficient de Hall n'a été mesuré qu'à la température de 20° C ; de même ρ n'a pas été mesuré aux températures inférieures à + 20° C.

Ces courbes rappellent celles obtenues sur le composé massif.

Toutes les couches sont de type n à la température ambiante. Aux basses températures, certaines couches restent nettement de type n, d'autres voient leur constante de Hall tomber à zéro, mais ce résultat estdouteux à cause de la grande résistance des couches ; aucune couche n'a été trouvée de type p aux basses températures.

Aux températures relativement basses, le régime de conduction est extrinsèque ; aux températures supérieures à la température ambiante, le régime devient intrinsèque et la valeur des pentes des différentes courbes $\log \rho(1/T)$ se rapproche de très près de la valeur correspondant à la loi $\rho \sim \exp\left(-\frac{\Delta E}{2kT}\right)$ où $\Delta E = 0{\cdot}17$ eV.

(E) LA PHOTOCONDUCTIVITÉ

Les couches de InSb ainsi préparées dans les meilleures conditions ont une grande sensibilité à la lumière

Le bruit de fond est très faible, inférieur à 1 μV, pour une bande passante de 1 c/s et une fréquence de récurrence de 900 c/s, le seuil de détection dans ces conditions est de 10^{-6} watt par mm² de cellule, la lumière étant celle d'un corps noir à 600° C

Quoique la sensibilité des couches demeure inférieure à celle du corps massif, il est probable qu'elle puisse être améliorée par un meilleur contrôle de la pureté et de la structure cristalline

Conclusion

Nous avons pu préparer des couches minces d'antimoniure d'indium ayant les propriétés essentielles du matériau massif, leur effet Hall et leur photoconductivité peuvent présenter un intérêt pratique

Références

1 Cité par Fan dans Photoconductivity Conference, Atlantic City, Novembre 1954, p 425
2 Presnov V S et Sironov, V F *J tech Phys Moscow*, 27, 1, 123–6 (1957)
3 Kurov, G A *J tech Phys Moscou*, 27, 9, 2181 2 (1957)
4 Kurov, G A et Pinsker, Z G *J tech Phys Moscow*, 28, 1, 29–34 (1958)
5 Launay J et Colombani, A *C R Acad Sci Paris*, 245, 12, 1008 11 (1957)
6. Paparoditis, C *C R Acad Sci, Paris*, 245, 18, 1526–8 (1957)

Physik der III-V-Halbleiter

H. WELKER

Siemens-Schuckertwerke A. G., Erlangen

Die III-V-Verbindungen—das sind Verbindungen zwischen den Elementen B, Al, Ga, In der dritten Gruppe und den Elementen N, P, As, Sb der fünften Gruppe des Periodischen Systems—können übersichtlich in einem rautenförmigen Schema dargestellt werden. Zur Konstruktion desselben ist in Fig. 1 ein Ausschnitt aus dem Periodischen System der Elemente dargestellt. In der vertikalen Mittellinie der Raute stehen die unmittelbaren Nachbildungen der Elemente der IV. Gruppe des Periodischen Systems, nämlich BN anstelle des Diamanten, AlP anstelle des Si, GaAs anstelle des Ge und InSb anstelle des grauen Zinns. Die Ergänzung zum rautenförmigen Schema erfolgt nun dadurch, daß zu den bisher genannten Verbindungen Nachbildungen im weiteren Sinne kommen. Wird z.B. anstelle von Ga das im Periodischen System darüberliegende Al verwendet und anstelle von As das darunterliegende Sb, so erhält man das AlSb, welches links neben GaAs in der Raute steht. Entsprechendes gilt für das rechts stehende InP, weiter für BAs und GaN. Betrachtet man die Nachbildungen der z.T. hypothetischen Zwischenkörper SiC, GeSi und SnGe, so gelangt man nach denselben Prinzipien zum vollständigen Rautenschema.

B	C	N				BN			
					BP		AlN		
Al	Si	P		BAs		AlP		GaN	
			BSb		AlAs		GaP		InN
Ga	Ge	As		AlSb		GaAs		InP	
					GaSb		InAs		
In	Sn	Sb				InSb			

Schmelzpunkt ↑
Aktivierungsenergie ↑
Beweglichkeit ↓
Brechungsindex ↓
undurchsichtig durchsichtig ↕

Fig. 1. Rautenschema der III-V-Verbindungen.

In der Raute stehen die Verbindungen mit geringem mittleren Atomgewicht oben, die mit hohem mittlerem Atomgewicht unten. Bezüglich der elektrischen Eigenschaften gelten dieselben Gesetzmäßigkeiten wie bei den halbleitenden Elementen der IV. Gruppe. So nehmen Schmelzpunkte und Breite der verbotenen Zone zu, wenn man von hohen zu niedrigen Atomgewichten übergeht. Dabei ist die Breite der verbotenen Zone der nachbildenden III-V-Verbindungen größer als die des nachgebildeten Elementes.

Die Elektronenbeweglichkeit nimmt bei Elementen und Verbindungen mit zunehmendem Atomgewicht von oben nach unten zu, wobei wiederum die Elektronenbeweglichkeit der nachbildenden Verbindungen im allgemeinen

großer ist als die des nachgebildeten Elementes Im einzelnen werden diese allgemeinen *Gesetzmaßigkeiten* durch die in Fig 2 zusammengestellten Zahlenwerte der Schmelzpunkte verbotenen Zonen und Elektronen beweglichkeiten bestatigt Eine eingehende Analyse der extrem hohen Beweglichkeitswerte bei InSb und InAs ergab daß diese auf besonders kleine effektive Massen der Leitungselektronen zuruckzufuhren sind Die Locherbeweglichkeiten der Nachbildungen sind vergleichbar oder sogar kleiner als die der zugehorigen Elemente Entsprechendes gilt fur die Lochermassen So kommt es daß fur III V Verbindungen ein mehr oder weniger großes Beweglichkeitsverhaltnis $b = \mu_n/\mu_p$ kennzeichnend ist Es soll hier auch erwahnt werden daß bei III V Verbindungen durchaus bemerkenswerte große Diffusionslangen fur Elektronen auftreten

	Breite der verbotenen Zone ΔE [eV]		*Beweglichkeit* [$cm^2/Vsec$]		*Relative effektive Massen*		*Diffusionslange* L_{max}	*Schmelzpunkt*
	(0° K)	(300° K)	μ_n ($T = 300°$ K)	μ_p	m_n/m_0	m_p/m_0	[μ]	[° C]
Si	1.18	1.04	1900	425	0.33	0.49	> 200	1420
Ge	0.73	0.63	3900	1700	0.22	0.28	> 1000	953
AlSb	1.6	1.49	40	230				1060
GaAs	1.53	1.38	6000	240	0.04		8	1240
InP	1.41	1.27	5000	60			150	1080
GaSb	0.8	0.68	4000	2000	0.2	0.4		702
InAs	0.43	0.33	27 000	280	0.064	0.33		936
InSb	0.24	0.162	77 000	1000	0.037	0.18		523

Fig 2 Zahlenwerte physikalischer Konstanten von III V Verbindungen

Aus dem bisher Gesagten ergibt sich daß zwar III V Verbindungen in ihren Eigenschaften den halbleitenden Elementen der vierten Gruppe sehr verwandt sind daß aber andererseits auch bemerkenswerte Unterschiede vorhanden sind Zur Erklarung dieser Unterscheide wurde bisher der Ladungsunterschied zwischen drei und funfwertigen Elementen und der dadurch hereinkommende zusatzliche Ionenanteil bei III V Verbindungen herangezogen Nach L Pauling sollte namlich bei einer Mischung des homoopolaren Grundanteils mit einem heteropolaren Zusatzanteil in der chemischen Bindung eine sogenannte Resonanzverfestigung auftreten Diese außert sich zunachst in einer erhohten Bindungsfestigkeit und ist wahrscheinlich auch fur die relativ zu den halbleitenden Elementen erhohten Schmelzpunkte verantwortlich Der Ionenanteil fuhrt im allgemeinen zu großeren Niveauunterschieden im elektrischen Kristallpotential und damit zu einer Vergroßerung der verbotenen Zone dieser Effekt des Ionenanteils auf die verbotene Zone wird durch Resonanzverfestigung noch weiter verstarkt

Damit ist das Verhalten der III-V-Verbindungen relativ zu den halbleitenden Elementen, was die verbotene Zone anlangt, befriedigend erklärt. Hingegen ist es nicht möglich, das Verhalten der einzelnen III-V-Verbindungen zueinander auf dieser Basis restlos zu klären. So nimmt nach den Elektronegativitätszahlen von Pauling der Ionenanteil in den beiden Reihen AlSb, GaAs, InP und GaSb, InAs (Fig. 3) zu, trotzdem aber die Breiten der verbotenen Zonen ab.

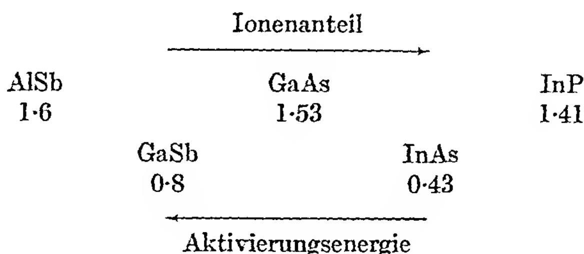

Fig. 3. Aktivierungsenergieen von isoelektronischen III-V-Verbindungen.

Durch die Erhöhung der Bindungsfestigkeit werden zwar die Amplituden der thermischen Gitterschwingungen verkleinert, da aber gleichzeitig wegen des Ionencharakters das Dipolmoment der schwingenden Gitterbausteine erhöht wird, ist der Effekt auf die Beweglichkeit schlecht abzuschätzen. Zudem sind die extrem hohen Elektronenbeweglichkeiten bei InSb und InAs auf extrem kleine Massen zurückzuführen. Auch dieses Verhalten läßt sich nicht allein aus der Annahme eines einfachen Ionenanteils erklären.

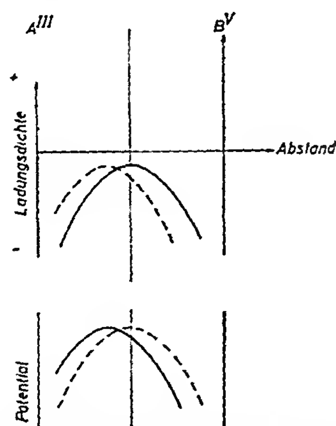

Fig. 4. Ladungsdichte und elektrisches Potential mit und ohne Polarisation.
– – – – mit Polarisation ———— ohne Polarisation

O. G. Folbert hatte den Gedanken, die durch den Ionenanteil hervorgerufene Polarisation der Bindungselektronen, die bei den bisherigen Überlegungen nie explizit betrachtet wurde, für die Erklärung dieser Unstimmigkeiten heranzuziehen. Zur Erklärung des Begriffes Polarisation sei in Fig. 4 die Elektronendichte auf der Verbindungslinie zwischen benachbarten Gitterbausteinen dargestellt. Die beiden Pfeile an den Eckpunkten sollen die unterscheidliche Punktladung der A^{III}- und B^{V}-Kerne andeuten.

Ohne Polarisation ist der Verlauf der Dichtekurve symmetrisch infolge Polarisation findet jedoch eine Dichteverschiebung in Richtung auf den starker geladnen BV Kern statt (gestrichelte Kurve) Betrachtet man die den Dichteverteilungen entsprechenden Kurven des elektrischen Potentials fur Elektronen so hat man ohne Polarisation der ungleichen Kernladung entsprechend ungleiche Potentialmulden Die Polarisation sucht die Muldenungleichheit zu neutralisieren Bei uberwiegendem Ionenanteil konnen sogar die umgekehrten Verhaltnisse auftreten indem durch die Bildung von negativen Ionen die Potentialmulde zum Potentialberg wird So wird es verstandlich daß Ionenanteil und Polarisation zusammen—im richtigen Verhaltnis gemischt—zu der bereits von Slater und Koster diskutierten neutralen Bindung fuhren konnen Das Potential der neutralen Bindung ist hinsichtlich seiner Wirkung auf die Valenzelektronen dem der halbleiten den Elemente der 4 Gruppe sehr ahnlich

Um zu einer mehr quantitativen Theorie zu gelangen zerlegt O Folberth das Kristallpotential in einen symmetrischen und einen antisymmetrischen Anteil und definiert einen Welligkeitsparameter ϵ durch das Amplitudenverhaltnis des antisymmetrischen zum symmetrischen Teil Dabei ist das Amplitudenverhaltnis in einem geeigneten Punkt zu nehmen der zwischen dem Mittelpunkt der beiden Kerne und einem Kern gelegen ist Fur die neutrale Bindung ist $\epsilon = 0$ Fur den Polarisationsgrad macht O Folberth den Ansatz

$$J = \frac{E_{on}}{E_{co}} (Z^{III} + Z^{V})^{3\,2}$$

Z^{III} und Z^{V} sind Kernladungszahlen Fur E_{on} wird der Paulingsche Ansatz gemacht

$$E_{on} = A(x_B \quad x_A)^2 \quad A \quad 4 \quad 23\,06 = 92\,24\ \frac{\text{kcal}}{\text{mol}}$$

Fur x_A x_B wird abweichend von Pauling der Mulliken sche Ansatz verwendet

$$x = \frac{\text{Ionisierungsenergie} + \text{Elektronenaffinitat}}{130}$$

Die Elektronenaffinitat kann im allgemeinen gegen die Ionisierungs energie vernachlassigt werden Fur E_{cov} wird die Bindungsfestigkeit des jeweiligen isoelektronischen Elementes gesetzt Es wird damit moglich fur jede III V Verbindung einen zugehorigen J Wert *anzugeben* (Fig 5) Nimmt man nun an daß die neutrale Bindung ($\epsilon = 0$) zwischen InSb und InAs vorliegt und daß in der Umgebung der neutralen Bindung die ϵ—J Beziehung linear ist so erhalt man den in Fig 5 dargestellten Zusammen hang Zu $\epsilon = 0$ gehoren die geringsten Unterschiede des elektrischen Potentials Deshalb wirkt sich eine Zunahme von ϵ vergroßernd auf ΔE aus In der neuen Argumentation tritt also der Begriff des Welligkeitspara meters ϵ an Stelle des fruher verwendeten Ionenanteils Wahrend aber die Bindungsfestigkeit wegen des steigenden *Ionenanteils in* der Reihe AlSb GaAs InP zunimmt nimmt ϵ in derselben Reihe ab Wegen dieser Gegenlaufigkeit wird es verstandlich daß die verbotene Zone in der Reihe AlSb GaAs InP sogar leicht abnimmt trotz wachsenden Ionenanteils Ferner ist klar daß in der Umgebung der neutralen Bindung die Grund voraussetzung fur hohe Elektronenbeweglichkeit namlich kleines Dipol

moment der Gitterschwingungen erfüllt ist. Der Effekt der Polarisation auf die Elektronenmasse ist zur Zeit nicht geklärt. Es kann sich nur um einen indirekten Einfluß handeln, da die Polarisation primär nur auf die Valenzelektronen wirkt. Hingegen wird es verständlich, daß die dem Valenzband angehörigen Defektelektronen durch die Polarisation eine

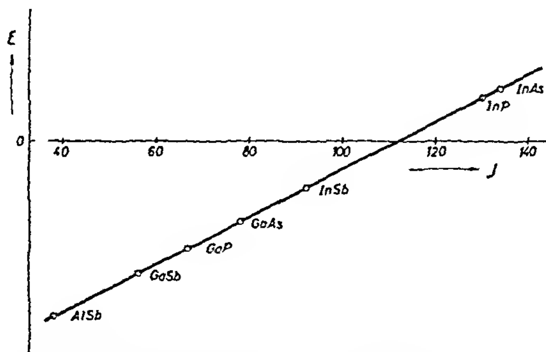

FIG. 5. Modulationsgrad ϵ des periodischen Kristallpotentials als Funktion der Polarisation J für III-V-Verbindungen.

Vergrößerung ihrer Masse erfahren. Durch die Konzentration der Valenzelektronenwolke auf den stärker geladenen Kern hin werden die Sprungwahrscheinlichkeiten in Richtung auf den schwächer geladenen Kern hin verkleinert. Dem entspricht eine Vergrößerung der effektiven Löchermasse.

Daß Elektronen- und Löcherbeweglichkeiten tatsächlich durch die Polarisation beeinflußt werden zeigt besonders deutlich die in Fig. 6

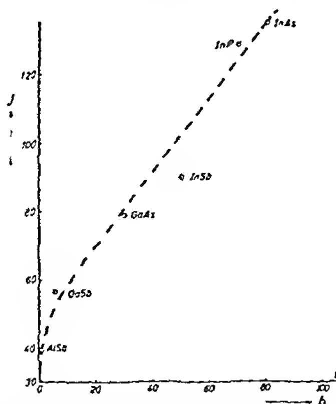

FIG. 6. Polarisation J als Funktion des Beweglichkeitsverhältnisses $b = \mu_n/\mu_p$ für III-V-Verbindungen.

dargestellte Auftragung des Beweglichkeitsverhältnisses $b = \mu_n/\mu_p$ als Funktion des Polarisationsgrades. Das Beweglichkeitsverhältnis nimmt mit steigendem Polarisationsgrad monoton zu.

O. Folberth konnte durch die Berücksichtigung der Polarisation auch Fragen der Mischkristallbildung bei III-V-Verbindungen klären und in die folgende Regel zusammenfassen :

Lückenlose Mischkristallbildung zwischen vorwiegend homöopolaren

Verbindungen wird begunstigt wenn neben einer hinreichenden Gleichheit von Gittertyp und Gitterkonstante auch noch hinreichende Gleichheit der Polarisationsgrade vorliegt

Beispiele fur die Moglichkeit luckenloser Mischkristallbildung sind die Systeme InAs InP und GaAs GaP mit jeweils sehr ahnlichen J Werten (siehe Fig 5) Hingegen ist im System AlSb GaSb trotz nahezu gleicher Gitterkonstante wegen der Verschiedenheit der J Werte die Mischkristall bildung verhaltnismaßig gering

Magnetoresistive Effects in Indium Antimonide and Indium Arsenide*

H. P. R. FREDERIKSE, W. R. HOSLER

National Bureau of Standards, Washington, D.C.

THE semiconductors InSb and InAs are characterized by a high electron mobility. As a result the conductivity is strongly influenced by a magnetic field : this has made possible a number of devices,[1] such as a magnetometer, current and voltage regulator, pressure gauge, Hall effect amplifier, etc. The magnetoresistive effect is very sensitive to the physical conditions under which it is measured, especially in materials like InSb and InAs. They offer therefore a unique opportunity to obtain information concerning the collision mechanism and the statistics of the conduction electrons ; at the same time, such measurements indicate the maximum values of the magnetoresistance that can be achieved with particular choices of the parameters.

The Wilson-Sommerfeld theory [2] predicts for the simplest case (electrons, isotropic conduction band, acoustical scattering, low magnetic field) a relative change of resistance

15713

$$\frac{\Delta\rho}{\rho_0} = \frac{9\pi}{16}\left(1 - \frac{\pi}{4}\right)\mu_e{}^2H^2, \tag{1}$$

where μ_e = electron mobility. There are, however, several factors which change Eq. (1) considerably. These factors are :

(a) More than one type of carrier (e.g. intrinsic semiconductor).
(b) Scattering mechanism (e.g. ionized impurity scattering, lattice scattering or mixed scattering).
(c) Degree of degeneracy.
(d) Anisotropic energy surfaces.
(e) Geometry (e.g. Corbino disc).
(f) High magnetic fields (quantum effects, " freeze-out ").
(g) High electric fields (" breakdown ").

By choosing the temperature and the magnetic and electric field strength, it is usually possible to separate the effects of the conditions (a)–(g) on the magnetoresistance. Furthermore, InSb (n-type) and InAs (n-type) have the advantage that the complications of condition (d) can be avoided : the electron energy surface is spherical and the energy-momentum relation is parabolic, at least at the bottom of the conduction band.

MAGNETORESISTANCE AT 300° K

Reasonably pure InSb is intrinsic and non-degenerate at room temperature ; the electrons are scattered by lattice vibrations. It can easily be shown that the magnetoresistance will not saturate when the number of

* Research supported by the Office of Naval Research, Washington, D.C., U.S.A.

electrons equals the number of holes, $n_e = n_h$ [3, 4] The value of $\Delta\rho/\rho_0$ (measured on a long thin sample) is about 0 5 at 10 kilogauss

Much larger values can be obtained if one changes the geometry of the sample [3, 5] Fig 1 shows the magnetoresistance of a Corbino disc The experimental points deviate from the quadratic behavior at high fields (H > 2 kilogauss) This is due to the influence of the low mobility holes At very high fields $\Delta\rho/\rho_0$ is still quadratic with H however with a smaller proportionality constant

$$\frac{\Delta\rho}{\rho_0} = \frac{9\pi}{16}\mu_e^2 H^2 \left(\frac{1+b^{-3}}{1+b^{-1}}\right) \qquad \text{(small } H\text{)} \quad (2\text{ a})$$

$$\frac{\Delta\rho}{\rho_0} = \frac{9\pi}{32}\frac{\mu_e^2}{b} H^2 \qquad \text{(large } H\text{)}, \quad (2\text{ b})$$

where b is the mobility ratio μ_e/μ_h (≈ 80 for InSb)

MAGNETORESISTANCE AT 78° K

At this temperature InSb is a simple extrinsic semiconductor and only one type of carrier contributes to the conduction in n type specimens On the other hand complications arise because the scattering is usually due both to the lattice and to ionized impurity centers The electron mobility reaches values of (2–5) × 10^5 cm²/volt sec at this temperature consequently the low field approximation is valid only at fields of less than 200 gauss ($\mu_e H \ll 1$)

The classical expression for the magnetoresistance at arbitrary magnetic field strength is a complicated function of the magnetic field parameter γ[= $(9\pi/16)\,\mu^2 H^2$] and the scattering parameter β[= 6 μ_L/μ_I μ_L and μ_I being the mobilities due to lattice scattering and impurity scattering respectively] [3, 4] At low fields a small amount of ionized impurity scattering reduces the magnetoresistance appreciably below the value for pure lattice scattering On the other hand a considerably larger *saturation* value ($H \to \infty$) is found when ion scattering becomes predominant At high magnetic fields however the above mentioned classical expression loses its validity because quantum effects begin to play a role [6] If the conditions

$$\omega\tau \gg 1 \qquad (3\text{ a})$$

$$\text{and } \hbar\omega \gg kT \qquad (3\text{ b})$$

(where ω = cyclotron frequency and τ = collision time) are fulfilled quantization of the electron orbits has to be considered this occurs in n type InSb at 78° K for $H > 7500$ gauss Provided the material is reasonably pure we are also dealing with a non degenerate situation and most of the electrons will be in the lowest quantum state (quantum limit) This case has been studied by Argyres [7], he predicts a linear dependence of the magnetoresistance at high fields

These effects are illustrated in Fig 2 The sample used in these measurements contains 9 × 10^{14} electrons per c c The Hall mobility is about 3 4 × 10^5 cm²/volt sec Using the low field approximation one calculates from the transverse magnetoresistance a mobility of 3 6 × 10^5 cm²/volt sec at magnetic fields of 100 or 200 gauss It is clear that $\Delta\rho/\rho_0$ deviates from a quadratic behavior when H exceeds 500 gauss

The top curve in Fig 1 represents the magnetoresistance of a Corbino disc with 2 × 10^{15} electrons per c c at 78° K Classically one expects a

quadratic behavior at high fields. Fig. 1 shows, however, that $\Delta\rho/\rho_0$ follows closely a linear magnetic field dependence above 10,000 gauss in accordance with Argyres's predictions.[7]

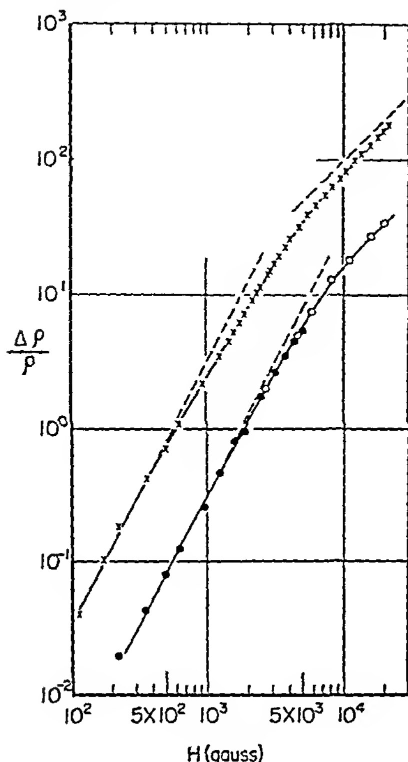

FIG. 1.

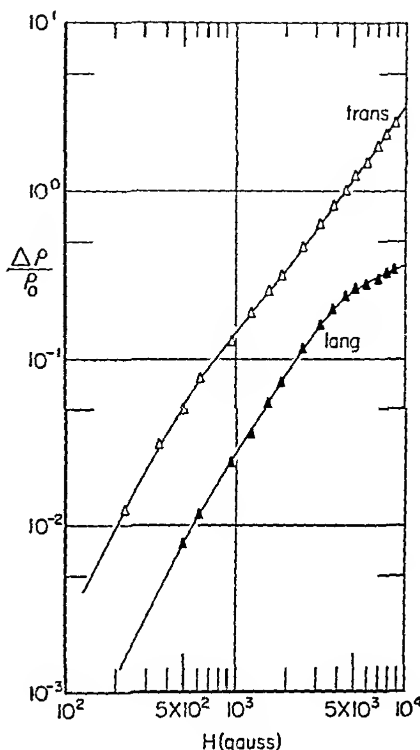

FIG. 2.

Fig. 1. Magnetoresistance of InSb (Corbino disc ; $n = 2 \times 10^{15}$/c.c.). ——●—— 300° K. ——x—— 78° K. ——o—— data by Beer *et al.* on a similar sample at 300° K (ref. 3). The dashed lines at low fields indicate a slope of 2, at high fields a slope of 1. FIG. 2. Magnetoresistance of InSb at 78° K. (Long narrow sample.)

MAGNETORESISTANCE AT LIQUID HELIUM TEMPERATURES

In semiconductors with a small effective mass like InSb and InAs, Eqs. (3 a) and (3 b) are satisfied at 4·2° K when H exceeds 1000 or 1500 gauss. Consequently, quantum effects will be important for magnetic fields of a few thousand gauss and higher. Furthermore, the electron distribution will be degenerate. As long as the Fermi energy $\zeta > \hbar\omega$ electrons will occupy several of the semidiscrete energy levels (Landau levels) ; this gives rise to an oscillatory behavior of the magnetoresistance (as well as the Hall coefficient). Recently the theory for this situation has been worked out. Assuming elastic lattice scattering, the formula for the transverse magnetoresistance looks as follows [7] :

$$\rho_H = \rho_0\left[1 + c\left(\frac{\hbar\omega}{\zeta}\right) + d\left(\frac{\hbar\omega}{\zeta}\right)^{1/2} \chi \frac{\sin\left(\frac{2\pi\zeta}{\hbar\omega} - \frac{\pi}{4}\right)}{\sin h\,\chi}\right] \qquad (4)$$

where c and d are numerical constants and $\chi = 2\pi^2 kT/\hbar\omega$ Actually the above expression was derived for $T = 0$, we have assumed here that the damping term $\chi/\sinh\chi$ enters in the transverse effect in the same way as in the longitudinal magnetoresistance and the susceptibility * The hyperbolic sin can be replaced by the exponential if $\chi \gg 1$, the amplitude A can then be written

$$A \sim TH^{1/2} \exp\left(-2\pi^2 kT/\beta^* H\right) \tag{5}$$

where $\beta^* H = \hbar\omega$, and β^* = double effective Bohr magneton Dingle [9] has pointed out that the amplitude is further affected by collision broadening He has shown that this can be taken into account if one replaces T in the exponential by a somewhat higher temperature $(T + T')$

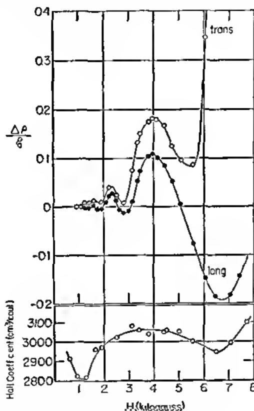

FIG 3 Magnetoresistance and Hall coefficient of InSb at 1 7° K (Sample 4 see Table 1)

Equation (4) indicates that the magnetoresistance will be periodic in $1/H$ with a period β^*/ζ The parameter ζ is the Fermi level in magnetic field, translating ζ in terms of ζ_0 $(H = 0)$ one can show that the resistance minima occur when the magnetic field obeys the following equalities

$$\left.\begin{aligned} \zeta_0 &= 1\,31\,\beta^* H, \\ \zeta_0 &= 2\,36\,\beta^* H \\ \zeta_0 &= 3\,38\,\beta^* H \\ \zeta_0 &= 4\,40\,\beta^* H, \text{ etc} \end{aligned}\right\} \tag{6}$$

* It can be shown that Eq (4) is also valid for impurity scattering if one assumes that the impurity potential can be represented by a δ function

The Fermi energy ζ_0 is easily calculable from the Hall coefficient and the ratio β^*/ζ_0 can therefore be determined. (Note that the effective mass drops out.) These values can be compared with the observed periods according to Eq. (6).

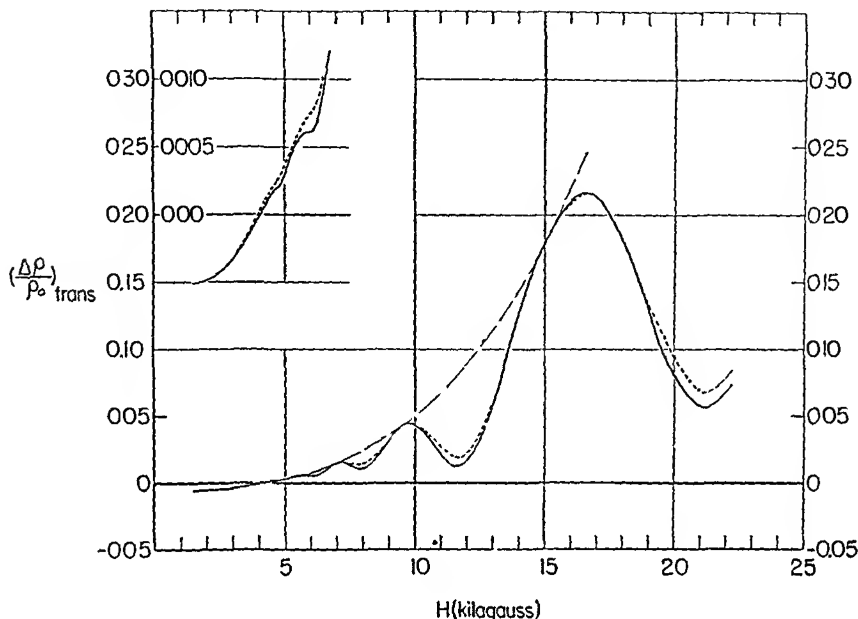

FIG. 4. Transverse magnetoresistance of InAs. - - - - - 4·2° K. ——— 3·05° K.

Measurements of the magnetoresistance have been made on a number of InSb[6] and InAs samples[10]; examples are shown in Figs. 3 and 4. Values of the observed and calculated periods are compared in Table 1.

Eq. (6) offers the possibility of determining β^* and therefore m^*. A plot of $\ln(AH^{-1/2})$ vs. $1/H$ at a given temperature should yield a straight line with a slope $-[2\pi^2k(T + T')]/\beta^*$. From data at different temperatures T' and β^* can be calculated. The values thus computed are: for InSb $m_e^* = (0{\cdot}009 \pm 0{\cdot}004)m_0$ and for InAs $m_e^* = (0{\cdot}018 \pm 0{\cdot}002)m_0$. These figures are somewhat smaller than the values resulting from electrical, optical and cyclotron resonance experiments.

"FREEZE-OUT" AND BREAKDOWN

Impurity states in semiconductors are often treated on the basis of a hydrogenic model. If the impurity concentration is not too small, the electron wave functions of neighboring donor (or acceptor) centers will overlap, thus giving rise to an impurity band. The activation energy of the donor band in InSb and InAs is very small and the width of the band is already appreciable at low impurity concentrations. Consequently the donor band will overlap the conduction band for donor concentrations of more than 10^{15}/c.c. Yafet, Keyes and Adams[11] have shown, however, that the overlap of the wave-functions can be reduced considerably by high magnetic fields: this means that the effective Bohr radius is decreased and

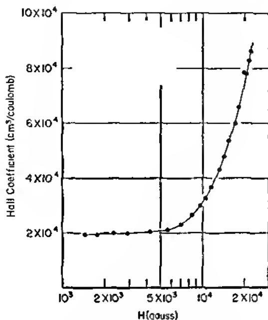

FIG. 5. Freeze out effect in InSb. $T = 4.2°$ K. $n = 3 \times 10^{14}$/c.c.

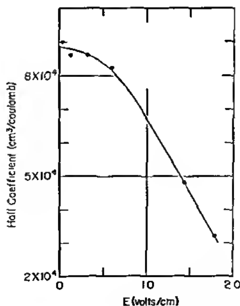

FIG. 6. Re-excitation in InSb. $T = 4.2°$ K. $H = 22{,}000$ gauss. $n = 3 \times 10^{14}$/c.c.

the activation energy increased. As a result, electrons will drop from the conduction band into the impurity states; this effect is called "freeze-out."[12] The decrease of the number of conduction band carriers is detected by a sharp rise of the Hall coefficient at high magnetic field strength (Fig. 5).

The magnetoresistance is also strongly affected by the freeze-out. Not only the mobility of the carriers in the conduction band is reduced, but also the number of those carriers is diminished. At the same time the number of electrons in the donor band increases, while the mobility in this band decreases exponentially.[13] This is the reason why the magnetoresistance rises at high fields with a much higher power of H than the theoretically predicted square law.[7] Magnetoresistance measurements on a very pure InSb sample at 1·7° K showed a resistance change of a factor 6500 at 22 kilogauss.

Re-excitation is possible by applying "high" electric fields. Fig. 6 shows the decrease of the Hall coefficient nearly back to its original value in an electric field of 1·8 volt/cm. This re-excitation is possible due to impact ionization, similar to the breakdown effect observed in germanium and other semiconductors in zero magnetic field.[14] In the latter cases the changes of the resistance and the Hall coefficient are, however, much more abrupt than in the present effect.

TABLE 1. Periods of Oscillations in Magnetoresistance

Sample		n_e	Obs. period Long.	Obs. period Trans.	Calc. period $a\beta^*/\zeta_0$
		cm^{-3}	$\times 10^{-4}$ gauss^{-1}		$\times 10^{-4}$ gauss^{-1}
InSb	1	$7{\cdot}0 \times 10^{15}$	1·24	—	0·88
	2	$5{\cdot}3 \times 10^{15}$	1·32	0·82	1·12
			0·92	—	1·10
			0·60 (?)	—	1·08
	3	$2{\cdot}4 \times 10^{15}$	2·13	1·75	1·87
			2·03	1·96	1·82
			—	1·72	1·80
	4	$2{\cdot}3 \times 10^{15}$	2·06	1·73	1·92
			2·03	2·01	1·86
			1·96	1·96	1·84
	5	$1{\cdot}35 \times 10^{15}$	3·15	2·75	2·71
	6	$1{\cdot}0 \times 10^{15}$	3·82	3·34	3·32
InAs	NOL-5	$2{\cdot}0 \times 10^{16}$	4·26	4·19	4·54
			4·16	4·22	4·45
			4·28	4·62	4·40
			4·40	4·33	4·35

References

1 Ross I M and Saker E W *J Electronics* **1** 223 (1955)
2 Wilson A H The Theory of Metals Cambridge University Press (1953)
3 Beer A C *et al* *Phys Rev* **107** 1506 (1957) and Reports of the Battelle Memorial Institute (unpublished)
4 Appel J *Z Naturf* **9 a** 167 (1954)
Madelung O *Z Naturf* **9 a** 667 (1954)
5 Weiss H and Welker H *Z Phys* **138** 322 (1954)
6 Frederikse H P R and Hosler W R *Phys Rev* **108** 1136 (1957)
7 Argyres P N *Phys Rev* **109** 1115 (1958) *J Phys Chem Solids* **4** 19 (1958)
8 Zilberman G E *J exp theor Phys* **29** 762 (1955) transl *Soviet Physics J E T P* **2** 650 (1956)
9 Dingle R B *Proc roy Soc* A **211** 500 (1952)
10 Frederikse H P R and Hosler W P *Phys Rev* (May 15 1958)
11 Yafet Y Keyes R W and Adams E N *J Phys Chem Solids* **1** 137 (1956)
12 Keyes R W and Sladek R J *J Phys Chem Solids* **1** 143 (1956)
13 Sladek R J *Phys Rev* (May 15 1958)
14 Sclar N Burstein E Turner W J and Davisson J W *Phys Rev* **91** 215 (A) (1953) Sclar and Burstein *J Phys Chem Solids* **2** 1 (1957)

Galvanomagnetic Effects in Indium Arsenide and their Applications

R. P. CHASMAR, E. COHEN

Research Department, Metropolitan-Vickers Electrical Co. Ltd. Manchester

1. Introduction

The practical utilization of the Hall effect, and, to a lesser extent, the magnetoresistive effect in semiconductors, has only recently come into prominence with the realization that these properties may enable certain electrical measurements to be made more simply and economically than heretofore. Germanium, because of its availability and advanced state of technological development has been used in a Hall-effect fluxmeter, as described by Pearson.[1] The linear product formation inherent in the Hall effect has been applied by Barlow, using germanium, to power measurements both at audio and power-supply frequencies [2] as well as at centimetric wavelengths.[3] The important application of a Hall multiplier to the needs of analogue computation has been considered by Keister [4] and by Lofgren,[28] while Mason *et al.*[5] have reported on Hall effect modulators and gyrators.

A limitation on these applications using germanium would be the dependence of the characteristics on temperature, and Keister and Lofgren have both suggested methods to overcome this problem in germanium multipliers.

It is the purpose of the following discussion to consider the relatively new semiconductor indium arsenide, whose properties promise to be particularly favourable from the temperature point of view, and which, unlike germanium, has a magnetoresistive effect large enough to use in control elements.

2. Properties of Indium Arsenide

Indium arsenide is one of the nine semiconducting compounds that can be formed by cross-combination of the elements aluminium, gallium and indium from group III of the periodic table with the elements phosphorus, arsenic and antimony from group V.[6] These compounds can be regarded in some sense as analogues of the intervening group IV semiconducting elements, in that they crystallize in the zinc blend structure,[7] have similar lattice constants and the binding is predominantly homopolar. In this way

Table 1

Semiconductor	*Lattice constant* (Å)	*Band gap at 20° C (eV)*
Germanium	5·65	0·72
Indium arsenide	6·04	0·33
Grey tin	6·46	0·08

indium arsenide can be considered as lying intermediate between germanium and grey tin as illustrated in Table 1

The value of 0 33 eV for the band gap of indium arsenide at 20° C is that found by Oswald [8] from optical measurements Measurements by various authors [9 10 11] of Hall effect and electrical conductivity have yielded values for the band gap at 0° K ranging from 0 42 to 0 5 eV while the value obtained by extrapolation of the optical data is 0 43 eV

It would not appear from the literature that indium arsenide which is substantially intrinsic at room temperature has yet been prepared but most laboratories have reported n type material containing a carrier concentration of about 1 7 10^{16} electrons/c c this is approximately ten times the intrinsic concentration The segregation coefficient of sulphur in indium arsenide has been shown to be unity [12] and it is likely that this is the donor impurity dominating the behaviour of the best reported samples

Indium arsenide has two surprising properties which it shares with indium antimonide and which largely distinguish these two compounds from the remaining group III V combinations First the electron mobility at room temperature is exceedingly large (25 000 cm^2/volt sec for InAs) due to a small effective electron mass which arises from a weak ionic component in the binding as discussed by Seraphin [13] Secondly the Hall coefficient is practically invariant with temperature from the onset of intrinsic conduction down to 1 3° K [11] This inability to freeze out donor electrons from the conduction band of even the purest samples has been attributed to the existence of an impurity conduction band overlapping the normal impurity band The small effective electron mass in indium arsenide would lead to extended electron orbits on the donor atoms and consequent large overlap of the wave functions Stern and Talley [14] have calculated the density of states distribution for an impurity band based on hydrogen like donor levels and found a reasonable fit of their results with the observed shift of optical absorption edge with donor concentration Their results are also consistent with values of effective electron mass deduced from electrical and thermo electric power data [10 15]

Thus it may be said that the large electron mobility and the temperature invariance of the extrinsic Hall coefficient both arise from the small effective electron mass in indium arsenide and this in turn is due to the unusual and critically balanced nature of the binding

3 The Hall Effect in Indium Arsenide

The temperature invariance of the extrinsic Hall coefficient and the high electron mobility in indium arsenide as discussed in the previous section are properties which make this material particularly suitable for Hall effect devices A Hall plate may be operated either into an open circuit if only voltage output is needed or into a matched load if power is required These two modes of operation will be discussed separately

(1) Open circuit operation

The Hall voltage (V_H) produced into an open circuit is

$$V_H \quad \frac{R_H \, H_G \, I_A \, 10^{\;5}}{t} \text{ millivolts} \tag{1}$$

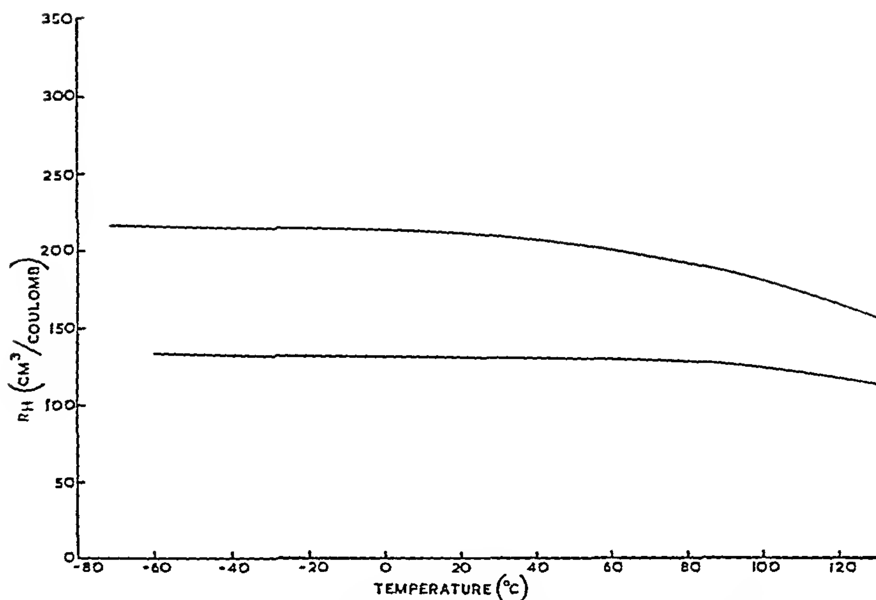

FIG. 1. Variation of Hall coefficient with temperature for indium arsenide.

FIG. 2. Performance of indium arsenide Hall plate at various temperatures.

R_H = Hall coefficient in cm^3/coulomb
I_A = plate current in amps
H_G = magnetic field in gauss
t = plate thickness in cm

V_H will then be a linear function of H and I if R_H is independent of magnetic field and temperature Measurements show R_H to be substantially independent of magnetic field up to 10 000 gauss at room temperature In Fig 1 are plotted curves showing the variation of Hall coefficient of indium arsenide with temperature between − 70° C and + 130° C, for two specimens having Hall coefficients at 20° C of 132 and 214 cm^3/coulomb Over the extreme practical range of working temperatures − 40° C to + 100° C the temperature variation is 0 06%/°C and 0 12%/°C respectively In Fig 2 is shown the performance at various temperatures of an indium arsenide Hall probe suitable for measuring or exploring magnetic fields The Hall coefficient of the plate was 100 cm^3/coulomb and it is seen that the temperature variation is in accordance with the data in Fig 1

(2) MATCHED OPERATION

It has been shown by Saker *et al*[16] that the efficiency of a Hall plate working into a matched load is given by

$$\text{Efficiency} = \frac{9\pi^2}{256}\ \frac{1}{K}\ 10^{-16}\ \mu^2 H_G^2 \tag{2}$$

μ = electron mobility
$K \simeq 5$ is a constant related to plate construction
This calculation only holds for weak magnetic fields where the magnetoresistance effect in the semiconductor is small It emphasizes however the importance of the high electron mobility in indium arsenide in producing for example, an advantage in efficiency of $\left[\frac{25\,000}{3600}\right]^2 \simeq 50$ times over germanium It has been shown from network theory by Wick[17] that ideally the efficiency can never exceed 17 per cent even for infinite mobilities and magnetic fields This limitation on maximum achievable efficiency arises owing to the magnetoresistance effect increasing the internal resistance of the sample at high magnetic fields

This effect is illustrated in Fig 3 where load curves are shown for an indium arsenide Hall plate at two values of magnetic field and it is seen that matching is achieved with load resistances of approximately 2 9 Ω and 4 2 Ω The resistance values obtained by direct measurement between current and Hall terminals of the plate are given in Table 2

TABLE 2

H (gauss)	0	4650	7750
R_C (ohms)	3·4	5·4	7 9
R_{HALL} (ohms)	1 9	2 9	4 2
Efficiency		2 9%	4 9%

If the efficiencies recorded in Table 2 are corrected so as to eliminate the effect of the magnetic field on the internal resistance of the specimen, values in reasonable agreement with those given by equation (2) are obtained. A further limitation imposed by the magnetoresistance effect for a loaded Hall plate, is in its effect on the linearity of the relationship between Hall output and magnetic field.[18] For devices such as the Hall multiplier (see

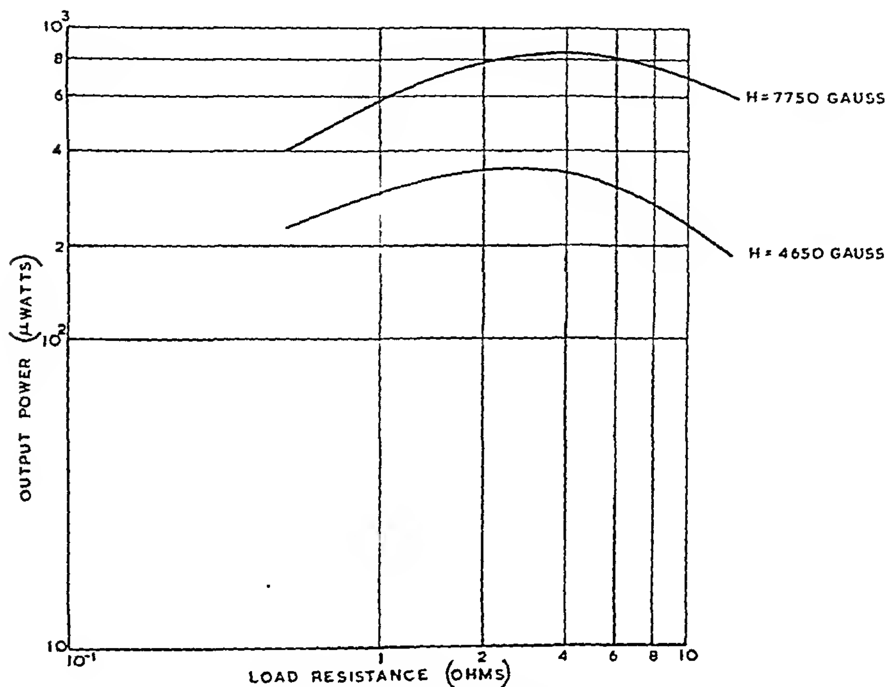

FIG. 3. Load curves for indium arsenide Hall plate.

§ 3 (4)) where linearity is of paramount importance, it is therefore preferable to use a Hall plate, working into an open circuit. For use as a fluxmeter which can be precalibrated, the effect is not serious and sufficient power can be obtained from a Hall plate to operate a milliammeter. Such a fluxmeter utilizing an indium antimonide Hall probe has been described by Saker.[16]

The temperature performance of the Hall plate when loaded is less favourable than when used on open circuit, since the output is now influenced by the change of internal resistance with temperature. The conductivity of a typical sample of indium arsenide is plotted against temperature in Fig. 4. Between $-40°$ C and $+100°$ C the temperature coefficient of resistance is 0·35%/°C. For comparison the relationship for an indium antimonide specimen of similar conductivity is also shown, and it is seen that above room temperature very marked changes occur due to this material becoming an intrinsic conductor.

(3) FIGURES OF MERIT FOR HALL PLATES

For rapid assessment of the performance of Hall plates it is proposed to define certain figures of merit Only open circuit working will be considered

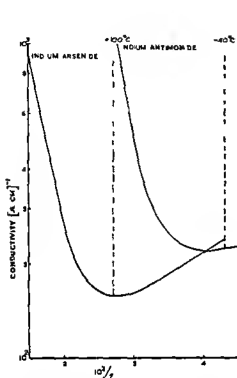

FIG 4 Conductivity of indium arsenide and indium antimonide as a function of temperature

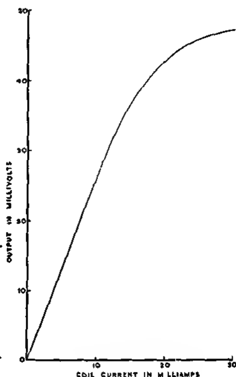

FIG 5 Hall effect multiplier

Responsivity

This is defined as the Hall voltage output in millivolts per unit plate current in mA and unit magnetic field in kilogauss From equation (1) we see that

$$\text{Responsivity} = R = \frac{V_H}{H_K I_M} = \frac{R_H}{t} \; 10^{-5} \text{ mV/mA kG} \qquad (3)$$

We can thus write

$$\frac{\Delta V_H}{\Delta I_m} = R \; H_K \text{ and } \frac{\Delta V_H}{\Delta H_K} = R \; I_M$$

R is therefore of the nature of a sensitivity defined without restriction on the plate current and power dissipation in the plate, and is of value for small signal conditions, such as the measurement of weak magnetic fields or small amounts of power, *it is proportional to the Hall coefficient of the semi* conductor and inversely proportional to plate thickness

Dissipation Constant

When it is desired to drive a Hall plate to its limit as set by temperature rise considerations in order to obtain maximum voltage output, a performance factor is required which is related to the plate dissipation. It is proposed to call this the "dissipation constant" (M) of the plate and to define it in terms of the power per unit area (P/A) dissipated in the plate such that

$$\frac{V_H}{H_K} = M \,.\, f(P/A)$$

Let V_H = Hall voltage in millivolts.
I_M = plate current in mA.
H_K = magnetic field in kilogauss.
ρ = specific resistivity of the plate material in ohm cm.
l = plate length in cm.
ω = plate width in cm.
t = plate thickness in cm.
A = total plate area in sq. mm.
P = power dissipated in the plate in milliwatts.

Then
$$P = I^2 \,.\, \rho \,.\, \frac{l}{\omega \,.\, t} \,.\, 10^{-3} \text{ milliwatts}$$
$$A = 2l \,.\, \omega \,.\, 10^2 \text{ mm}^2$$

$\therefore$ By definition

$$\frac{V_H}{H_K} = M \,.\, f\left[\frac{I_M^2 \,.\, \rho \,.\, 10^{-5}}{2\omega^2 \,.\, t}\right] \tag{4}$$

From equation (1)

$$\frac{V_H}{H_K} = \frac{R_H \,.\, I_M \,.\, 10^{-5}}{t} \tag{5}$$

We have from equations (4) and (5)

$$f(P/A) = \sqrt{P/A}$$

Then

$$M = \frac{V_H}{H_K}\sqrt{A/P} \text{ mV/kG}\sqrt{\text{mm}^2\text{/milliwatt}} \tag{6}$$

$$= 3{\cdot}16 \,.\, 10^{-3}\, R_H \,.\, \omega \,.\, \sqrt{2/t \,.\, \rho} \tag{7}$$

M is thus the Hall output in millivolts for a field of 1 kilogauss and a dissipation of 1 milliwatt per sq. mm. and is given in terms of the plate constants by equation (7).

For a semiconductor of given R_H and ρ the value of M increases with increasing width and decreasing thickness of the Hall plate. If, on the other hand, the plate dimensions are fixed and the material characteristics are changed then

$$M \propto \frac{R_H}{\sqrt{\rho}} \propto \sqrt{\mu \,.\, R_H}.$$

Thus in comparison with other semiconductors of similar Hall coefficient indium arsenide has an advantage due to its large mobility.

As an example of the performance figures that might be obtained in practice consider a Hall plate of dimensions 8 mm × 4 mm × 0 05 mm made from indium arsenide of Hall coefficient 100 cm³/coulomb Then from equations (3) and (7)

$$R = 0\,2 \text{ mV/mA kG}$$
$$M = 40 \text{ mV/kG } \sqrt{\text{mm}^2/\text{mW}}$$

Plates having these characteristics have been successfully made in the laboratory and this would seem to be near the limit of performance for material of $R_H = 100$ since 0 05 mm is probably a minimum practical thickness Higher values of M can be obtained by increasing the width of the plate as shown by equation (7) but the length of the plate must also be increased in proportion to avoid short-circuiting of the Hall potential by the current electrodes Examples of the uses of such Hall plates have been given by Hartel [19]

(4) THE HALL EFFECT MULTIPLIER

An obvious application of the Hall effect is to a simple linear multiplier for use in analogue computers Such a device would also be of value as a frequency changer or as a carrier suppressed double side-band modulator The frequency response for most computer applications ranges from D C to a few hundred cycles, and one input signal can be utilized in the form of a current in a coil wound on a ferromagnetic core to provide the magnetic field for the Hall plate The other signal is provided as a current supply to the plate Since the Hall voltage will be linearly related to the currents in the coil and the plate it is essential that these are supplied from high impedance sources in order to eliminate the effect of the coil reactance and the magnetoresistance effect in the plate

Experimental multipliers have been made in this laboratory using an indium arsenide Hall plate mounted in a gap in a ferrite core The characteristic of a typical multiplier is given in Fig 5 in terms of the Hall voltage output into an open circuit for various values of coil current and for a plate current of 50 mA The characteristic is linear up to values of coil current of 13 mA and measurements showed the ratio of fundamental to second harmonic introduced by this multiplier to be greater than 40 db The curvature at higher coil currents is due to saturation of the ferromagnetic core In this multiplier the coil had an inductance of 4 7 henrys and was self resonant at 6 kc/s The figures of merit for the Hall plate were

$$R = 0\,18 \text{ mV/mA kG and } M = 33 \text{ mV/kG } \sqrt{\text{mm}^2/\text{mW}}$$

4 The Transverse Magnetoresistance Effect in Indium Arsenide

When a semiconductor carrying an electric current is placed in a magnetic field transverse to the current direction, a Hall voltage is set up as discussed in the previous sections The effect of the Hall electric field is to annul the deflecting force due to the magnetic field and enable the current carriers to pass through the semiconductor substantially undeflected Owing to the spread of thermal velocities of the current carriers, this balance only occurs for carriers of a certain mean velocity Carriers differing from this critical velocity are deflected by the magnetic field and their path length through the

semiconductor is enhanced, giving rise to an increase in the specimen resistance : this effect is known as the transverse magnetoresistance effect to distinguish it from the longitudinal magnetoresistance effect observed when the magnetic field is parallel to the current direction. The magnitude of the magnetoresistive effect will depend on the energy distribution of the current carriers and on the relation between their energy and mean free path as determined by the scattering mechanism in the semiconductor. The effect will thus vary both with degree of degeneracy and with purity. This subject has been treated by a number of authors and a comprehensive review has been made by Champness.[20] Considering the case of a pure semiconductor with covalent lattice scattering and for weak magnetic field ($\mu H \ll 1$), it can be shown that the magnetoresistance expressed as ratio of the change of resistivity ($\Delta\rho$) due to the magnetic field, to the resistivity (ρ_0) in zero field is given by $\frac{\Delta\rho}{\rho_0} = 0{\cdot}38\,(\mu H)^2$ for a specimen long compared to its width. The effect is therefore exceptionally great in semi-conductors of high electron mobility such as indium arsenide [21, 22] and indium antimonide.[23, 24]

If the constraining effect of the Hall field is removed, for example, by short-circuiting a pair of Hall connections placed on the sides of the specimen, the magnetoresistive change is increased since all the current carriers are now deflected by the magnetic field. The same effect can be obtained by altering the dimensions of the specimen. If the length is made small compared to the width, the end electrodes tend to short-circuit the Hall voltage and again the magnetoresistive change is greatly enhanced. A device in which it may be considered that the Hall voltage is completely short-circuited is the Corbino disc : here, the electrons flowing in at the centre execute spirals in the plane of the disc as they travel to the circumferential electrode and their path length is thus greatly increased, due to the magnetic field. The magneto-resistance in indium antimonide has been measured by Weiss, Welker [23] for various geometric configurations. A Corbino disc of this material had a value $\frac{\Delta\rho}{\rho_0}$ of 23·6 at a field of 10,000 gauss.

In Fig. 6 are shown measurements on a square plate of n-type indium arsenide ($R_H \simeq 200$) and on a construction approximating to a Corbino disc. Measurements by Ramer *et al.* are included for comparison, while Welker has reported a value of $\frac{\Delta\rho}{\rho_0} = 4{\cdot}5$ at 10,000 gauss for an indium arsenide disc. The discrepancy between the various measurements may perhaps lie in the essentially low resistance of the Corbino disc configuration and the consequent importance of small amounts of contact resistance to the leads. The effect of temperature on the magnetoresistance effect in the square plate is given in Fig. 7. In practical applications the variation of zero field resistance with temperature could be balanced out by using a pair of matched elements in a bridge circuit, only one of which was introduced into the field.

Practical applications utilizing magnetoresistance do not appear to have been developed as far as those involving the Hall effect ; this may be in part due to the low resistance of suitable specimens. For example, the disc and plate in Fig. 6 had a zero field resistance of the order of 1 or 2 ohms.

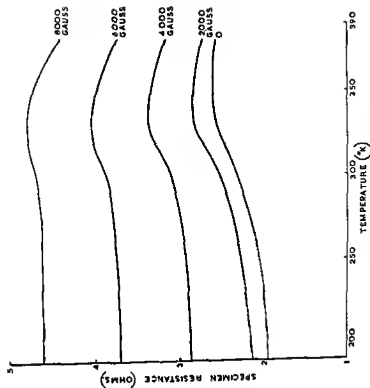

Fig 7 Variation of resistance with temperature and magnetic field for indium arsenide square plate

Fig 6. Transverse magneto resistance in indium arsenide.

However. the plates can be made small and a number connected in series to give a resistance of between 10 and 20 ohms occupying an area of about 1 sq. cm. An ingenious method of doing this has been described by Welker [25] in which a long plate of semiconductor is effectively divided into a number of short, wide specimens by means of evaporated silver strips ; essentially the strips serve to short-circuit the Hall voltage and thus increase the magnetoresistive effect.

A number of possible applications have been discussed by Willardson and Beer.[26] These include voltage and current regulators, rectifiers and a contactless potentiometer. Ross and Saker [27] have described a magnetoresistive displacement gauge using two small indium antimonide plates moving differentially in a strong magnetic field gradient ; with this arrangement a movement of 1 micron was easily detected. A similar sensitivity has been obtained with indium arsenide magnetoresistive elements made in this laboratory.

Acknowledgments

Thanks are due to many of our colleagues for assistance with the measurements and to Dr. R. W. Sillars for much valuable criticism and advice. The authors wish to thank Sir Willis Jackson, F.R.S., Director of Research and Education, Metropolitan-Vickers Electrical Co. Ltd., for permission to publish.

References

1. Pearson, G. L. *Rev. sci. Instrum.* **19**, 263 (1948).
2. Barlow, H. E. M. *Proc. Instn elect. Engrs* B **102**, 186 (1955).
3. Barlow, H. E. M. and Stephenson, L. M. *Proc. Instn elect. Engrs* B **103**, 110 (1956).
4. Keister, G. L. *Control Engng* p. 94 (November 1955).
5. Mason, W. P., Hewitt, W. H. and Wick, R. F. *J. appl. Phys.* **24**, 166 (1953).
6. Welker, H. *Physica, Eindhoven* **20**, 893 (1954).
7. Iandelli, A. *Gazz. chim. ital.* **71**, 58 (1941).
8. Oswald, F. *Z. Naturf.* **10a**, 927 (1955).
9. Folberg, O. G., Madelung, O. and Weiss, H. *Z. Naturf.* **9a**, 954 (1954).
10. Antell, G. R., Chasmar, R. P., Champness, C. H. and Cohen, E. *Phys. Soc. Meeting on Semi-Conductors*, p. 99 (1956).
11. Harman, T. C., Goering, H. L. and Beer, A. C. *Phys. Rev.* **104**, 1562 (1956).
12. Schillman, B. *Z. Naturf.* **11a**, 463 (1956).
13. Seraphin, B. *Z. Naturf.* **9a**, 450 (1954).
14. Stern, F. and Talley, R. M. *Phys. Rev.* **100**, 1638 (1955).
15. Chasmar, R. P. and Stratton, R. *Phys. Rev.* **102**, 1686 (1956).
16. Saker, E. W., Cunnell, F. A. and Edmond, J. T. *Brit. J. appl. Phys.* **6**, 217 (1955).
17. Wick, R. F. *J. appl. Phys.* **25**, 741 (1954).
18. Kuhrt, F. *Siemens-Z.* **28**, 370 (1954).
19. Hartel, W. *Siemens-Z.* **28**, 376 (1954).
20. Champness, C. H. M.Sc. Thesis, University of London (May 1957).
21. Weiss, H. *Z. Naturf.* **12a**, 80 (1957).
22. Champness, C. H. and Chasmar, R. P. *J. Electronics* **3**, 494 (1957).

23. Weiss, H. and Welker, H. *Z. Phys.* **138**, 322 (1954).
24. Raimer, P., Strutt, M. J. O. and Von Willisen, F. K. *Archiv elektr. Übertr.* **11**, 1 (1957).
25. Welker, H. *Electrotech. Z. A.* **76**, 513 (1955).
26. Willardson, R. K. and Beer, A. C. *Elect. Mfg* **57**, 79 (1956).
27. Ross, I. M. and Saker, E. W. *Nature, Lond.* **175**, 1196 (1956).
28. Lofgren, L. *Proc. int. Anal. Compt. Meeting*, Brussels (1955).

Infra-Red Faraday Effect Due to Conduction Electrons in Indium Antimonide

S. D. SMITH, T. S. MOSS

Ministry of Supply, Royal Aircraft Establishment Radio Department, Farnborough, Hants.

Introduction

A plane polarized wave passing through a material may be resolved into two circularly polarized waves with opposite directions of rotation. Under the influence of a magnetic field parallel to the radiation, one of the waves travels faster, and the other slower than in the absence of the field. The result of this is a rotation of the plane of polarization in the material, which is known as the Faraday effect.

When this effect is due only to free carriers, it in fact measures the dispersion due to cyclotron resonance absorption by these carriers. Mitchell (1955) suggested that measurement of Faraday effect would give a value for the effective mass of free carriers in a semiconductor, and we consider that such a measurement has accuracy comparable with a cyclotron resonance determination without the necessity of the stringent conditions required to observe this resonance. Mitchell [1] and Spitzer and Fan [2] point out that dispersion in general is independent of the collision time τ. Thus determination of effective mass from dispersion or Faraday effect measurements is independent of the scattering characteristics of the crystal.

The Faraday effect is preferable to a direct measurement of dispersion in that it is unaffected by lattice vibrational dispersion and can be used over a wide range of carrier concentrations. Thus, in indium antimonide, the change in effective mass as the conductive band is filled progressively can be studied. (See Moss,[9] Smith *et al.*[10])

The effect varies inversely as the square of the effective mass and is thus very large in InSb. It is possible to obtain a rotation of one revolution for 10,000 gauss, so that rotations of $\sim 45°$ as might be required in applications can be produced with fields $\sim$ 1000 gauss.

Theory

Consider free carriers of density N in a band characterized by an isotropic effective mass m. Let the plane polarized wave be split into circular components $Ee^{\pm i\omega t}$, with the wave travelling parallel to the magnetic induction B. The equations of motion will not contain a restoring force term, and the displacement s will be given by

$$md^2s/dt^2 + (m/\tau)ds/dt - ieBds/dt = eEe^{\pm i\omega t} \qquad (1)$$

where τ is the collision time.

The only useful solutions of this equation will be of the form

$$s = Se^{\pm \iota\omega t} \tag{2}$$

Substitution of (2) in (1) gives $S = \dfrac{Ee/m\omega}{-\omega \pm Be/m \pm \iota/\tau}$ (3)

which is the complex amplitude of the displacement

Now the complex dielectric constant is given by

$$(n - \iota k)^2 = \mathscr{E} + (Ne/\mathscr{E}_0)S/E \tag{4}$$

$$= \mathscr{E} + \frac{Ne^2/m\omega\mathscr{E}_0}{-\omega \pm Be/m \pm \iota/\tau}$$

Hence $$n^2 - k^2 = \epsilon - \frac{(Ne^2/m\omega\mathscr{E}_0)(\omega \pm Be/m)}{(\omega \pm Be/m)^2 + \iota/\tau^2} \tag{5}$$

and $$\sigma = 2nk\omega = \frac{Ne^2/m\tau\mathscr{E}_0}{(\omega \pm Be/m)^2 + \iota/\tau^2} \tag{6}$$

It should be noted that Eq (6) is the normal cyclotron resonance absorption equation so that Eq (5) gives the dispersion due to cyclotron resonance

If we assume that the absorption is small (so that $k^2 \ll n^2$) and that we are working at frequencies well above the cyclotron resonance frequency so that $(Be/m)^2 \ll \omega_0$ then

$$n_1^2 - n_2^2 = (Ne^2/m\mathscr{E}_0)\{2\ Be/m\omega(\omega^2 + 1/\tau^2)\} \tag{7}$$

Now $$\theta = \tfrac{1}{2}\omega(n_1 - n_2)/c = \omega(n_1^2 - n_2^2)/4nc \tag{8}$$

since the changes in n are small

Thus $$\theta = BNe^3/2nc\mathscr{E}_0 m^2(\omega^2 + 1/\tau^2) = NBe^3/2nc\mathscr{E}_0\omega^2 m^2 \tag{9}$$

at high frequencies where $\omega^2 \gg 1/\tau^2$

By use of this equation and measurement of B N n and ω we can determine the effective mass of the carriers The measurement is potentially accurate as the equation gives m^2 also since m is very small in InSb the rotation should be very large This equation has been derived previously by Mitchell (1955)

Alternatively θ can be related to the dispersion of the material To the same degree of approximation as is used above

$$n^2 = \mathscr{E} - Ne^2/m\mathscr{E}_0\omega^2$$

$$n\,dn/d\omega = Ne^2/m\mathscr{E}_0\omega^3$$

$$\theta = (Be/2m\ c)\omega\,dn/d\omega = (Be/2m\ c)\lambda\,dn/d\lambda \tag{10}$$

In this case measurement of N is eliminated and except for determining B the experiment is a purely optical one

It should be noted that neither Eq (9) nor (10) involve the collision time τ Thus the Faraday effect is independent of the scattering mechanism and it is not necessary to average over τ if it is energy dependent Spitzer and Fan [2] have pointed out that the same is true of the normal free carrier dispersion and that measurement of dispersion is thus superior to measurement of absorption

As the E k curve for the conduction band of InSb is not a simple parabola the effective mass will be energy dependent and will also vary with impurity content Any measurement involving transitions from one energy

level to another therefore gives an average over part of the band. In the Faraday effect, the measurements can be made with small fields and hence small values of $\hbar\omega_c$ are involved. However, the effective electrons will be distributed over a range of energies so that some average value over this range is obtained.

The Faraday effect due to electrons in a non-parabolic conduction band has been discussed by Lidiard and Stephen.[3] By considering the Boltzmann equation in the presence of a magnetic field they find that m^* in Eq. (9) above gives

$$m^* = \frac{\hbar^2 (k)_F}{\left(\frac{\partial E}{\partial k}\right)_F}$$

where k_F is the value of k at the Fermi surface, for the case of degenerate electrons, assuming spherical energy surfaces. This is not identical with the usual expression from the curvature of the band $\left(\text{i.e. } m^* = \hbar^2 / \frac{\partial^2 E}{\partial k^2}\right)$, unless the band *is* parabolic.

When classical statistics apply it is necessary to assume a shape for the E–k curve, so that m^* can be expressed in terms of $E(k)$.

The absorption constant K is given by

$$K = (Ne^2/mcn\mathscr{E}_0)\tau/(1 + \omega^2\tau^2) \tag{11}$$

so from Eq. (9)

$$\theta/K = Be\tau/m = \mu B \tag{12}$$

The ratio of Faraday rotation to absorption constant is thus independent of frequency and depends on the Hall angle.

For a specimen of thickness t, the maximum product of rotation and transmittance occurs when

$$Kt = 1$$

i.e. for an absorption of $e : 1$.

The rotation then is

$$\theta t = \mu BKt = \mu B \tag{13}$$

The Faraday effect at long wavelengths (i.e. radio frequencies) has been studied by Rau and Caspari.[4] However, since the rotation is then independent of m but involves τ, this experiment is not comparable with the present work.

Experimental Details

Since the Faraday rotation depends upon the square of the wavelength and since there is dispersion due to the intrinsic absorption across the forbidden gap at wavelengths near the absorption edge (Moss, Smith and Hawkins),[5] it is desirable to measure the rotation at wavelengths greater than 15μ.

Polarizers suitable for such wavelengths were constructed from stacks of polythene sheets, each approximately 8 μ thick, inclined at the Brewster angle. Twelve sheets were used in each pile and a polarization of over 90 per cent. was obtained. Beyond 15 μ polythene shows good transparency at least as far as 40 μ and probably further. At shorter wavelengths pronounced absorption bands are found, but the polarizers may be used at

selected points between the bands At visible wavelengths the polarizing stacks scatter significantly and images formed by rays passing through the polarizers show poor definition However for wavelengths 10 or more times greater than in the visible the scattering is greatly reduced and it was found that the image definition improved markedly The crossed position of the polarizers was found by continuously rotating the analyzer through the minimum and recording the signal on a chart with the magnetic field in one direction The field was then reversed the procedure repeated, and the rotation was found by the shift on the chart required to bring the two tracks into coincidence

An electro magnet with pole pieces of elliptical cross section was used to provide a uniform field which was usually at 50° to the direction of the radiation so that the specific rotation was given by $\theta/tB \cos 50°$, where t is the thickness When the highest fields obtainable from the magnet are required the specimen may be placed perpendicularly to the field at some angle ψ to the radiation Due to the high refractive index of indium antimonide the radiation will then be refracted such that it passes almost normally through the specimen (i e parallel to the magnetic field) and a correction has to be applied to the measured angle because of different reflection coefficients R_s R_p of rays polarized in and perpendicular to the plane of incidence as follows

$$\theta = \tan^{-1}\left\{\left(\frac{1 - R_p}{1 - R_s}\right)^{\frac{1}{2}} \tan\theta\right\}$$

where θ' is the apparent rotation

Convenient thickness of specimens were 890 μ for intrinsic InSb which had $n_i = 1\ 8 \times 10^{16}\text{cm}^{-3}$ at 24° C and 130μ for n type material with $n = 7 \times 10^{17}\text{cm}^{-3}$ Thicknesses were measured with a dial gauge to better than 2 per cent

Wavelength dependence was measured from 10–22 μ for pure material and from 6 5–19 μ for n type material In the case of the intrinsic material the number of carriers was sensitive to the temperature to the extent of ~2 per cent per °C The rotation was therefore measured at a given wave length and field as a function of temperature from 18° C to 30° C and small corrections made to the field and wavelength dependence determinations to reduce all values to 24° C A stream of air blown past the specimen ensured that its temperature was primarily determined by forced convection and that equilibrium conditions were rapidly established No such corrections were necessary for the n type material

Experimental Results

1 *Intrinsic InSb with $N = 1\ 8 \times 10^{16}\text{cm}^{-3}$ at 24° C*

The wavelength dependence of specific rotation for a field of 4230 gauss at 24° C is shown in Fig 1

Since
$$n\theta = \frac{BNe^3}{8m^{*2}\pi^2c^3\mathcal{E}_0}\ \lambda^2$$

a plot of $n\theta$ cf λ^2 reveals how well the theory is satisfied and this is shown in Fig 2 Values of n were taken from a previous determination of dispersion

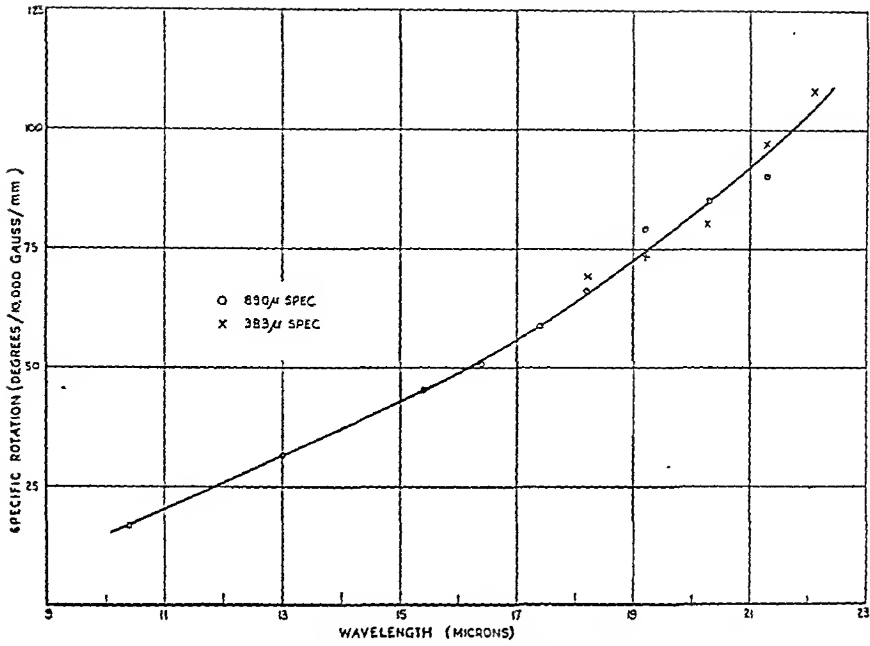

Fig. 1. Wavelength dependence of Faraday effect in pure InSb at 24° C. $N = 1{\cdot}8 \times 10^{16}$ cm^{-3}.

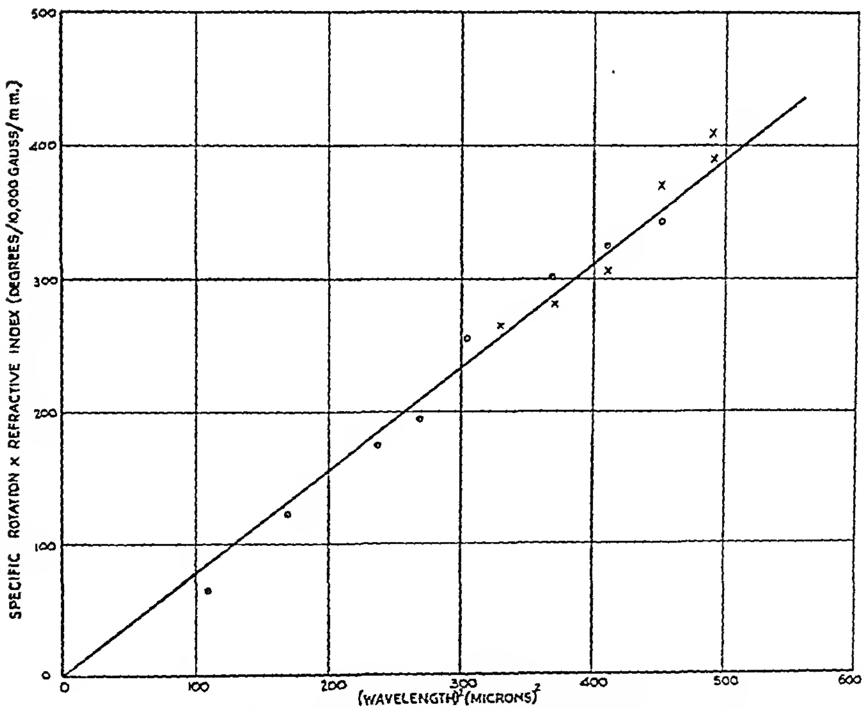

Fig. 2. Wavelength dependence of Faraday effect in intrinsic InSb. $N = 1{\cdot}8 \times 10^{16}$ cm^{-3}.

Fig 3 Magnetic field dependence of Faraday effect in intrinsic and n type InSb ($N = 1\ 8 \times 10^{16}$ cm^{-3}, $N = 6\ 4 \times 10^{17}$ cm^{-3})

Fig 4 Wavelength dependence of Faraday effect in n type InSb $N = 6\ 4 \times 10^{17}$ cm^{-3}

in this material (Moss, Smith and Hawkins),[5] and n changes by only 2 per cent. throughout the region considered. It was also shown that free carrier effects are only dominant beyond 15 μ and consequently the straight line in Fig. 2 is biased in favour of the points at larger wavelengths. The field dependence, given by curve A of Fig. 3, again shows good linearity.

The slope of $n\theta$ against λ^2 in Fig. 2 gives $\dfrac{BNe^3}{8m^{*2}\pi^2c^3\varepsilon_0} = 13{\cdot}6 \times 10^{12}$ radians per m^3 whence $m^* = 0{\cdot}018(5)$ m.

2. *n-type InSb with* $N = 6{\cdot}5 \times 10^{17}$ cm^{-3}

The wavelength variation in this material is shown in Fig. 4. The rotation is sufficiently large in this case to be measured down to wavelengths near the absorption edge (i.e. near 6 μ). The plot of $n\theta$ cf. λ^2 is shown in Fig. 5—in this case there is a marked variation in n with wavelength and values were obtained by making a very small correction to a determination of Spitzer and Fan [2] of the refractive index for material with $6{\cdot}2 \times 10^{17}$ cm^{-3}. The dispersion obtained agreed well with an interfermetric determination of *relative* dispersion made on our own material. The λ^2 dependence was again satisfied, as was the linearity with magnetic field (Fig. 2, curve B).

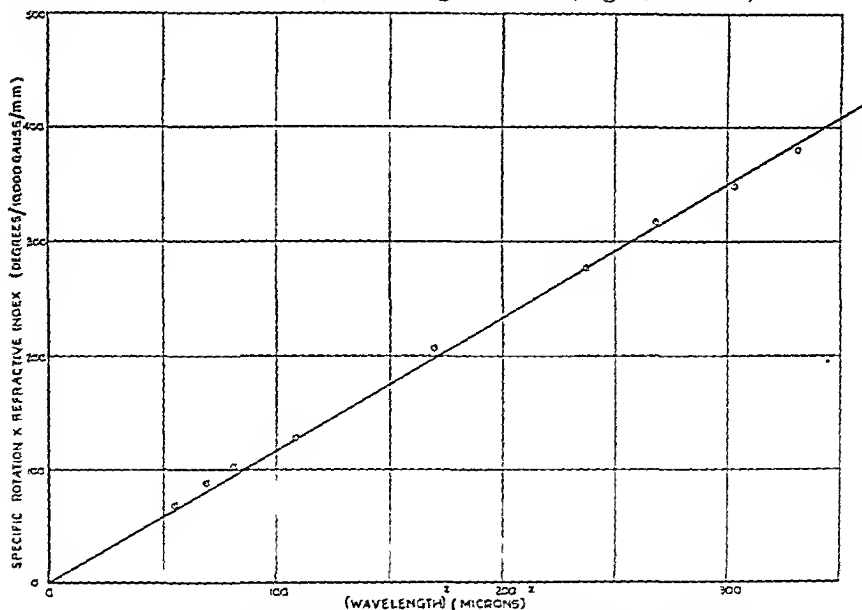

Fig. 5. Wavelength dependence of Faraday effect in n-type InSb. $N = 6{\cdot}4 \times 10^{17}$ cm^{-3}.

From the slope of $n\theta$ against λ^2 we have.

$$m^* = 0{\cdot}028 \text{ m}.$$

The effective mass in this material was also determined from dispersion data, using Eq. (10). At $\lambda = 16{\cdot}37\,\mu$, which was the wavelength used for the measurement of Fig. 2B, the specific rotation is $1{\cdot}66 \times 10^4$ radians/m/weber m^{-2}, and our measured value for the dispersion is $\lambda dn/d\lambda = 1{\cdot}69$; hence $m^* = 0{\cdot}030$ m. The two determinations of m^* are thus in good agreement.

More recent results are given by Moss[9] and Smith *et al.*[10]

DISCUSSION

The experimental results show that accurate measurement of Faraday effect may be made with carrier concentrations varying by a factor of at least 30 That this range may be extended to lower concentrations has been shown by preliminary measurements at liquid air temperatures when the electron concentration in our material is $1\ 84 \times 10^{15}$ cm $^{-3}$ The concentration may be extended upwards by making thinner specimens

At the highest concentrations measured $6\ 5 \times 10^{17}$ cm $^{-3}$, the value of effective mass obtained (0 028 m) agrees well with that of Spitzer and Fan[2] from direct dispersion measurements (0 029 m) and I R pulsed field cyclotron resonance values by Keyes *et al*[7] The Faraday effect determination should be more accurate than the dispersion measurements because of the square root dependence of m^* on n, N and θ

At intrinsic concentrations ($1\ 8 \times 10^{16}$ cm^{-3} at 24° C) the free carrier contribution to the dispersion is less than the contribution of the Restrahlen band at 20 μ (Moss Smith and Hawkins)[5] (Thus the direct dispersion measurement which does not discriminate against vibrational dispersion, cannot be used) However the band to band absorption still contributes a negligible amount to the dispersion The value of effective mass obtained (0 018) should be reliable and has been measured with small magnetic fields (< 5000 gauss) This mass is somewhat higher than the value of 0 015 m found by Burstein Picus and Gebbie[6] by infra red cyclotron resonance with a field of the order of 50 kilogauss The number of carriers in the conduction band was comparable in the two experiments

The measurements at 90° K suggest that with the band containing only one tenth of the number of electrons present at room temperature there is a significant fall in mass towards the value obtained by Dresselhaus *et al*[8] of 0 013 m for microwave cyclotron resonance

The experimental observation that the λ^2 dependence and the linear magnetic field dependence is well satisfied justifies the theory employed to analyse the measured Faraday rotation However in interpreting the effective mass in terms of the non parabolic energy band a further extension of the theory is required for the case of non degenerate electrons

The large rotation obtained with moderate fields shows that the Faraday effect may have practical application as a high frequency modulator or chopper, on infra red radiation

ACKNOWLEDGMENTS

Thanks are due to Dr D G Avery for assistance in supplying indium antimonide, to Dr K W Taylor and Miss D Webber for assistance in the measurements and to Dr E W J Mitchell for helpful discussion

REFERENCES

1 Mitchell, E W J *Proc phys Soc Lond* **B 68** 973 (1955)
2 Spitzer, W G and Fan, H Y *Phys Rev* **106,** 882 (1957)
3 Lidiard, A B and Stephen M J *J Phys Chem Solids* **9,** 43 (1959)
4 Rau, R R and Caspari M *Phys Rev* **100,** 632 (1955)

5. Moss, T. S., Smith, S. D. and Hawkins, T. D. H. *Proc. phys. Soc. Lond.* B **70**, 776 (1957).
6. Burstein, E., Picus, G. S. and Gebbie, H. A. *Phys. Rev.* **103**, 825 (1956).
7. Keyes, R. J., Zwerdling, S., Foner, S., Kolm, H. H. and Lax, B. *Phys. Rev.* **104**, 1804 (1956).
8. Dresselhaus, G., Kip, A. F., Kittel, C. and Wagoner, G. *Phys. Rev.* **98**, 556 (1955).
9. Moss, T. S. "Optical Properties of Semiconductors," Butterworths, London; Academic Press, New York (1959).
10. Smith, S. D., Moss, T. S. and Taylor, K. W. *J. Phys. Chem. Solids* **11**, 131 (1959).

L'Effet Magnetothermoelectrique dans l'Antimoniure d'Indium

M RODOT

Laboratoire du Magnétisme et de Physique du Corps Solide Bellevue (Seine et Oise)

DIVERS effets de transport dans l antimoniure d indium ont ete largement etudies notamment la conductivite et l effet Hall l effet Seebeck la con ductivite thermique la magnetoresistance Il ressort de ces etudes que les electrons ont dans ce corps une tres grande mobilite et une faible masse efficace et que le rapport $b = \mu_n/\mu_p$ des mobilites des electrons et des trous est grand de l ordre de 50

Des travaux anterieurs il ressort aussi que le mecanisme predominant de dispersion des electrons dans InSb est incertain Il a ete releve en effet que l hypothese classique selon laquelle la mobilite des electrons est limitee par les chocs avec les vibrations acoustiques du reseau conduit a un desaccord [1] entre la théorie et l experience si l on adopte pour masse efficace la valeur $m_n = 0\ 013\ m_0$ fournie par la methode de mesure la plus directe la resonance de cyclotron

Le present travail a pour but de lever cette incertitude par l etude d un autre effet de transport l effet magnetothermoelectrique (M T E) qui est defini par l alteration de l effet Seebeck par un champ magnétique transversal L effet M T E des électrons libres qu on peut prevoir important vu la valeur élevee de μ_n doit fournir des indications sur le mécanisme de dispersion predominant [2] L étude a ete menee de façon à mettre en évidence la presence eventuelle d un effet ambipolaire effet du a la presence simultanee d electrons et de trous libres

1 CHOIX DES ÉCHANTILLONS ET METHODES MESURE

Comme la bande de conduction de l antimoniure ndium presente la symetrie spherique on doit s attendre a ne pas trouver de difference de comportement notable entre des monocristaux et des polycristaux a purete et mobilite égales Ce fait a ete vérifie et des echantillons des deux categories ont ete utilises Leur purete est determinee au moyen de leur constante de Hall R_{H_s} à 77° K dans un fort champ magnetique (6000 gauss) la difference des nombres de donneurs et d accepteurs est $N_d - N_a = n_s = -1/eR_{H_s}$

Des mesures d effet Hall et de conductivité electrique fournissent en fonction de la température la mobilite de Hall $\mu_H = R_H/\rho$

Le tableau 1 resume les caracteristiques des echantillons etudies

Pour la mesure des effets thermomagnétiques on a utilise un mani pulateur represente sur la Fig 1 L echantillon F est place entre deux plaques de cuivre A et B dont l une est en contact thermique etroit avec une grosse e loppe de cuivre E jouant le role de reservoir thermique et l autre

TABLEAU 1

Ech.	A 77° K: R_s (cm³/A.s)	A 77° K: $n_s = N_d - N_a$ (cm⁻³)	T (°K)	η	$s = n/p$	μ_H (10³cm²/V.s)	$\Delta Q(0)/H^2$ (10⁻¹²V/g².°)	$B(0)$ (10⁻⁹V/g.°)	$\Delta Q(0)/y^2$ (10⁻⁶V/°)	$B(0)H/y$ (10⁻⁶V/°)	r_{calc} (équ. 20c.)
SX	− 26	+ 2·4 . 10¹⁷	203	+ 4·20		20		− 4·0		− 20	+ 0·29
			303	+ 2·84		18		− 2·1		− 12	+ 0·12
HXβ	− 45	+ 1·4 . 10¹⁷									
OXβ	− 54	+ 1·2 . 10¹⁷	203	+ 2·64		29	+ 1·10	− 1·6	+ 13	− 5·5	+ 0·05
			303	+ 1·42	194	33	+ 0·45	− 5·6	+ 4·1	− 17	+ 0·08
R'X	− 87	+ 7·2 . 10¹⁶	203	+ 1·71		22	+ 0·80	− 3·1	+ 16·5	− 14	+ 0·08
			303	+ 0·63		14	+ 0·92	− 5·4	+ 19	− 39·5	+ 0·09
C6	− 320	+ 1·9 . 10¹⁶	203	− 0·10		117					
			303	− 0·55		86					
IXδ	− 6900	9·1 . 10¹⁴	205	− 3·14		98					
			267	− 2·08		77					
FXα	+ 1850	− 3·4 . 10¹⁵	303			76					
DXα	+ 1040	− 6·0 . 10¹⁵	303	− 1·72	0·61	78	+ 0·90	− 12·5			
M24α* / M24β*	+ 270	− 2·3 . 10¹⁶									
JXα	+ 170	− 3·7 . 10¹⁶									
M32*	+ 81	− 7·7 . 10¹⁵	303	− 3·41	0·022		+ 4·40	− 28·5			
M38*	+ 40	− 1·6 . 10¹⁷	203			$\mu_p = 1·4$					

* Monocristaux.

est ısolee et chauffee par une resistance electrique Le tout est place dans un Dewar et peut etre porte à une temperature moyenne variable par une resistance R Des thermocouples mesurent la temperature en a et b Le champ magnetique H (100 a 7000 gauss) est fourni par un electro aimant

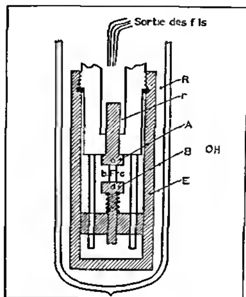

FIG 1

muni d un arbre à cames qui permet de realiser automatiquement le cycle $H > 0$ $H = 0$ $H < 0$ $H = 0$ Quatre fils sont soudes en a b c d et les tensions ab et cd ainsi que les temperatures sont enregistrées sur un potentiometre M E C I de construction speciale où l on peut mesurer simultanément des tensions inferieures au millivolt à 5 μV pres et des tensions plus elevées avec une précision plus faible Soit en fonction de la temperature (de 77 a 330° K) soit en fonction du champ magnétique on enregistre simultanement l effet Seebeck et les effets Nernst et M T E pour ces derniers effets on prend la moyenne des lectures pour $H > 0$ et $H < 0$

Nous avons vérifie que les mesures sont faites dans des conditions iso thermes ' c est a dire que l appareillage est tel que la difference des tem peratures en c et d est nulle ($<$ 1/50° pour une difference de 60° entre T_a et T_b)

Le signe de l effet Nernst est determiné par comparaison avec celui de l effet Hall en appliquant simultanément en a et b une difference de tem pérature et une difference de potentiel electrique Nous avons adopté la convention de signe suivante le champ magnetique etant dirigé suivant 0_z et le gradient de temperature dT/dx suivant $0x$ le coefficient de Nernst est défini par

$$B = + \frac{E_y}{H dT/dx}$$

2. Résultats Expérimentaux

La Fig. 2 représente l'effet M.T.E. en fonction de la température pour $H = 3000$ gauss. Les échantillons de type p (courbes pleines) présentent un maximum aigu de l'effet, témoignant qu'il s'agit là de l'effet " ambipolaire " ; les échantillons de type n (courbes en pointillé) ont un effet dépendant peu de la température, qui est l'effet propre des seuls électrons.

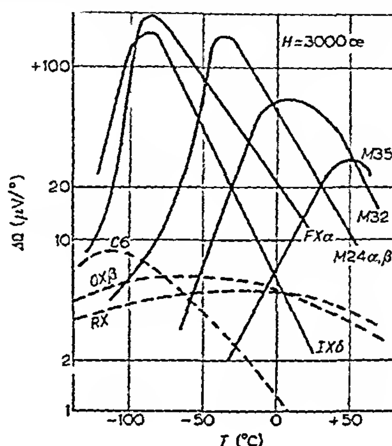

Fig. 2.

Le maximum de l'effet ambipolaire se déplace vers les températures élevées et décroît quand l'échantillon devient plus impur ; quand le champ magnétique varie il reste à une température à peu près constante (Fig. 3).

En fonction du champ magnétique à une température déterminée, l'effet M.T.E. $\triangle Q$ commence par croître paraboliquement, pendant que le co-

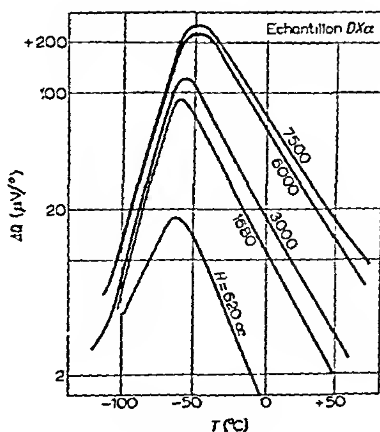

Fig. 3.

efficient de Nernst B varie peu (Fig. 4). Aux champs plus élevés, $\triangle Q/H^2$ et B diminuent (Figs. 5 et 6), et $\triangle Q$ tend vers une limite $\triangle Q(\infty)$, pendant que B tend vers zéro. La saturation de $\triangle Q$ est rarement atteinte aux champs inférieurs à 7000 gauss. Elle est plus vite atteinte aux basses températures.

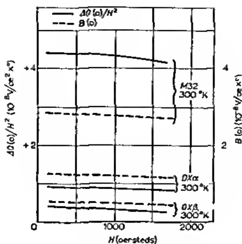

FIG 4

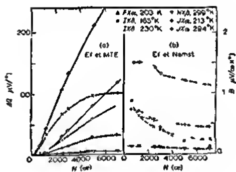

FIG 5

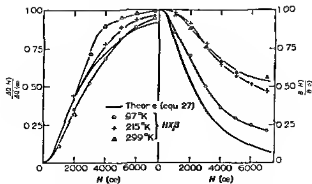

FIG. 6

Il faut souligner le fait que dans tous les échantillons et à toute température, $\triangle Q$ est positif et B est négatif, qu'il s'agisse de l'effet " simple " ou de l'effet " ambipolaire ".

3. Théorie des Effets Thermomagnétiques

(A) Résolution de l'équation de Boltzmann

Considérons un cristal d'antimoniure d'indium contenant un seul type de porteurs de charge, soit des électrons. Le gaz d'électrons est fréquemment dégénéré ; nous emploierons comme fonction de distribution à l'équilibre la fonction de Fermi-Dirac :

$$f_0(\epsilon) = \frac{1}{1 + e^{(\epsilon - \zeta)/kT}} \equiv \frac{1}{1 + e^{x - \eta}} \qquad (1)$$

où ζ est le niveau de Fermi et ϵ l'énergie de l'électron comptés vers les énergies positives à partie du bas de la bande de conduction.

Le nombre d'électrons libres dépend par ailleurs du nombre de niveaux dans la bande de conduction. Posons :

$$F_i(\eta) = \int_0^\infty \frac{x^i dx}{1 + e^{x - \eta}} \qquad (2)$$

Si la bande de conduction a la forme " standard " que nous appellerons parabolique :

$$\epsilon = \frac{\hbar^2 k^2}{2m_n} \ (k = \text{vecteur d'onde}) \qquad (3)$$

le nombre d'électrons libres est :

$$n_p = -\frac{8\pi}{3h^3}(2m_n)^{3/2}\int_0^\infty \epsilon^{3/2}\frac{\partial f_0}{\partial \epsilon}d\epsilon = \frac{4\pi}{h^3}(2m_n kT)^{3/2} F_{1/2}(\eta) \qquad (4)$$

En fait, la bande de conduction dans InSb n'est pas parabolique [3] et il faut substituer à (3) et (4) :

$$\epsilon = \frac{\hbar^2 k^2}{2m_0} + \frac{1}{2}\left[\left(E^2_g + 2\hbar^2 k^2 E_g \frac{m_0 - m_n}{m_0 m_n}\right)^{1/2} - E_g\right] \qquad (3')$$

$$n = n_p\Bigg[1 + \frac{kT}{E_g^*}\left(\frac{5}{2} - 5\frac{m_n}{m_0}\right)\frac{F_{3/2}(\eta)}{F_{1/2}(\eta)} + \left(\frac{kT}{E_g^*}\right)^2\left(1 - 21\frac{m_n}{m_0}\right)\frac{F_{5/2}(\eta)}{F_{1/2}(\eta)} - 4\frac{m_n}{m_0}\left(\frac{kT}{E_g^*}\right)^3\frac{F_{7/2}(\eta)}{F_{1/2}(\eta)}\Bigg] \qquad (4')$$

où E^*_g diffère légèrement de la lacune d'énergie E_g en ce que sa dépendance avec T est dûe uniquement à la dilatation du réseau.

Nous aurons besoin de façon générale des intégrales du type $\int_0^\infty \epsilon^i dn$, que nous appellerons $< \epsilon^i >$, et qui s'écrivent respectivement, pour les bandes " parabolique " et " de Kane " :

$$< \epsilon^i >_p \equiv \int_0^\infty \epsilon^i dn_p = \frac{8\pi}{3h^3}(2m_n)^{3/2}(kT)^{i+3/2}(i + 3/2)F_{i+1/2}(\eta) \qquad (5)$$

$$< \epsilon^i > = \int_0^\infty \epsilon^i dn = < \epsilon^i >_p \left[1 + \frac{kT}{E_g^*}\left(\frac{5}{2} - 5\frac{m_n}{m_0}\right)\frac{F_{i+3/2}(\eta)}{F_{i+1/2}(\eta)} + \quad \right] \quad (5')$$

Les intégrales $F_i(\eta)$, dans les cas particuliers où la distribution est " classique " (distribution de Boltzmann) ou " métallique " (complètement dégénerée), s'écrivent

$$(i + 1)F_i(\eta) = \Gamma(i + 2)e^\eta \text{ (" classique ")} \quad (6)$$

$$(i + 1)F_i(\eta) = \eta^{i+1}\left(1 + \frac{i\pi^2}{6\eta^2} + \quad \right) \text{ (" métallique ")} \quad (7)$$

En présence de champs électriques **E** *et magnétiques* **H** *et de gradients thermiques* $\triangle T$ la distribution des électrons est perturbée Soit f la nouvelle fonction de distribution [4] L'équation exprimant que f est stationnaire, c'est à dire que le cristal est à l'état d'équilibre, est l'équation de Boltzmann

$$\frac{q}{\hbar}\left[E + \frac{1}{c} v_\wedge H\right]\nabla_k f + v \quad \nabla_r f = \left(\frac{\partial f}{\partial t}\right)_c \quad (8)$$

$\triangle_k f$ et $\triangle_r f$ sont les gradients de f dans l'espace des vecteurs d'onde et dans l'espace des coordonnées , $q = \pm e$ est la charge du porteur, v sa vitesse Le deuxième terme de (8) est la variation dans le temps de la fonction de distribution dûe aux collisions des électrons Il est courant de supposer qu'il existe un temps de relaxation τ c'est à dire que

$$\left(\frac{\partial f}{\partial t}\right)_c = -\frac{f - f_0}{\tau} \quad (9)$$

Souvent, de plus, τ est proportionnel à une puissance de ϵ

$$\tau = \tau_0 \epsilon^r \quad (10)$$

Ainsi $r = -1/2$ dans le cas de la dispersion par les phonons acoustiques , $r = +3/2$ dans le cas de la dispersion par les impuretés ionisées dans le cas de la dispersion par les phonons optiques, dite ' dispersion polaire ", (9) et (10) ne sont pas vérifiées mais (9) et (10) sont approximativement vérifiées pour les électrons de très faible ou de très grande énergie

$$\text{si } \epsilon \ll h\nu_l,\ r = 0\ , \quad \text{si } \epsilon \gg h\nu_l \quad r = +1/2$$

ν_l étant la fréquence des vibrations de nombre d'ondes nul

Nous supposons dans les sections 3a 3b 3c que (9) et (10) sont vérifiées

Pour résoudre l'équation de Boltzmann, on développe f au voisinage de f_0 sous la forme

$$f = f_0 - v \quad \varphi \frac{\partial f_0}{\partial \epsilon} \quad (11)$$

On trouve que φ a pour valeur

$$\varphi = \frac{\tau}{1 + (\alpha\tau H)^2}[P - \alpha\tau H_\wedge P] \qquad \left(\alpha = \frac{q}{mc}\right) \quad (12)$$

$$P = qE - T\nabla_r\left(\frac{\zeta}{T}\right) - \frac{\epsilon}{T}\nabla_r T \quad (13)$$

Il est alors possible de calculer la densité de courant $J = \frac{q}{4\pi^3}\int vf dk$ Exprimant que $J_x = J_y = 0$, et tenant compte de notre condition aux limites

$\partial T/\partial y = 0$, et de ce que, par définition :

$$Q = \frac{E_x - \frac{1}{q}\, d\zeta/dx}{dT/dx} \; ; \quad BH = \frac{E_y}{dT/dx} \tag{14}$$

nous obtenons pour l'effet Seebeck et l'effet Nernst les expressions suivantes :

$$\frac{q}{k} Q = \frac{1}{kT} \frac{\frac{K_2}{K_1} + \left(\frac{L_1}{K_1}\right)^2 \frac{L_2}{L_1}}{1 + \left(\frac{L_1}{K_1}\right)^2} - \eta \; ; \quad \frac{q}{k} BH = \frac{1}{kT} \frac{\frac{L_1}{K_1}\left(\frac{K_2}{K_1} - \frac{L_2}{L_1}\right)}{1 + \left(\frac{L_1}{K_1}\right)^2} \tag{15}$$

où :

$$\begin{cases} K_1 = \left\langle \dfrac{\tau}{1 + (\alpha\tau H)^2} \right\rangle \; ; \quad K_2 = \left\langle \dfrac{\tau\epsilon}{1 + (\alpha\tau H)^2} \right\rangle \\ L_1 = \left\langle \dfrac{\tau . \alpha\tau H}{1 + (\alpha\tau H)^2} \right\rangle \; ; \quad L_2 = \left\langle \dfrac{\tau . \alpha\tau H . \epsilon}{1 + (\alpha\tau H)^2} \right\rangle \end{cases} \tag{15bis}$$

(B) EFFETS THERMOMAGNÉTIQUES DUS AUX ÉLECTRONS LIBRES [5]

Il résulte des formules (14) que l'effet Seebeck pour $H = 0$ s'écrit :

$$\frac{q}{k} Q(0) = \frac{1}{kT} \frac{K_2(0)}{K_1(0)} - \eta = \frac{< \epsilon^{r+1} >}{< \epsilon^r >} - \eta \tag{16}$$

et l'effet M.T.E. $\triangle Q(H) = Q(H) - Q(0)$:

$$\frac{q}{k} \triangle(QH) = \frac{\frac{1}{kT}\left[\frac{K_2(H)}{K_1(H)} - \frac{K_2(0)}{K_1(0)}\right]}{1 + \left[\frac{L_1(H)}{K_1(H)}\right]^2} + \frac{\frac{1}{kT}\left[\frac{L_2(H)}{L_1(H)} - \frac{K_2(0)}{K_1(0)}\right]\left[\frac{L_1(H)}{K_1(H)}\right]^2}{1 + \left[\frac{L_1(H)}{K_1(H)}\right]^2} \equiv$$

$$\equiv \frac{q}{k} \triangle_1 Q(H) + \frac{q}{k} \triangle_2 Q(H)$$

Dans le cas des *champs magnétiques faibles*, les termes $\triangle_1 Q$ et $\triangle_2 Q$ s'écrivent :

$$\begin{cases} \dfrac{q}{k} \triangle_1 Q(0) = \dfrac{1}{kT}\left[\dfrac{K_2(H)}{K_1(H)} - \dfrac{K_2(0)}{K_1(0)}\right] = \dfrac{\alpha^2 H^2}{kT}\left(\dfrac{< \tau^3 >}{< \tau >} - \dfrac{< \tau^2 \epsilon >}{< \tau\epsilon >}\right) \\ \dfrac{q}{k} \triangle_2 Q(0) = \dfrac{1}{kT}\left[\dfrac{L_1(0)}{K_1(0)}\right]^2 \left[\dfrac{L_2(0)}{L_1(0)} - \dfrac{K_2(0)}{K_1(0)}\right] = \\ \qquad = \dfrac{\alpha^2 H^2}{kT}\left(\dfrac{< \tau^2 >}{< \tau >}\right)^2 \left(\dfrac{< \tau^2\epsilon >}{< \tau^2 >} - \dfrac{< \tau\epsilon >}{< \tau >}\right) \end{cases} \tag{17a}$$

et le coefficient de Nernst, d'après (14) :

$$\frac{q}{k} B(0)H = -\frac{\alpha H}{kT}\frac{< \tau^2 >}{< \tau >}\left(\frac{< \tau^2\epsilon >}{< \tau^2 >} - \frac{< \tau\epsilon >}{< \tau >}\right) \tag{17b}$$

Ainsi l'effet M.T.E. est parabolique et l'effet Nernst linéaire en H aux faibles champs, conformément à l'expérience.

Pour obtenir des résultats numériques relatifs à un échantillon donné, on calcule à chaque température son niveau de Fermi réduit η, en résolvant

l équation $n - p = n_s$ compte tenu de la structure exacte, non parabolique, de la bande de conduction Dans les formules (17) on fait $\tau = \tau_0 \epsilon^r$ et on calcule les integrales en y portant la valeur de η obtenue precedemment On peut voir qu on ne commet qu'une faible erreur en calculant les integrales $< \tau^i \epsilon^j >$ comme si la bande de conduction etait parabolique a condition d y introduire le niveau de Fermi exact Nous ecrirons les expressions ainsi obtenues pour un gaz d'*electrons* ($q = - e$) par application de la formule (5) ainsi que les resultats approchés obtenus dans les cas limites ' classique ' et ' metallique ", par application des formules (6) et (7) Nous exprimerons ici $\triangle Q$ et B en fonction, non de H, mais de

$$y = | a | H \frac{< \tau^2 >}{< \tau >} = \frac{\mu_H H}{c} \quad (\mu_H = \text{mobilite de Hall})$$

Dans le cas general degenere ou non dégenere

$$\left\{ \begin{aligned} & \frac{e}{k} \triangle_1 Q(0) = \\ & \qquad y^2 \frac{(5/2+3r)F_{3/2+3r}\,(3/2+r)F_{1/2+r} - (3/2+3r)F_{1/2+3r}\,(5/2+r)F_{3/2+r}}{(3/2+2r)^2\, F^2_{1/2+2r}} \\ & \frac{e}{k} \triangle_2 Q(0) = y^2 \left[\frac{(5/2 + r)F_{3/2+r}}{(3/2 + r)F_{1/2+r}} - \frac{(5/2 + 2r)F_{3/2+2r}}{(3/2 + 2r)F_{1/2+2r}} \right] \\ & \frac{e}{k} B(0)H = y \left[\frac{(5/2 + r)F_{3/2+r}}{(3/2 + r)F_{1/2+r}} - \frac{(5/2 + 2r)F_{3/2+2r}}{(3/2 + 2r)F_{1/2+2r}} \right] \end{aligned} \right. \tag{19}$$

Dans l'approximation ' métallique "

$$\left\{ \begin{aligned} & \text{(a)} \ \frac{e}{k} \triangle_1 Q_m(0) = \frac{\pi^2}{6\eta} 4ry^2 , \quad \frac{e}{k} \triangle_2 Q_m(0) = - \frac{\pi^2}{6\eta} 2ry^2 \\ & \text{(b)} \ \frac{e}{k} \triangle Q_m(0) = \pi^2 r y^2 / 3\eta \\ & \text{(c)} \ \frac{e}{k} B_m(0)H = - \pi^2 r y / 3\eta \end{aligned} \right. \tag{20}$$

Dans l approximation ' classique "

$$\left\{ \begin{aligned} & \text{(a)} \ \frac{e}{k} \triangle_1 Q_c(0) = y^2 \frac{\Gamma(7/2+3r)\,\Gamma(5/2+r) - \Gamma(5/2+3r)\,\Gamma(7/2+r)}{[\Gamma(5/2 + 2r)]^2} = y^2 \theta r , \\ & \qquad\qquad \frac{e}{k} \triangle_2 Q_c(0) = - y^2 r \\ & \text{(b)} \ \frac{e}{k} \triangle Q_c(0) = r y^2 (\theta - 1) \\ & \text{(c)} \ \frac{e}{k} B_c(0)H = - r y \end{aligned} \right. \tag{21}$$

ou $(\theta - 1)$ designe un nombre positif et faible, croissant avec $| r |$

Toutes ces formules montrent que $\triangle Q$ *est du signe de* r *et* B *du signe opposé* L'experience indique donc que $r > 0$ Les valeurs experimentales de $\triangle Q(0)/y^2$ et de $HB(0)/y$ sont portees sur le tableau I pour une serie d'echantillons de type n Ces deux nombres sont differents, comme le pre

voient les formules générales (19) ; ils seraient égaux seulement dans le cas d'un échantillon très dégénéré. On peut tirer un ordre de grandeur de r en utilisant la formule (20c) ; cette valeur $r_{\text{calc.}}$, portée dans le tableau I, est toujours voisine de 0·05 *a* 0·30 *quels que soient l'échantillon et la température*, et tend à augmenter avec η.

De ce résultat on peut conclure que *le mode de dispersion prédominant* ne peut être ni la dispersion par les phonons acoustiques, ni la dispersion par les impuretés ionisées ; c'est probablement la *dispersion " polaire "*.

Dans le cas des *champs magnétiques forts*, L_1/K_1 augmente avec H, et à la limite des champs infinis,

$$\begin{cases} B(\infty) = 0 \\ \dfrac{q}{k}\,\triangle Q(\infty) = \dfrac{1}{kT}\left[\dfrac{L_2(\infty)}{L_1(\infty)} - \dfrac{K_2(0)}{K_1(0)}\right] \end{cases} \tag{22}$$

$$\begin{cases} K_1(\infty) = \dfrac{1}{a^2H^2}\left\langle\dfrac{1}{\tau}\right\rangle ; \quad K_2(\infty) = \dfrac{1}{a^2H^2}\left\langle\dfrac{\epsilon}{\tau}\right\rangle \\ L_1(\infty) = \dfrac{1}{aH} < 1 > ; \quad L_2(\infty) = \dfrac{1}{aH} < \epsilon > \end{cases} \tag{23}$$

On obtient le résultat très simple, *indépendant du mode de dispersion* :

$$\frac{q}{k}\,Q(\infty) = \frac{5\;F_{3/2}(\eta)}{3\;F_{1/2}(\eta)} - \eta \tag{24}$$

Dans les cas limites étudiés,

$$\frac{e}{k}\,\triangle Q_m(\infty) = r\pi^2/3\eta \tag{25}$$

$$\frac{e}{k}\,\triangle Q_c(\infty) = r \tag{26}$$

Un rapprochement des formules (20) et (25) amène à écrire les formules suivantes :

$$\triangle Q(H) = \frac{y^2}{1+y^2}\,\triangle Q(\infty) ; \quad B(H) = \frac{1}{1+y^2}\,B(0) \tag{27}$$

$$\triangle Q(\infty) = -\,B(0)c/\mu_H \tag{27bis}$$

Ces formules, dont la première est assez bien vérifiée par l'expérience (Fig. 6), sont valables en toute rigueur seulement pour l'approximation métallique.

(c) EFFETS THERMOMAGNÉTIQUES AMBIPOLAIRES

Si les indices 1, 2 et 3 s'appliquent respectivement aux effets des électrons seuls, des trous seuls, et totaux, nous écrirons avec Chambers [6] :

$$\begin{cases} \varphi_3(1+t_3{}^2)Q_3 = \varphi_1[(1+t_1t_3)Q_1 + (t_1-t_3)B_1H] + \\ \qquad\qquad + \varphi_2[(1+t_2t_3)Q_2 + (t_2-t_3)B_2H] \\ \varphi_3(1+t_3{}^2)B_3H = \varphi_1[(1+t_1t_3)B_1H + (t_3-t_1)Q^2] + \\ \qquad\qquad + \varphi_2[(1+t_2t_3)B_2H + (t_3-t_2)Q_2] \end{cases} \tag{28}$$

où

$$t_1 = R_{H1}\sigma_1H = -\,y_1 ; \; t_2 = R_{H2}\sigma_2H = y_2 ; \; t_3 = R_{H3}\sigma_3H$$

$$\varphi_1 = \frac{\sigma_1}{1 + t_1^2}, \quad \varphi_2 = \frac{\sigma_2}{1 + t_2^2}, \quad \varphi_3 = \frac{\sigma_2}{1 + t_3^2}$$

$$\varphi_3 = \varphi_1 + \varphi_2, \quad \varphi_3 t_3 = \varphi_1 t_1 + \varphi_2 t_2$$

$\sigma =$ conductivité electrique

Ces formules, valables si les bandes de valence et de conduction sont independantes et isotropes sont employees en supposant en outre (1) H faible, c'est a dire $Q_2 = B_2 = 0$, (2) $V_1 = \frac{\sigma_1}{\sigma_1 + \sigma_2}$ n'est pas voisin de 1 ni de 0, (3) Q_1 et B_1 sont donnes par les formules " classiques " (21) et enfin (4) $r_1 = r_2 = r$ On obtient

$$\begin{cases} \triangle Q_3(0) = v_1 \triangle Q_1(0) + v_1(1 - v_1)\triangle Q_a(0) \\ B_3(0) = v_1 B_1(0) + v_1(1 - v_1)B_a(0) \end{cases} \tag{29}$$

les effets d'origine ambipolaire ayant la valeur

$$\begin{cases} \frac{e}{k}\triangle Q_a(0) = y_1^2\{(a_3 - v_1)(5 + 2r + \delta) + r[1 - a_3(\theta - 1)]\} \\ \frac{e}{k} B_a(0)H = -y_1[5 + 2r + \delta - a_3 r] \end{cases} \tag{30}$$

Ici $\delta = E_g/kT$, $a_3 = \frac{\Gamma(5/2 + 3r)\Gamma(5/2)}{[\Gamma(5/2 + 2r)]^2}$ a_3 est voisin de 1 dans le cas où r est voisin de 0 Des formules (30) on peut conclure que *l'effet M T E ambipolaire est positif et l'effet Nernst ambipolaire est négatif*, conformément à l'expérience a cause du terme en $5 + \delta$ (nombre voisin de 12 à la tem perature ambiante) ces effets sont importants Le facteur $v_1(1 - v_1)$ des formules (29) rend compte de l'allure des courbes de la Fig 2 Enfin il est clair que ces effets *dépendent peu de r*, en particulier ils existent même si $r = 0$, contrairement aux effets des seuls électrons libres, ils s'ecrivent dans ce cas

$$\begin{cases} \triangle Q_a(0) = \frac{k}{e} y_1^2(1 - v_1)(5 + \delta) \\ B_a(0)H = -\frac{k}{e} y_1 (5 + \delta) \end{cases} \tag{31}$$

On peut tirer des résultats experimentaux une valeur de v_1 qui se trouve en accord avec la valeur $b \simeq 50$

(D) SUR L'ORIGINE DES EFFETS THERMOMAGNÉTIQUES DES ÉLECTRONS LIBRES DANS LE CAS DE InSb

Revenant au cas d'un echantillon de type n ne contenant que des électrons libres, observons que les effets thermomagnétiques, de même que les effets galvanomagnétiques magnetorésistance et variation de R_H avec H, sont dûs aux differences de mobilite des electrons d energie différente, ils sont nuls si $r = 0$, même si l'on tient compte complètement de la structure non parabolique de la bande de conduction

Dans le cas du mecanisme de dispersion polaire ces effets sont importants,

mais ne sont pas rigoureusement calculables au moyen de la théorie qui précède. On peut répartir les électrons en trois groupes selon leur énergie :

Si l'énergie est inférieure à $h\nu_l$, il n'existe pas de temps de relaxation, sauf si $\epsilon \simeq 0$.

Si l'énergie est juste supérieure à $h\nu_l$, il existe un temps de relaxation qui est une fonction très décroissante de ϵ.

Si l'énergie est largement supérieure à $h\sigma_l$, jusqu'à atteindre le niveau de Fermi, il existe un temps de relaxation qui est une fonction croissante de $\epsilon : \tau \sim \epsilon^{1/2}$.

Les effets thermomagnétiques des deux derniers groupes se compensent partiellement ; ceux du premier groupe ne sont pas calculables par la théorie précédente.

Conclusions

En conclusion, les résultats théoriques concordent bien, dans l'ensemble, avec les mesures présentées. Nous retiendrons le fait que *la mobilité des électrons dans l'antimoniure d'indium est limitée par les chocs avec les vibrations optiques du réseau.*

Références

1. Voir, pour la *conductivité électrique* : Ehrenreich, H. *J. Phys. Chem. Solids* **2**, 131–49 (1957), qui montre que les résultats expérimentaux s'accordent avec l'hypothèse de la dispersion par les phonons optiques ; pour l'*effet Seebeck* : Tauc, J. et Matyas, M. *Czechoslov. J. Phys.* **5**, 369 (1955) ; Weiss, H. *Z. Naturf.* **11a**, 131 (1956) ; Rodot, M., Duclos, P., Köver, F. et Rodot, H. *C.R. Acad. Sci., Paris.* **242**, 2522–5 (1956).
2. Rodot, M. *J. Phys. Radium* **19**, 2, 140–50 (1958).
3. Kane, E. O. *J. phys. Chem.* **1**, 249 (1957).
4. Le calcul de ce paragraphe suit celui de Blatt, dans " Solid State Physics," No. 4, p. 214, Academic Press Inc., New York (1957).
5. Nous négligeons dans la présente étude la variation de ζ avec H, c'est-à-dire les effets oscillatoires susceptibles de se produire aux basses températures, ainsi que la variation de τ avec H, qui peut également donner lieu à des effets particuliers aux basses températures ; nous excluons enfin l'effet Gurevitch, dont il n'a pas été trouvé de trace expérimentalement dans le domaine de température étudié.
6. Chambers. *Proc. phys. Soc. Lond.* **65**, 391A, 903 (1952). La convention que nous avons choisie pour le signe de B est l'opposée de celle de Chambers.

C21 KO 18713

Sur les Propriétés de Semi-Conducteurs Utilisables comme Thermoéléments

H. RODOT, H. BENEL

Laboratoire du Magnétisme et de Physique du Corps Solide, Bellevue (Seine-et-Oise)

Introduction

Afin de préparer des matériaux utilisables comme thermoéléments, nous avons étudié les différents moyens d'améliorer le rendement des corps déjà connus tels que le tellurure de bismuth et le tellurure d'antimoine.

Si l'on choisit $Z = \frac{\alpha^2 \sigma}{K}$, comme facteur de mérite d'un élément d'une substance donnée, où α = pouvoir thermoélectrique, σ = conductivité électrique, K = conductivité thermique, il s'agit d'imprimer des variations à ces différents facteurs afin d'augmenter Z.

Nous savons que pour de faibles concentrations d'impuretés, dans un semi-conducteur, il est possible de faire varier la conductivité électrique et le pouvoir thermoélectrique par addition d'atomes étrangers. Le nombre d'impuretés augmentant, σ croît, α passe par un maximum puis décroît, le produit $\alpha^2\sigma$ passe par un maximum[1]. Le dopage sera donc un moyen pour agir sur le produit $\alpha^2\sigma$ sans action sensible sur K, à condition de rester dans le domaine où la contribution électronique dans la conductivité thermique est inférieure à celle des phonons. Lorsque la conduction thermique par électrons est trop grande les modifications de σ et de K se compensent et le dopage entraîne une diminution de Z.

Une seconde méthode consiste à augmenter très fortement la concentration des impuretés, comme par exemple dans le cas des solutions solides; les impuretés représentent un obstacle additionnel pour les phonons, le libre parcours moyen des phonons diminue et la résistance thermique augmente. La longueur d'onde des électrons étant beaucoup plus grande que celle des phonons, ils sont moins sensibles à l'altération du réseau cristallin; les propriétés électroniques (α, σ) peuvent n'être que faiblement modifiées; le rapport $\frac{\sigma}{K}$ croît[2].

Deux voies sont donc favorables à l'amélioration des matériaux thermoélectriques: les dopages faibles et les additions massives d'impuretés, en particulier la formation de solutions solides.

Nous avons préparé tout d'abord les composés Bi_2Te_3 et Sb_2Te_3; nous avons recherché l'influence de différents agents dopants sur ces composés. Puis les solutions solides $Bi_2Te_3 - Sb_2Te_3$ ont été étudiées, et l'action d'impuretés sur ces solutions déterminée.

Pour connaître les caractéristiques des échantillons obtenus nous avons mesuré leur pouvoir thermoélectrique, leur résistivité électrique, leur con

ductivité thermique. Il a été fait en plus quelques mesures de pouvoir thermoélectrique à haute température.

Les fusions ont toutes été faites suivant le même procédé : une nacelle de graphite contenant les éléments composants est placée dans un tube de quartz sous atmosphère d'argon. Le chauffage est réalisé par haute fréquence. La fusion et le refroidissement sont faits très rapidement. Ce procédé a été adopté après différents contrôles qui montraient la reproductibilité des résultats. Nous avons aussi réalisé des fusions de zône sur Bi_2Te_3.

Les matières premières, antimoine et tellure, utilisées pour les deux composés, étaient purifiées par voie chimique dans nos laboratoires et présentaient une teneur, pour chaque impureté, inférieure à 10^{-6}.[3] Le bismuth était purifié par fusion de zône.

Étude sur le Tellurure de Bismuth

Par simple fusion des éléments tellure et bismuth, nous avons obtenu pour une proportion de 47·7% de tellure, un tellurure de bismuth de type p ($a = 177 \mu V/°$). Pour une proportion de 47·95% de tellure, nous avons obtenu un lingot de type n ($a = -150\, \mu V/°$).

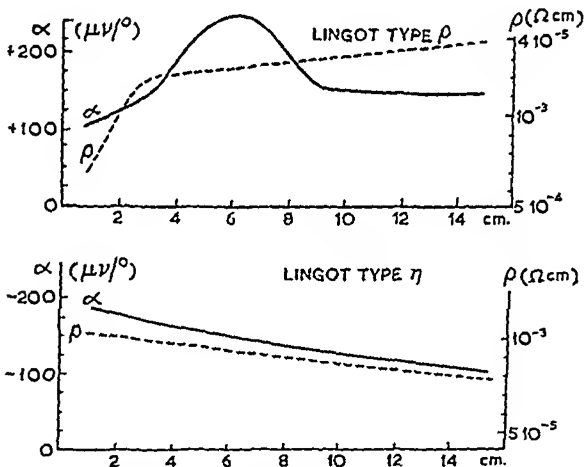

Fig. 1.

Sur des lingots de type p et de type n, de 17 cm. de longueur, après deux passes de fusion de zône, nous obtenons les répartitions des caractéristiques indiquées sur le Fig. 1.

Sachant que le tellure se comporte comme un donneur dans le tellurure de bismuth, nous avons étudié les variations du pouvoir thermoélectrique en fonction de la quantité de tellure introduite dans le lingot. Tenant compte de la perte de tellure inhérente à la technique employée, nous avons obtenu la courbe représentée sur la Fig. 2, en accord avec des résultats antérieurs.[4]

Ayant constaté que le lithium se comportait tantôt comme donneur tantôt comme accepteur dans le tellurure de bismuth, nous avons recherché

son influence sur ce composé en fonction de la teneur en tellure Les principaux resultats de cette etude ont ete portés sur la Fig 3 Les courbes A, B, C, D, representent les variations du pouvoir thermoélectrique en fonction de la teneur en lithium Chaque courbe représente les valeurs d'une serie

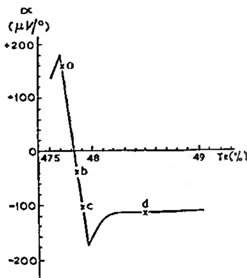

Fig 2

d'échantillons ayant la même teneur en tellure, correspondant respectivement aux points a, b, c, d, de la Fig 2, Nous n'entrerons pas ici dans le détail de l'etude publiee par ailleurs [5] Nous soulignerons seulement quelques résultats

Dans le cas des courbes A et B (Fig 3), representant l'action du lithium

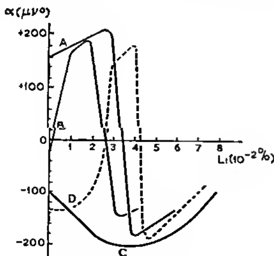

Fig 3

sur du tellurure de bismuth de faible teneur en tellure, le lithium semble d'abord être un accepteur (ce comportement s'accentuant avec la quantite de tellure), puis, à partir d'une certaine concentration, devient donneur Pour la courbe C il est toujours donneur (maximum—$200\mu V/°$) Enfin

sur la courbe D, l'influence du lithium est en apparence identique à celle des courbes A et B avec un décalage de 20 à 25 . 10^{-3} % dans la concentration en lithium.

Nous voyons que le comportement du lithium est déterminé par ses interactions avec le tellure. Ceci est dû aux formes de liaisons chimiques existant dans le réseau cristallin du tellurure de bismuth qui permettent au lithium de s'introduire en position intersticielle, soit entre deux couches atomiques faiblement liées, soit dans les couches atomiques fortement liées ; son rôle d'accepteur ou de donneur correspond respectivement à ces deux cas.

Quelques autres impuretés ont été étudiées. Le plomb s'est comporté comme un accepteur, faisant passer un lingot de tellurure de bismuth du type *n* au type *p*. Le magnésium (en faible proportion), l'iodure de zinc, l'iodure de cuivre, le chlorure d'iode, le bromure d'iode et le bromure de cuivre se sont comportés comme des donneurs, l'iodure de cuivre ayant donné les meilleurs résultats.

TABLEAU 1

Composition		α ($\mu V/°$)	ρ (Ω cm.)	K ($W/cm.°$)
Bi_2Te_3	stoechiom.	+ 190	2·3 . 10^{-3}	1·7 . 10^{-2}
Bi_2Te_3	+Te	− 172	1·1 . 10^{-3}	
Bi_2Te_3	+Li	+ 190	2 . 10^{-3}	
Bi_2Te_3	+Te +Li	− 200	2·2 . 10^{-3}	2·5 . 10^{-2}
Bi_2Te_3	++Te ++Li	− 160	1·25 . 10^{-3}	2·1 . 10^{-2}
Sb_2Te_3	stoechiom.	+ 83	4 . 10^{-4}	3·3 . 10^{-2}
Sb_2Te_3	+BrCu	+ 75	2 . 10^{-4}	
Sb_2Te_3—Bi_2Te_3	50/50	+ 140	8 . 10^{-4}	
Sb_2Te_3—Bi_2Te_3	70/30 +Li	+ 166	8 . 10^{-4}	
Sb_2Te_3—Bi_2Te_3	90/10 +I_2Zn	− 135	1 . 10^{-3}	
Sb_2Te_3—Bi_2Te_3	90/10 +I_2Cu	− 128	6 . 10^{-4}	

ÉTUDE SUR LE TELLURURE D'ANTIMOINE

Par simple fusion de l'antimoine et du tellure dans les proportions de 39% d'antimoine pour 61% de tellure, nous avons obtenu du Sb_2Te_3 ayant les caractéristiques suivantes : $\alpha = + 83\,\mu V/°$ et $\rho = 4 . 10^{-4}$ Ω.cm.

Afin d'obtenir des variations de $\alpha^2\sigma$ pour Sb_2Te_3, nous l'avons dopé avec du tellure, de l'antimoine, du bismuth ; α et ρ n'ont pratiquement pas subi de variation. Avec du cadmium, du lithium, du zinc, du magnésium, du plomb, de l'étain, le pouvoir thermoélectrique s'est trouvé réduit (30 à 50 μV/°), sans changement important dans la résistivité. Les halogénures, iodure de zinc, bromure de plomb, chlorure d'iode, bromure d'iode, bromure de cuivre, n'ont provoqué aucune variation appréciable de $\alpha^2\sigma$.

ÉTUDE DES SOLUTIONS SOLIDES TELLURURE DE BISMUTH-TELLURURE D'ANTIMOINE

Étant donné les structures isomorphes de Sb_2Te_3 et Bi_2Te_3 (rhomboédriques), les solutions solides possibles de ces deux composés nous ont

paru intéressantes à étudier Une etude métallographique a montré que ces solutions existaient dans tout le domaine de composition

Les résultats de la preparation des solutions solides ont été portes dans la Fig 4 La courbe I donne α en fonction des proportions de Bi_2Te_3 et Sb_2Te_3 la courbe II donne ρ On obtient des grandeurs intéressantes de $\alpha^2\sigma$ pour les solutions aux environs de 50% Bi_2Te_3 70% Bi_2Te_3 et 80% Bi_2Te_3

Comme on pouvait le prevoir la conductivite thermique des solutions solides est plus faible que celle des composants

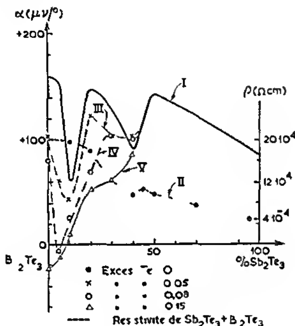

Fig 4

Une etude de l action du tellure sur les solutions solides a ete faite Les resultats portés sur la Fig 4 (courbes III IV V) ont montre que pour des teneurs de 100 a 60% de tellurure de bismuth l action du tellure va en décroissant jusqu a s annuler Au delà de 60% de Bi_2Te_3 elle est con stamment nulle

De meme en etudiant l action d halogenures sur des solutions solides nous avons constate la plus grande sensibilite aux agents dopants des solutions de teneur en tellurure de bismuth plus grande que 60% Par exemple la solution 90/10 $Bi_2Te_3 - Sb_2Te_3$ est devenue de type n pour divers halogenure (tableau I) Les resultats les plus caracteristiques ont *eté obtenus avec l iodure de zinc* le bromure d iode le chlorure d iode le bromure de plomb et l iodure de cuivre (Avec I_2Zn $\alpha = -135$ $\mu V/°$ $\rho - 1$ 10^{-3} Ω cm) Avec le chlorure d iode et le bromure d iode nous avons tout de meme obtenu un changement de signe du pouvoir thermo électrique de la solution 50/50 $Bi_2Te_3 - Sb_2Te_3$ (-27 5 μV ° et -44 4 μV /) (Fig 5)

Étude du Pouvoir Thermoélectrique en Fonction de la Température

Afin de déterminer la sensibilité de nos composés et solutions solides à la température, nous avons mesuré le pouvoir thermoélectrique de différents échantillons en faisant varier le température ambiante de 15 à 400° C.

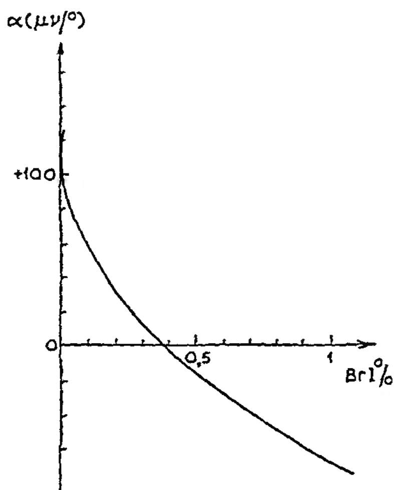

Fig. 5.

Les résultats obtenus ont été portés sur la Fig. 6. On voit qu'avec un accroissement de la température ambiante un échantillon de tellurure de bismuth voit son pouvoir thermoélectrique varier rapidement et passer de positif à négatif. Pour un échantillon de tellurure d'antimoine le pouvoir

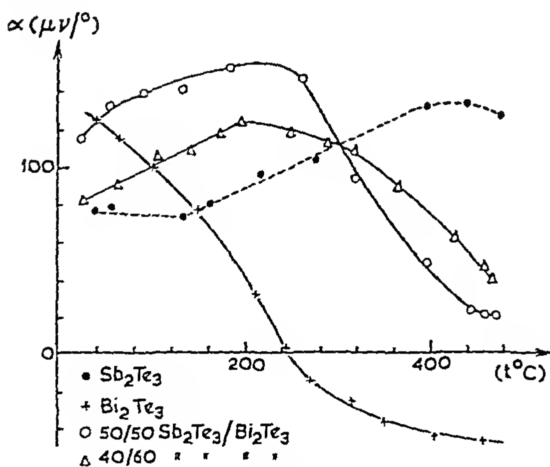

Fig. 6.

thermoélectrique croît avec la température. Les solutions solides présentent un comportement intermédiaire entre les deux composés ; leur pouvoir thermoélectrique croît, puis à partir d'une certaine température décroît.

Conclusion

Nous avons pu constater la possibilite de faire varier $\alpha^2\sigma$ dans le tellurure de bismuth par faible dopage avec diverses impuretes, sans action sur la conductivité thermique Les divers moyens d'incorporer des electrons ou des trous dans un compose pour l'amener a son facteur de merite maximum ne sont pas indifferents Certaines impuretes peuvent rendre la fabrication plus aisee

Le comportement electrique d'une impurete dépend essentiellement des liaisons chimiques, comme le montre notre etude du dopage de Bi_2Te_3 au lithium Il y a un interet evident à bien connaitre le reseau cristallin d'un corps pour faire varier ses proprietes d'une maniere contrôlable

Pour les solutions solides $Bi_2Te_3 - Sb_2Te_3$ nous avons obtenu des resultats previsibles, en particulier une faible conductivite thermique L'action des impuretés s'est revelee grande pour les solutions riches en tellurure de bismuth et presque nulle pour les solutions riches en tellurure d'antimoine Ceci est en rapport avec leur structure cristalline Nous pouvons conclure que ces solutions judicieusement dopees presentent un intérêt comme thermoelements

References

1 Price, P J *Phys Rev* 104, 1223 (1956)
2 Ioffe A F *J Phys Radium* 18, 4 14 (1957)
3 Duclos P Communication au Congres de Bruxelles (1958)
4 Vlasova, P M et Stilbans, L C *J tech Phys*, *Moscow* 25, 4 (1955)
5 Rodot, H *C R Acad Sci*, *Paris* 6 paraitre

Bismuth Telluride and its Thermoelectric Applications

D. A. WRIGHT

Communication from the Staff of the Research Laboratories of The General Electric Company Ltd., Wembley

1. Performance of Thermojunctions for Refrigeration

If current i is passed through a thermojunction made from materials a and b, with the hot junction at temperature T_1, the cold junction can be maintained at a lower temperature T_2 which depends on the properties of the materials used for the thermojunction, and on the heat input to the cold junction. If W is the rate of supply of energy to the circuit, then :

$$W = i^2R + i(\eta_a - \eta_b)(T_1 - T_2)$$

where R is the circuit resistance, η_a is the thermoelectric power of one component of the junction and η_b that of the other.

In equilibrium the rate of heat flow Q into the cold junction from external sources is equal to the rate of transfer from the junction. This is given by the Peltier term, less the heat flow to the cold junction from the Joule heating in the material and from the hot junction :

$$Q = T_2\, i(\eta_a - \eta_b) - \tfrac{1}{2}\, i^2R - K(T_1 - T_2)$$

K is the thermal conductance of the junction.

The " coefficient of performance " of the junction ϕ is defined as the ratio Q/W. To obtain the highest value of ϕ for a given junction material, it is necessary to relate the length, l and cross sections S of the two components of the junction :

$$l_aS_b/l_bS_a = (\lambda_a\sigma_a/\lambda_b\sigma_b)^{\frac{1}{2}}$$

where λ is the thermal and σ the electrical conductivity, and also to choose the optimum current i given by :

$$i_m = \frac{(\eta_a - \eta_b)\,(T_1 - T_2)}{(R\sqrt{1 + F^2\, T_m} - 1)}.$$

Here T_m is the mean temperature $\dfrac{T_1 + T_2}{2}$, and F is the " figure of merit " of the junction.

F has the value :

$$F = \frac{\eta_a - \eta_b}{(\lambda_a/\sigma_a)^{\frac{1}{2}} + (\lambda_b/\sigma_b)^{\frac{1}{2}}}.$$

When these conditions are satisfied, ϕ has its highest value $\phi_{\max}$ consistent with maintaining a temperature difference $T_1 - T_2$.

$$\phi_{\max} = \frac{T_2(1 + T_mF^2)^{\frac{1}{2}} - T_1}{(T_1 - T_2)[1 + (1 + T_mF^2)^{\frac{1}{2}}]}.$$

When ϕ_{max} becomes zero the particular junction is maintaining the maximum temperature difference of which it is capable Then

$$T_1/T_2 = (1 + T_m F^2)^{\frac{1}{2}},\ (T_1 - T_2)_{max} = \tfrac{1}{2}F^2 T_2^{\,2}$$

A plot of $T_1 - T_2$ against F is shown in Fig 1 for $T_1 - 300°$ K $= 27°$ C

2 The Use of Semiconductors

In the case of a semiconductor it is possible to 'dope' a material to give either n or p type conductivity by suitable control of the concentration of impurity If n and p type samples of one semiconductor have similar electrical conductivities i e $\sigma_a \approx \sigma_b$ then the thermal conductivities will be similar i e $\lambda_a \approx \lambda_b$ If in addition η_a is similar numerically to η_b i e $\eta_a \approx -\eta_a$ then the value of F becomes

$$F = \eta\sqrt{\sigma/\lambda}$$

If values are substituted for the three parameters η σ and λ taking the simplest semiconductor theory it can be shown [1] that there is an optimum value for the thermoelectric power near 200 μV/°C whatever the material

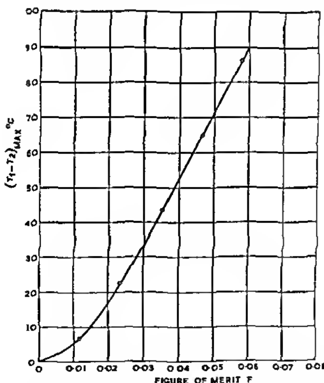

Fig 1 Relation between maximum temperature difference and figure of merit Hot junction at 300° K

More complex semiconductor models appropriate for practical materials, lead to similar conclusions the optimum value lying between 200 and 300 μV/°C in all cases Provided values of this order are chosen the value of F^2 is proportional to $\dfrac{\mu}{\lambda_0}\left(\dfrac{m^*}{m}\right)^{3/2} T^{3/2}$ Thus in comparing different materials

at a given temperature, a good performance requires a high value of $\frac{\mu}{\lambda_0}\left(\frac{m^*}{m}\right)^{3/2}$. Here μ is the mobility of electrons or holes, λ_0 is the lattice component of the thermal conductivity, m^* is the "effective mass" of electrons or holes, and m the mass of the free electron. The electron values apply to n-type materials, and the hole values to p-type. It is with these considerations in mind that special attention has been paid to lead telluride and bismuth telluride. since λ_0 decreases as atomic weight increases, and these two materials have the highest atomic weights of any known semiconductors. μ and m^* do not vary systematically through the periodic table, but it appears that few semiconductors have values of $\mu\left(\frac{m^*}{m}\right)^{3/2}$ greater than those for Bi_2Te_3 and PbTe, and that those which do have low atomic weights and high values of λ_0: they are not therefore, overall, as good as these two compounds.

3. Bismuth Telluride and its Alloys

Bismuth telluride Bi_2Te_3 can be prepared by melting the constituent elements and zone refining, so producing ingots in which the crystals are orientated with their cleavage planes aligned in the direction of zone refining. Single crystals can be prepared by directional freezing.

The crystal structure is rhombohedral, and there is ready cleavage along planes perpendicular to the axis of rotation. There is marked anisotropy in the electrical and thermal conductivities, and in the Hall effect and magnetoresistance. There is slight anisotropy also in the thermoelectric power and in the optical properties. The energy gap at 290° K is near 0·13 eV. The dielectric constant has a high value near 80,[2] with the result that impurity scattering is not appreciable over a wide temperature range. The mobility varies with temperature in the range 150–300° K according to the laws:

$$\mu \propto T^{-1\cdot 72} \text{ for electrons and}$$
$$\mu \propto T^{-1\cdot 94} \text{ for holes.}$$[3]

Stoichiometric proportions in the initial material give p-type crystals with resistivity near $2\cdot 10^{-3}$ ohm cm. for current flow in the direction of the cleavage planes, and near $5\cdot 10^{-3}$ for the perpendicular direction. Group II impurities raise the p-type conductivity. Group VII impurities, and certain others as well, lower the p-type conductivity and ultimately convert the material to n-type. By suitable adjustment of impurity concentration, the optimum thermoelectric power η near 200 μV/°C can be obtained for both n- and p-type material. The resistivity is then near 10^{-3} ohm cm. in each case,[3, 4] for current flow in the direction of the cleavage planes.

The value of λ the thermal conductivity is given by $\lambda_0 + \lambda_e$, where λ_0 is the lattice component and λ_e the component due to free electrons. λ_e has a value near $2 \,.\, (k/e)^2 \, T\sigma$, where k is Boltzmann's constant and e the electronic charge. At 300° K, λ_0 in the direction of the cleavage planes is 0·0157 watt cm.$^{-1}$ °C^{-1}, while for $\sigma = 10^3$ ohm^{-1}cm^{-1}, λ_e is about 0·004 watt cm^{-1}°C^{-1}.[4, 5] The value of F is therefore $\eta\sqrt{\sigma/\lambda} = 0\cdot 0445$. With a mean temperature of 290° K this corresponds with a maximum $(T_1 - T_2)$ of 65° C.

A coefficient of performance of unity can be achieved provided $(T_1 - T_2)$ is not greater than 22° C, as shown in Fig 3 below

The Hall mobility for bismuth telluride at 300° K is near 300 cm²volt⁻¹ sec⁻¹ for electrons and holes Assuming simple covalent lattice scattering the value of $\mu\left(\frac{m^*}{m}\right)^{3/2}$ deduced from σ and η is about 340 cm²volt⁻¹sec⁻¹ for

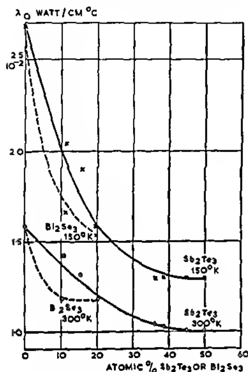

Fig 2 Lattice component of thermal conductivity as a function of antimony or selenium concentration in bismuth telluride

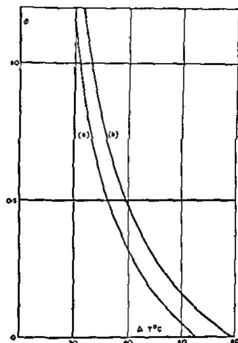

Fig 3 Coefficient of performance for refrigeration against temperature difference for thermocouples at a mean temperature of 290° K (a) Bi_2Te_3 (b) Alloy of Bi_2Te_3 with $F = 0.049$

electrons and 260 for holes Taking the scattering laws indicated by the way in which μ varies with temperature, the value of $\mu\left(\frac{m^*}{m}\right)^{3/2}$ is near 420 for both types of carrier [3] The interpretation of these values in terms of drift mobility and effective mass is not yet complete though clarification follows the study of magnetoresistance [6] this shows that a 6 valley model probably applies for the energy band structure, leading to a density of states mass about half that of the free electron

To obtain further improvement in performance, it is not possible at present to increase $\mu\left(\frac{m^*}{m}\right)^{3/2}$ by treatment or modification of the material It is possible however to lower λ_0 by substituting foreign elements in the lattice, and if this can be done without lowering $\mu\left(\frac{m^*}{m}\right)^{3/2}$, an advantage is obtained Elements from the same columns of the periodic table do give

this result, although in some cases the amount which can be used without lowering μ or m^* is restricted. Dr. Goldsmid in this laboratory has found that substitution of Sb for Bi lowers λ_0 to near 0·010 watt $cm^{-1}°C^{-1}$ at 50 atomic per cent., while substitution of *Se* for *Te* has a similar but smaller effect, as shown in Fig. 2.

It has not yet been possible at all compositions to obtain *n*- and *p*-type material with the required thermoelectric power, so that full advantage of $\lambda_0 = 0{\cdot}010$ cannot be taken for both *p*- and *n*-type material. The best junctions we have so far prepared have a value of F of 0·05, corresponding with a maximum $T_1 - T_2$ exceeding 80° C, when $T_m = 290°$ K.[7] The coefficient of performance ϕ with this material can exceed unity provided $(T_1 - T_2)$ is not greater than 26° C (Fig. 3).

4. Applications of Thermoelectric Cooling

With figures of merit of the order 0·05, many useful applications are possible. The coefficient of performance for a given temperature difference is still considerably below that of the compressor type of refrigerator, so that for cooling-powers exceeding about 100 watts, it is not yet clear how widespread the application of thermoelectric cooling will be ; its advantage lies in silence, in a very long expectation of life, and probably in reduced size of the cooling unit ; the scale of use for domestic refrigeration will depend on the relative cost, which is not yet established. However, there will clearly be special applications where the absence of moving parts offers an important advantage. For powers below about 100 watts the compressor type cannot be used, and applications in this range are likely to develop, for example, for dew-point hygrometry, and for cooling electronic equipment. Germanium diodes and triodes do not tolerate high operating temperatures, and it is possible to cool them thermoelectrically, either by mounting individual devices on a cooled junction, or by mounting an

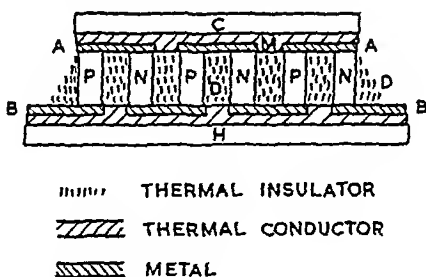

Fig. 4. Three junctions in series in one stage.

assembly in a cooled enclosure. Some types of infra-red detector require temperatures below normal ambient, and their cooling might also be done by this method. The cooling of a baffle in the throat of an oil diffusion pump improves the vacuum, and is conveniently done using a thermoelectric junction ; this is also relevant, though indirectly, to the electronic industry. It is possible, furthermore, to use thermoelectricity to maintain an enclosure at a constant temperature, using a control switch to reverse the current

through a set of thermojunctions this is useful for example to maintain constant temperature for crystal oscillators

The thermojunction elements are formed by slicing and cutting zone refined ingots to form small rectangular bars which can conveniently be 3 mm or more square and 5 to 10 mm long A simple junction between two such elements will operate at 5 10 amp to give the maximum coefficient of performance the power consumption will be of the order $\frac{1}{2} - 1$ watt and the cooling power of this order therefore for a temperature difference of about 25° C If larger cooling powers are required the sectional area can be increased or a number of junctions can be arranged electrically in series as in Fig 4

A greater temperature difference can be attained by using two sets of junctions thermally in series as in Fig 5 Here the cold face is cooled by the first stage of junctions and the second stage must have a larger cooling power

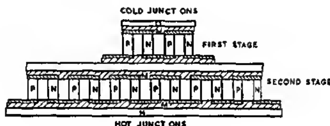

FIG 5 Two stage cool ng un t

since it must remove the heat generated in the first stage in addition to that incident upon it It can be shown that addition of yet a third stage results in no worthwhile improvement since the temperature drop between successive stages is not negligible and the further improvement in coefficient of performance is small

5 THERMOELECTRIC GENERATION

It may be noted that thermoelectric generators may be of value in the communication industry in connection particularly with supplies for radio equipment or for telephone repeater stations in remote areas Such units may be based on bismuth telluride or its alloys provided the hot junction temperature is not too high The heat can be provided by solid or liquid fuel or by solar energy

The thermoelectric power of a semiconductor mat rial should be 200/300 μV/degree as indicated above Improvement in material does not modify this figure but only the value of F and therefore of the efficiency available Thus whatever the material one thermocouple produces about 0 05 volts for 100° C temperature difference Only part of this approximately half of it can be used across the load Thus a large number of junctions in series is required for most practical applications

The efficiency for bismuth telluride and its alloys though higher than for other thermojunctions is not very high with $F = 0\ 04$ it is 3 per cent for a temperature difference of 100° C and with $F = 0\ 05$ it is 5 per cent This refers of course to the temperature difference maintained between the hot

and cold junctions, which is less than that between the surfaces used for heat exchange. Thus interest is restricted at present to special applications such as those mentioned.

References

1. Goldsmid, H. J. and Douglas, R. W. *Brit. J. appl. Phys.* 5, 386 (1954).
   Goldsmid, H. J. *J. Electronics.* 1, 218 (1955).
2. Austin, I. G. *Proc. phys. Soc. Lond.* 72, 545 (1958).
3. Goldsmid, H. J. *Proc. phys. Soc. Lond.* 71, 633 (1958).
4. Goldsmid, H. J., Sheard, A. R. and Wright, D. A. *Brit. J. appl. Phys.* 9, (1958).
5. Goldsmid, H. J. *Proc. phys. Soc. Lond.* B 69, 203 (1956) ; *Proc. phys. Soc. Lond.* 71, (1958).
6. Drabble, J. R. and Wolfe, R. *Proc. phys. Soc. Lond.* B 69, 1101 (1956).
   Drabble, J. R., Groves, R. D. and Wolfe, R. *Proc. phys. Soc. Lond.* 71, 430 (1958).
   Drabble, J. R. *Proc. phys. Soc. Lond*, 72, 380 (1958).
7. Wright, D. A. *Nature, Lond.* 181, 834 (1958).

Modern Applications of Hall Effect in Semiconductor Compounds

M J O STRUTT

Department of Advanced Electrical Engineering
Swiss Federal Institute of Technology Zurich

1 Introduction

In the semiconductor compounds indium antimonide (JnSb) and indium arsenide (JnAs) the Hall effect is much stronger than e g with germanium or silicon [10] Assuming a probe shaped as shown in Fig 1 with a magnetic field of flux density B (Weber/m²) perpendicular to its upper flat surface we obtain an open circuit Hall voltage between the points 3 and 4 of Fig 1

$$U_{h_0} = \frac{k_h}{h} f\left(\frac{l}{b}\right) IB \qquad (1)$$

In this formula k_h is the Hall coefficient h is the thickness of the probe (see Fig 1) f is a function of the ratio of length l to width b of the probe

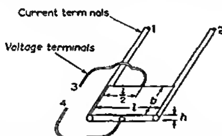

Fig 1 Shape of Hall probe The contacts 1 and 2 carry the current I through the probe The contacts 3 and 4 are the Hall contacts Between them the Hall voltage U_h arises The magnetic field of flux density B is perpendicular to the upper surface of the probe

(see Fig 1) I is the current in amperes through the contacts 1 and 2 of Fig 1 The function f is zero for l zero and attains the value unity for l/b about 2 5 For larger values of this ratio f stays unity [5]

With the JnSb probes under consideration k_h is about $0\,25\;10^{-3}$ m³/Coulomb and with the JnAs probes k_h is about half this value As we shall show experimentally these values stay constant if the current I or the magnetic flux or both alternate at frequencies up to about 10 mc/sec

With JnSb the Hall voltage U_{h_0} according to Eq (1) is dependent on temperature according to Fig 2 [8] The resistance of the Hall probe of Fig 1 between the contacts 1 and 2 is indicated by r_i This resistance r_i is dependent on temperature according to Fig 3 [8] Similarly the resistance

r_h of the Hall probe of Fig. 1 between the contacts 3 and 4 is also dependent on temperature, the curve being similar to Fig. 3. The resistances r_i and r_h of the Hall probe are also dependent on magnetic flux density B at constant values of the current I and of the temperature. This is called the C.F. Gauss

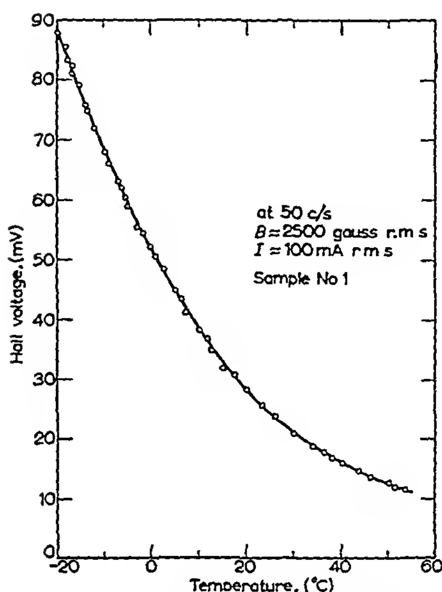

FIG. 2. Open circuit Hall voltage (vertical scale) at a magnetic flux density of 2·5 kilogauss = 0 25 Weber/m² effective value at a frequency of 50 c/s and an A C. I of 0 1 A effective value at a frequency of also 50 c/s as dependent on temperature in degrees centigrade (horizontal scale).

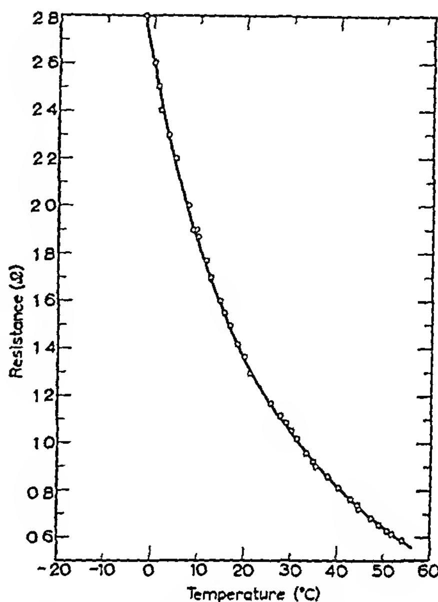

FIG. 3. Resistance r_i between the contacts 1 and 2 of the Hall probe of Fig. 1 (JnSb) (vertical scale, ohms) as dependent on temperature in degrees centigrade (horizontal scale).

effect. The Gauss effect is shown in Fig. 4 for different shapes of the Hall probe.[10]

Measurements have shown, that the Hall contacts 3 and 4 of Fig. 1 may be displaced to the immediate vicinity of the current contacts (see Fig. 5), without alteration of the Hall voltage (see Fig. 6).[8]

2. Multiphase Hall Wattmeters

It has been shown that the Hall probes according to Figs. 1 and 5 may be applied to obtain wattmeters, measuring the real power, or the imaginary power, or the apparent power, going into a consumer.[3]

A simple arrangement, suitable for measuring the imaginary power of a single phase A.C. consumer Z is shown in Fig. 7. According to this arrangement, we have (see Eq. (1)):

$$I = k_I I_{max} \sin(\omega t + \varphi)$$

$$B = k_U U_{max} \sin\left(\omega t + \frac{\pi}{2}\right)$$

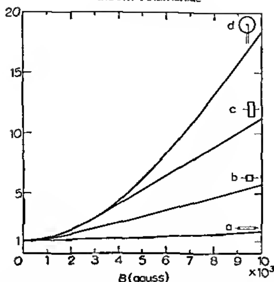

FIG 4 *Ratio of resistance (vertical scale) between the current contacts of* Hall probes of different shapes (shown at the right side) to its value at flux density zero as dependent on flux density expressed in kilogauss (horizontal scale)

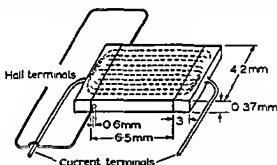

FIG 5 Hall probe, with Hall contacts adjacent to one of the current contacts This arrangement is used in multiphase Hall wattmeters

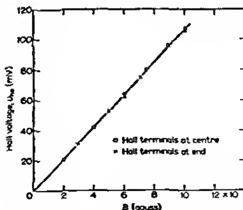

FIG 6 Open circuit Hall voltage (vertical scale) of Hall probe of Fig 5 as dependent on magnetic flux density (horizontal scale) at a current of 0 1 A The circles pertain to an arrangement of the Hall contacts according to Fig 1 The crosses pertain to an arrangement of the Hall contacts according to Fig 5

Here the coefficient k_I is determined by the shunt Sh. and the resistance r of Fig. 7, whilst k_U is determined by the coil and corresponding core of Fig. 7. Obviously, according to Eq. (1), we have :

$$U_{h_0} = \frac{1}{2}\frac{k_h}{h} f\, k_I k_U I_{\max} U_{\max} \cos\left(\varphi - \frac{\pi}{2}\right) - \\ - \frac{1}{2}\frac{k_h}{h} f\, k_I k_U I_{\max} U_{\max} \cos\left(2\omega t + \varphi + \frac{\pi}{2}\right)$$

The D.C. part of U_{h_0} is proportional to the imaginary power consumed in the impedance Z of Fig. 7.

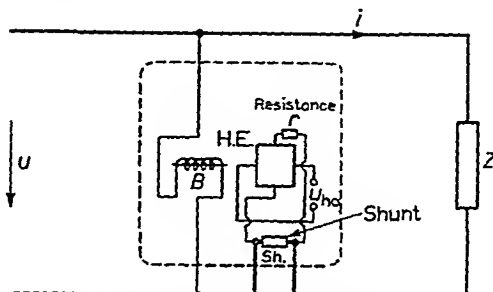

FIG. 7. Wattmeter arrangement, using a Hall element H.E., the current of which is supplied by the shunt Sh. in conjunction with the series resistance r. It is proportional to the single phase current i. The magnetic flux density B is supplied by the tension u between the single-phase conductors.

If we invert the current I through the Hall element and its magnetic flux density B, we obtain a Hall wattmeter suitable for measuring the real power consumed in the impedance Z of Fig. 7. In this case, the terminals of the shunt Sh. of Fig. 7 must be connected to the coil, causing the flux density B. The two terminals on the power line must be connected to the current contacts of the Hall probe (see Fig. 1) via the resistance r of suitable value. We have then :

$$I = k'_U U_{\max} \sin \omega t \,;$$

$$B = k'_I I_{\max} \sin (\omega t + \varphi)$$

Hence :

$$U_{h_0} = \frac{1}{2}\frac{k_h}{h} f\, k'_I k'_U I_{\max} U_{\max} \cos\varphi - \frac{1}{2}\frac{k_h}{h} f\, k'_I k'_U I_{\max} U_{\max} \cos(2\omega t + \phi)$$

Obviously, the D.C. component of U_{h_0} is proportional to the real power, consumed by the impedance Z. For this connection, measuring the real power, reference is made to Fig. 9, pertaining to a three-phase system.[8]

It is also possible to build a Hall wattmeter, measuring the apparent power consumed in the impedance Z of Fig. 7.[8] An appropriate arrangement is shown in Fig. 8, which may be considered as self-explanatory.

If we try to apply the arrangement of Fig. 7, or its inverse (for measuring the real power) to a multiphase power system, we run into trouble. One difficulty is that considerable A.C. voltages arise between the Hall contacts of the Hall probes to be used. By these A.C. voltages, considerable currents would arise, destroying the Hall probes. A simple method of avoiding

this difficulty is shown in Fig. 9 Here, three Hall elements (H.E.) are used, with which Hall contacts are arranged according to Fig 5. Hereby, the above A C. voltages are reduced to almost zero The D C components of the

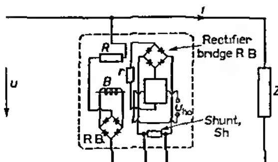

FIG 8 Wattmeter arrangement, suitable for measuring the apparent power (i e product of peak current and peak voltage), consumed by the impedance Z Two separate rectifiers are used to supply the flux density B and the current I respectively of the Hall element H E

Hall voltages of the three Hall elements are connected in series Their sum is proportional to the real three phase power, consumed in the three load impedances Z_a, Z_b and Z_c *Another method of avoiding the said* difficulty consists in the application of suitable transformers, by which the

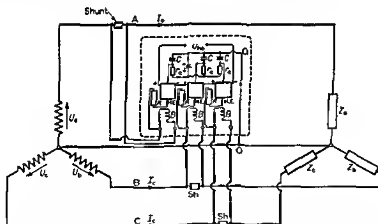

FIG 9 Hall wattmeter suitable for measuring the real power consumed in the impedances Z_a, Z_b and Z_c of a three phase system One of the current contacts of each of the three Hall elements H E is connected to earth (zero point) via a suitable large condenser C The three resistances r_c are required, if the condensers C are of electrolytic type, in order to *apply a polarizing voltage to their terminals* The series resistances R and the corresponding condensers C *must satisfy the relationship* $R \gg 1/\omega C$, or $\omega RC \gg 1$ This relation warrants, that the A C through the Hall elements is in phase with the corresponding phase voltages of the three phase system

current I and the flux density B of the Hall elements are supplied These transformers must, of course, be devoid of spurious phase angles A Hall wattmeter *according to* Fig. 9 has been actually built and tested Its performance was satisfactory.[8]

3. Temperature Compensation

The temperature dependence of the open-circuit Hall voltage according to Fig. 2 is detrimental to the performance of Hall wattmeters, if not compensated. The open-circuit Hall voltage may be made nearly independent of temperature at a constant magnetic flux density by using the temperature dependence of r_t, according to Fig. 3 as a means of compensation. The current I through the Hall element must rise at rising temperature in a way, which makes U_{h_0} independent of temperature. An appropriate circuit is shown in Fig. 10. The current i_R of Fig. 10 is divided into a current i_s through the Hall element H.E. and a current i_{r_t} through the auxiliary resistance r_t. This resistance r_t is slightly dependent on temperature

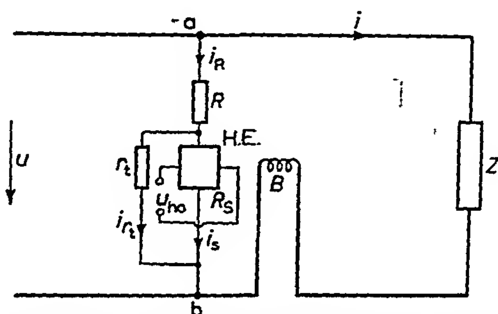

Fig. 10. Practical circuit for the compensation of the temperature dependence of the open circuit Hall voltage U_{h_0}. A suitable shunt resistance r_t is connected in parallel to the Hall element H.E.

according to a precalculated curve. In a practical case, the resistance r_t was composed of a manganin wire of 0·0875 ohms (see curve 3 of Fig. 11). It is possible, by using suitable series combinations for the resistance r_t of Fig. 10, to obtain a Hall voltage curve, independent of temperature in a considerable range within 0·5 per cent. (curve 5 of Fig. 11).[8]

Obviously, this temperature compensation at a definite flux density B is upset, as soon as this flux density is altered. For such an alteration, by the Gauss effect of Fig. 4, alters the resistance R_s of Fig. 10 between the current contacts of the Hall element H.E. The compensation is based on the particular value of R_s at room temperature, corresponding to the flux density under consideration. It is possible, however, to avoid this upsetting of the above temperature compensation. According to Fig. 4, the variation of R_s with flux density is small, if the ratio l/b of the Hall probe is large. Thus, Hall probes of considerable length l compared to the width b (see Fig. 1) are favourable for the temperature compensation in question. We may use a supplementary bias D.C. flux density of fixed value (e.g. 2·5 kilogauss), on which the flux density caused by the current i of Fig. 10 is superimposed. As long as the superimposed alternating flux density is small with respect to the fixed D.C. flux density (e.g. caused by a suitable permanent magnet), the resistance R_s of Fig. 10 will be very nearly constant at constant temperature and current i_s at varying flux densities. The remaining relatively small variations of R_s with flux density will in this case have no influence on the D.C. component of the Hall voltage of the Hall element

in question. Hence, in this way the temperature compensation may be applied quite correctly.

The internal resistance r_h between the Hall contacts varies with temperature in a similar way as the resistance between the current contacts of the Hall element (see Fig. 3). This temperature variation of r_h prohibits

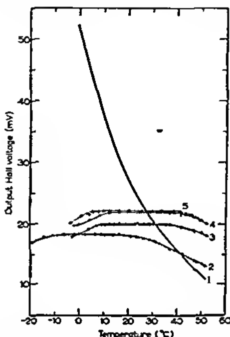

Fig. 11. Resulting temperature-compensated curves of the open-circuit Hall voltage U_{h_0}. This is shown on the vertical scale as dependent on temperature in degrees centigrade (horizontal scale). Curve 1. un compensated (see Fig. 2). Curve 2: at a current i_R of Fig. 10 of 0.5 A at a flux density B of 2.5 kilogauss. The shunt r_t of Fig. 10 was a manganin wire of 0.157 ohms in this case. Curve 3. at a current i_R of 0.8 A and r_t was a manganin wire of 0.0875 ohms. Curve 4: at a current i_R of 0.7 A and r_t a nickel wire of 0.116 ohms at 20° C. grade. Curve 5: at a current i_R of 0.7 A and r_t consisting of a nickel wire of 0.103 ohms at 20° C. in series with a manganin wire of 0.029 ohms. The flux density is the same for all curves (2.5 kilogauss).

the full use of the D.C. available power at the Hall contacts of the Hall element. Assuming the outer load on these contacts to be r, we obtain a Hall voltage at these terminals:

$$U_h = U_{h_0} \frac{r}{r + r_h} = \frac{U_{h_0}}{\dfrac{r_h}{r} + 1}$$

The power, consumed in the Hall-circuit load resistance r is:

$$P_h = \frac{P_{h_0}}{\dfrac{1}{2} + \dfrac{1}{4}\dfrac{r_h}{r} + \dfrac{1}{4}\dfrac{r}{r_h}}$$

where P_{h_0} is the available power at the Hall contacts:

$$P_{h_0} = \frac{U_{h_0}^2}{4 r_h}$$

Obviously, if $U_h \approx U_{h0}$, we have $r \gg r_h$ and in this case the load power P_h is a very small fraction of the available Hall power P_{h0}. This condition must be adhered to in order to avoid the upsetting of the temperature compensation of U_{h0} by the temperature dependence of r_h. The result is that only very small effective load powers P_h may be obtained, being mostly in the microwatt range. In order to apply the Hall voltage as a means of regulation of power systems, much larger powers, of the order of milliwatts at least, should be available. This may be achieved by means of suitable power amplifiers. We have made effective use of an appropriate magnetic amplifier, affording linear power amplification of about 2000 times.[8]

4. Hall Effect Oscillators

A simplified picture of a Hall effect oscillator is shown in Fig. 12.[9] The open-circuit Hall voltage U_q between the Hall contacts 5 and 6 of Fig. 12,

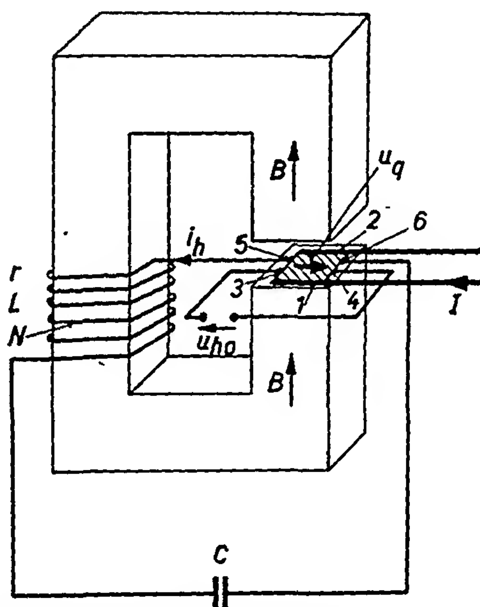

Fig. 12. The Hall probe bears the current contacts 1 and 2, through which the D.C. supply current I flows. The Hall contacts 5 and 6 are connected to the feed back coil of N turns, having a resistance r and an inductance L. Through this coil flows the Hall current i_h. A pair of subsidiary Hall contacts 3 and 4 generate the open-circuit Hall voltage U_{h0}. The condenser C is connected in series with the feed-back coil. The ferrite core causes a magnetic flux of density B perpendicular to the paths of the currents I and i_h.

as well as between the contacts 3 and 4 is given by Eq. (1). If the remanent flux density of the ferrite core is B_m, the flux density in the air gap of width g is approximately

$$B = \frac{\mu_0}{g} i_h N + B_m \tag{2}$$

where the relative permeability μ_r of the core material is assumed to be

large compared with unity and μ_0 is the vacuum permeability The current i_h is given by

$$i_h = \frac{U_q}{r + r_h} \tag{3}$$

Insertion of the value of Eq (2) into Eq (1) and of the resulting value of U_q into Eq (3) yields

$$U_q = \frac{k_h}{h} f B_m I + \frac{\mu_0 k_h}{gh} f I N i_h$$

or

$$U_q = \frac{k_h}{h} f B_m I (1 - KI)^{-1}$$

where the feed back factor K is

$$K = \frac{\mu_0 k_h}{gh} f \frac{N}{r + r_h} \tag{4}$$

Obviously, if KI is unity, a Hall voltage U_q may be obtained at a zero value of the remanent flux density B_m This means that oscillations may start in this case In a practical case, the value of K was 1 75 (ampere)$^{-1}$

It may be shown that oscillations build up if $KI > 1$ and this process continues until KI reduces to unity The reduction of K has several causes, such as increase of r and r_h by rising temperature, additional losses in the core, mismatch The build up of oscillations occurs according to

$$U_q = U_m \cos(\omega t + \varphi) \exp\left[-\frac{t}{2T}(1 - KI)\right] \tag{5}$$

Here, T is equal to $L/(r + r_h)$ i e the time constant for the circuit The angular frequency is given by

$$\omega^2 = \frac{1}{LC} - \left(\frac{1 - KI}{2T}\right)^2$$

At $KI = 1$, we obtain $\omega^2 = 1/LC$, which corresponds to the stationary case

In Fig 13 some experimental build up curves corresponding to Eq (5) are shown [9] The calculated values for the exponents are in satisfactory agreement with experimental values of Fig 13 The decline of the stationary values of oscillatory voltages after reaching a peak value is due to the heating up of the circuit and of the Hall probe The values of u_{h_0} were obtained at the contacts 3 and 4 of Fig 12

The peak levels of the oscillatory voltages in Fig 13 are determined by the saturation flux densities of the ferrite core under consideration This may be checked by discussion of the curves of Fig 14 These curves show saturation at a definite value of the supply current I for each curve Disconnecting the coil N of Fig 12 from its Hall contacts, the magnetic hysteresis loop of the core was projected on an oscilloscope screen One pair of oscilloscope plates was connected to the contacts 3 and 4 of the Hall probe (see Fig 12), whereas the other pair was connected to an A C voltage, proportional to the A C through the coil N of Fig 12 Using one of the frequencies of Fig 14, the hysteresis loop showed saturation at exactly the U_{h_0} value, corresponding to Fig 14

We have investigated experimentally the efficiency of the Hall effect

oscillator.[9] In doing so at 20° C. and 60 c/s, at a supply current I of 1·0 A, the optimal output power at the contacts 3 and 4 of Fig. 12 was obtained, by connecting these contacts to 3 ohms. The Hall oscillator was self-oscillating according to Fig. 14. The power, dissipated in the said resistance

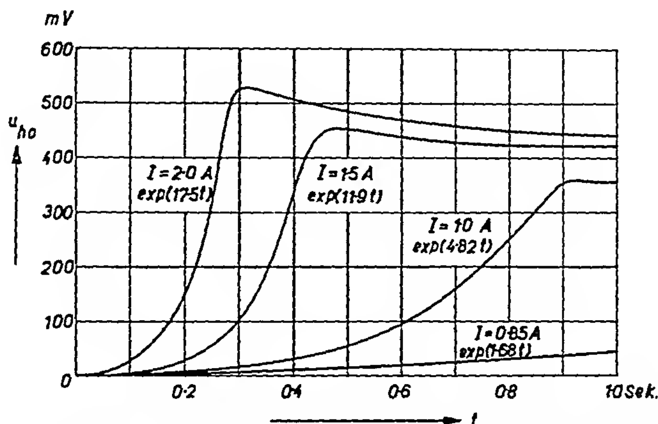

Fig. 13. Effective value of U_{h_0} (see Fig. 12) (vertical scale) as dependent on time t in seconds (horizontal scale) at room temperature, drawn from oscilloscope screen pictures at different values of the supply current I (see Fig. 12). The exponents correspond to Eq. (5). These experimental values are in satisfactory agreement with calculated values from Eq. (5) for the set-up in question.

was 12 mW (see point 1 of Fig. 14). The supply power corresponding to the supply current I was 810 mW. The Hall probe, between the contacts 1 and 2 of Fig. 12, dissipated a power of 756 mW. Hence, only 54 mW (the difference of the above values) is available for the oscillations. The output

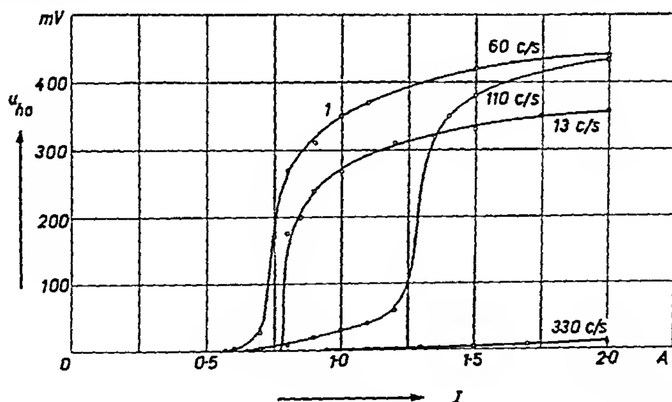

Fig. 14. Vertical scale: Effective value of Hall voltage U_{h_0} of Fig. 12 (see Hall contacts 3 and 4) at different frequencies as indicated at the curves as dependent on supply D.C. I (horizontal scale).

power being 12 mW, the efficiency is 12/54 = 0·22. The power, dissipated in the Hall probe (756 mW) may be compared to the cathode heating power of a tube, which usually is not taken into account in discussing the efficiency of a tube oscillator.

The fact that efficiency of oscillation according to Fig 14, drops at higher frequencies is due to rising losses in the ferrite core, this one being unsuited to high frequencies, in the coil and in the Hall probe, causing mismatch *It is not due to a decline of the Hall coefficient k_h of Eq (1)*

The frequency dependence of k_h was investigated by measuring the Gauss effect (see Fig 4) at different frequencies[6] Some relevant values are shown in Figs 15 and 16 The probe of Fig 15 was of length $l = 2\,7$ mm,

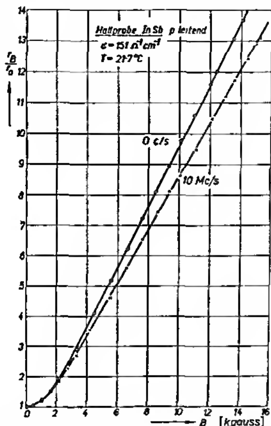

FIG 15 Gauss effect of Hall probe (InSb) at zero and at 10 mc/s Vertical scale Ratio of resistance of Hall probe at a definite transverse flux density (horizontal scale) to the resistance at zero flux density

width $b = 6\,1$ mm and thickness $h = 1\,6$ mm Its conductivity (of p type) was 151 mho/cm It is seen that a slight decline of Gauss effect and hence of the Hall coefficient k_h of Eq (1) is obtained at 10 mc/s as compared to its value at zero frequency The probe used in the measurements of Fig 16 was of length $l = 3\,0$ mm, of width $b = 5\,8$ mm and of thickness $h = 0\,15$ mm Its conductivity (InSb of n type) was 90 mho/cm From this Fig 16, a considerable decline of Gauss effect, and hence of the Hall coefficient k_h of Eq (1) is evident at 300 and at 600 mc/s as compared to the values at zero frequency

5 Hall Effect Flux Density Meter

Flux density meters, using germanium crystals, have been in use for many years With the semiconductor compounds, much more sensitive

meters may be built.[4] Here an arrangement, designed to attain the highest possible sensitivity, will be described.

The Hall probe is of width $b = 2$ mm., of length $l = 4$ mm. and of thickness $h = 0{\cdot}2$ mm. Its material is InAs, which was chosen because of its Hall coefficient k_h being far less dependent on temperature, around

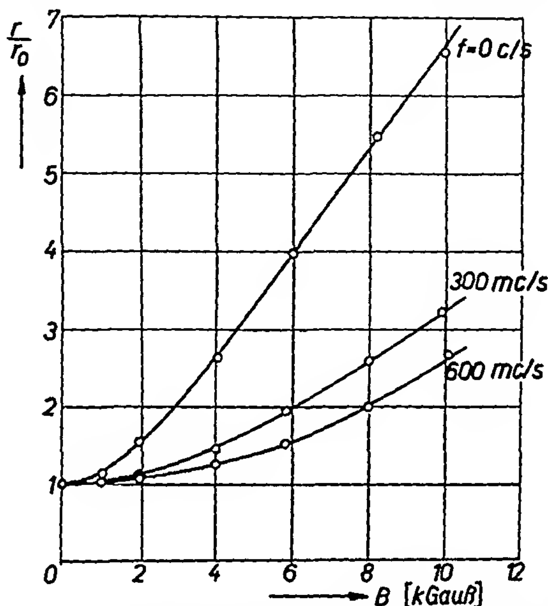

FIG. 16. Vertical scale: Ratio of resistance of Hall probe at a definite transverse flux density (horizontal scale) to the resistance at zero flux density. Curves at 0, 300 and at 600 mc/s of the current through the probe. A significant decline of Gauss effect is shown in these curves.

room temperature, than with JnSb. Its Hall coefficient k_h was found to be $0{\cdot}12.10^{-3}m^3$/Coulomb. The function f of Eq. (1) being about 0·83, the open-circuit Hall voltage is given by

$$U_{h_0} = 0{\cdot}5\ BI \qquad (6)$$

A current I of 1·2 A caused a stationary temperature of the probe of about 100° C.

Consideration was given to the use of probes of less thickness h. According to Eq. (1), the open-circuit Hall voltage U_{h_0} goes up, if h is reduced, at constant values of B and of I. However, if h is reduced, leaving the width b constant, the maximum current I must be reduced, as the heat dissipation in the probe must not cause an undue rise of temperature. It should be borne in mind that the probe's temperature must remain well below 150° C. in order to avoid disintegration of the material. Considering different possibilities, such as reduction of I, increase of width b with or without corresponding increase of l, it was found, that only a slight increase, if any, of U_{h_0}, at a given value of flux density B, may be achieved by reduction of h.

A block diagram of the experimental set-up is shown in Fig. 17. As seen from this Fig., an A.C. of 10 kc/s is supplied to the Hall probe by a

suitable transistor oscillator[7] with transistor power output stage The reasons for this are as follows It is easier to build a stable transistor amplifier for a range between 9 and 11 kc/s, than for a range between zero and 1 kc/s Amplifiers, either of tube or of transistor type, always show high inherent flicker noise at frequencies f adjacent to zero This flicker

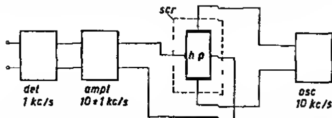

Fig 17 The Hall probe h p is supplied by a current of effective value I at a frequency of 10 kc/s by the transistor oscillator osc The Hall voltage of the probe is amplified by a transistor amplifier with a range between 9 and 11 kc/s The amplified Hall voltage is then detected by the transistor detector circuit det, its output giving signals of frequencies between zero and 1 kc

noise tapers off about proportionally to f^{-1} and is very much less at 10 kc/s Here, noise is mainly of shot and of Nyquist type[1 2]

Noise measurements were carried out at the Hall terminals of the Hall probe h p of Fig 17 Some resulting values are shown in Fig 18 Here the equivalent noise resistance R_{aqu} is shown as dependent on the current I (horizontal scale) through the Hall probe Its dependence on I may approximately be expressed by the equation

$$\frac{R_{aqu}(I)}{R_{aqu}(0)} = 1 + 1\ 14\ I^2$$

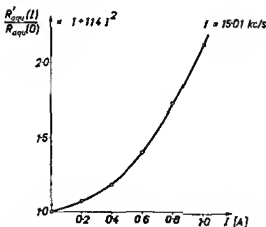

Fig 18 Vertical scale Ratio of equivalent noise resistance $R_{aqu}(I)$ at a current I through the Hall probe (horizontal scale) to the value $R_{aqu}(0)$ at zero current The value of $R_{aqu}(0)$ was shown to correspond exactly to the effective resistance between the Hall contacts of the Hall probe The frequency is 15 01 kc/s

While this curve of Fig 18 corresponds to a frequency of 15 kc/s, similar curves were taken at lower and at higher frequencies, showing a tendency for the ratio to drop at rising frequency at a definite value of I It is seen

from Fig. 18 that the noise at a current of 1·2 A is about 2·5 times the Nyquist noise at 15 kc/s. At 10 kc/s this figure rises to somewhat less than three times the Nyquist noise.

The transistor amplifier has a measured noise figure of 2.[1] These figures enable us to calculate the total equivalent effective noise voltage at the Hall terminals of the Hall probe, taking into account the noise of the amplifier and of the Hall probe itself. For the latter we assume that the equivalent noise resistance is three times the actual resistance between the Hall terminals. The equivalent noise resistance due to the amplifier noise is about twice the actual resistance at the Hall terminals. Hence, the total equivalent noise resistance at the Hall terminals of the probe is about five times its effective resistance. The latter value, at a current of 1·2 A is about 1·0 ohm. The total mean square effective noise voltage at the Hall terminals is given by the equation

$$\overline{U^2_n} = 4kTR_{\text{äqu total}}\,\Delta f$$

Here, k is Boltzmann's constant $1{\cdot}38.10^{-23}$ J/°K., T the temperature in °K. and Δf the effective band width, which is 2000 c/s in our case. We obtain, at a temperature T of 393 °K., a square root mean square value of the noise voltage of about 0·015 microvolts.

Assuming that the minimum Hall voltage is equal to the noise voltage, we obtain $U_h = 0{\cdot}015$ microvolts. If the Hall terminals of the probe are matched to the input of the amplifier, this Hall voltage U_h under optimum load conditions is half the open circuit Hall voltage U_{h_0}, which is hence 0·03 microvolts. The corresponding flux density B is obtained from Eq. (6) :

$$B = 2\,\frac{U_{h_0}}{I}$$

At a current I of 1·2 A, we obtain an effective value of $B \approx 5.10^{-8}$ volt sec/m^2 or 5.10^{-4} gauss.

It should be borne in mind that the above figure corresponds to a band width at the detector output (see Fig. 17) of 1000 c/s. Hence, variations of flux density up to 1000 c/s may be detected. In many cases, only much slower variations of flux density are to be measured. If, for instance, the output of the detector is connected to an indicator, registering up to 0·5 c/s, the corresponding minimum effective value of B to be detected would be $\sqrt{2000}$ times smaller, or about 10^{-5} gauss. If, furthermore, suitable pole pieces of mu-metal are applied, this minimum effective value of B is still about 400 times smaller, or about 2.10^{-8} gauss. Comparing this value with the best ones published so far, it is seen to be about 250 times smaller.[4]

The use of a transistor oscillator and of a transistor amplifier-detector results in a very compact and easily transportable arrangement, adaptable to many applications.

6. Hall Effect Mixer Stage

Mixer stages for superheterodyne receivers may be constructed using a Hall probe. The set-up is shown in Fig. 19. The antenna signal causes a current $I_{\max} \sin \omega_i t$ through the Hall probe 6. The local oscillator causes a

transverse magnetic flux density $B_{max} \sin \omega_{osc} t$ at the Hall probe 6 Here from a Hall voltage

$$U_{h0} = \frac{k_h}{h} f \frac{1}{2} I_{max} B_{max} \cos(\omega_{osc} - \omega_i)t \tag{7}$$

results, which constitutes the intermediate frequency signal This is filtered amplified and detected at the stages 11 and 12

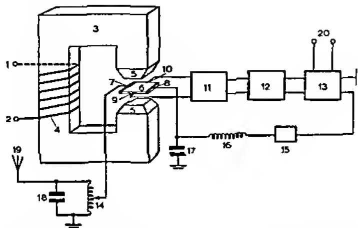

FIG 10 The signal from the antenna 10 is filtered by the resonance circuit 18 14 and then by a suitable transformation ratio (tap 14) supplied to the Hall probe 6 by means of the contacts 7 and 8 The h f circuit is closed by means of the condenser 17 The local oscillator signal is connected to the terminals 1 and 2 of the coil 4 which is arranged on the ferrite core 3 with the pole pieces 5 concentrating the magnetic flux on the Hall probe 6 The i f signal is taken from the Hall contacts 9 and 10 is then filtered amplified and detected at 11 and 12 A power supply 20 is fed to the power rectifier stage 13 which supplies a D C through the filter 15 and the choke 16 to the Hall probe 6 through the contacts 7 and 8

This mixer stage behaves differently from other mixer stages using mixer tubes transistors or diodes in that no distortion is involved in the mixing process The Hall voltage is proportional to the first power of I_{max} and does not contain any higher power components The Hall voltage does contain a component of angular frequency $\omega_{osc} + \omega_i$ but this is filtered out by the intermediate frequency stage 11 which is tuned to $\omega_{osc} - \omega_i$ The ferrite core by its non linear characteristic causes some harmonic components of the flux density B These cause Hall voltage components of angular frequencies $n\omega_{osc} \pm \omega_i$ where n is 2 3 4 - - - - However, these Hall voltage components are also filtered out by the stage 11

The behaviour of the Hall mixer stage is mainly determined by its gain g and by its noise figure F In the case of InSb the Hall coefficient k_h of Eq (1) is about 0 25 10 ³ m³/Coulomb In a practical set up, we have $h = 0\ 1$ mm and hence

$$U_{h_0} = 2\ 5\ BI$$

if f of Eq (1) is about unity The resistance between the Hall contacts is r_h at an effective temperature T_h Then the available Hall power of angular frequency $\omega_{osc} - \omega_i$ at the Hall contacts of the probe is

$$P_h = \frac{\frac{1}{2}(\frac{1}{2}\ 2\ 5\ B_{max}\ I_{max})^2}{4r_h}$$

The available input power of angular frequency ω_i is

$$P_i = \frac{\frac{1}{2}I_{\max}^2 r_0^2}{4r_0} = \frac{1}{8} I_{\max}^2 r_0$$

where r_0 is the effective internal resistance of the antenna circuit between the tap 14 on the coil (see Fig. 19) of the resonant antenna circuit and earth. The temperature of r_0 is assumed to be room temperature T_0. The gain of the mixer stage is :

$$g = \frac{P_h}{P_i} = \frac{(2{\cdot}5\ B_{\max})^2}{4r_h r_0},$$

In a practical set-up, the value of $B_{\max}$ was 3000 gauss or 0·3 volt sec/m². In this case, the oscillator connected to the contacts 1 and 2 of Fig. 19 had to supply a power of some 10 milliwatts. Furthermore, r_0 and r_h were both about 1 ohm. Hence, a gain g of about 1/7 or $-$ 8·5 db is obtained.

The noise figure F may be evaluated as follows. The available input noise power is $kT_0\Delta f$, where k is Boltzmann's constant and Δf is the effective band width under consideration. This gives an equivalent output noise power $gkT_0\Delta f$. The Hall resistance r_h causes an available output noise power $kT_h\Delta f$. Hence, the total available output noise power is $gkT_0\Delta f + kT_h\Delta f$. The noise figure F is obtained by division of this available output noise power by $gkT_0\Delta f$:

$$F = 1 + \frac{T_h}{gT_0}.$$

If $T_h = T_0$, this yields $F = 8$, if $g = 1/7$. The intermediate frequency stage 11 of Fig. 19 is assumed to have a noise figure F_1. Then the overall noise figure will be :

$$F_{\text{tot}} = F + \frac{F_1 - 1}{g}$$

Assuming $F_1 = 2$, we obtain $F_{\text{tot}} \approx 15$. This value compares favourably with noise figures of known mixer stages in the radio-frequency and high-frequency ranges. As the Hall voltage drops considerably above 30 mc/s, the Hall mixer stage becomes less favourable beyond this frequency.

In mixer stages, automatic volume control is a desirable feature. This may be obtained with Hall mixer stages by application of the temperature dependence of the Hall voltage according to Fig. 2. Hereby, the Hall coefficient k_h of Eq. (7) is affected. As this coefficient is independent of B and of I, *no distortion* is generated by varying the temperature. Thus, we have a *unique* volume control, which is entirely free of distortion. This feature compares favourably with the volume controls of all other known mixer stages. The temperature of the Hall probe may be varied by supplying a suitable auxiliary heating current. This may be obtained from a stage 13 (see Fig. 19), which is controlled automatically by the intermediate frequency output of the stage 12. The heating current is supplied to the Hall probe through a suitable filter 15 and a choke 16. The heating time of the Hall probe may be used as a means of obtaining a suitable time constant of the volume control in question.

In a practical set-up a small Hall probe was heated up by a heating current of about 1 A and a temperature difference of about 60° C. was obtained. According to Fig. 2, a reduction of Hall voltage by a factor 5

may be expected at this temperature difference The time constant was some tenths of a second, depending on the surface cooling of the Hall probe As the Hall resistance r_h is also reduced at rising temperature according to Fig 3, a further gain control is obtained by mismatch of the mixer stage to the subsequent intermediate frequency stage

By the heating current, the effective noise tempertaure T_h of the Hall probe goes upwards, causing a rise of noise figure As, however, volume control is applied at high input signal levels, this rise of noise figure does not constitute an impairment of the performance of the mixer stage

Acknowledgments

The work reported here was carried out in co operation with my co workers Dr P Ramer, Mr B Schneider, Dr S F Sun, Mr E Voegele, Mr F von Willisen and Mr W Wunderlin It was supported by grants from the Swiss Aluminum Foundation and from the Swiss Federal Institute of Technology I want to express my thanks for this support

References

1 Guggenbuehl, W and Strutt M J O Transistoren in Niederfrequenz Anfangsstufen, *Sci elect* 2, 47–57 (1956)
2 Guggenbuehl, W and Strutt, M J O Transistoren in Hochfrequenz Anfangsstufen, *Sci elect* 2, 99–115 (1956)
3 Hartel, W Anwendung der Hallgeneratoren, *Siemens Z* 28, 376 (1954)
4 Hieronimus, H and Weiss, H Ueber die Messung kleinster magnetischer Felder mit Hallgeneratoren, *Siemens Z* 31, 404–409 (1957)
5 Kuhrt, F Eigenschaften der Hallgeneratoren *Siemens Z* 28, 370–376 (1954)
6 Ramer, P, Strutt, M J O and von Willisen, F K Messungen des Gausseffektes verschiedener Halbleiter bei 10, 300 and 600 MHz, *Arch elektr Übertr* 11, 1–7 (1957)
7 Schaffhauser H Beschreibung eines stabilisierten LC Transistoroszillators im Niederfrequenzgebiet, *Sci elect* 4, 23 30 (1958)
8 Strutt, M J O and Sun, S F Leistungsmessung und Leistungsregulierung in Mehrphasennetzen mittels Halbleitern, *Arch Elektrotech* 42, 155–164 (1955)
9 Strutt, M J O and Sun, S F Experimentelle und theoretische Unter suchung von Halbleiter Halleffektoszillatoren, *Arch elektr Übertr* 11, 261 265, (1957)
10 Welker, H Neuere Untersuchungen der Halbleitereigenschaften von III V Verbindungen, *Sci elect* 1, 4, 152 (1954)

Eigenschaften und Anwendungen der Hallgeneratoren

W. HARTEL

Siemens-Schuckertwerke A.G., Nürnberg

HALLGENERATOREN sind Bauelemente der Elektrotechnik, die die technische Ausnützung des Hall-Effektes gestatten. Die folgenden Ausführungen geben einen kurzen Überblick über die wesentlichsten physikalischen und elektrischen Eigenschaften der Hallgeneratoren, die bei der Anwendung in der Praxis berücksichtigt werden müssen.

Der Hallgenerator ist in Fig. 1 schematisch als Rechteckplatte dargestellt, die vom Magnetfeld B durchsetzt und vom Steuerstrom i_1 durchflossen wird. Der Hallgenerator kann als Vierpol mit den Eingangsklemmen 1, 2 und mit den Ausgangsklemmen 3, 4 aufgefaßt und durch die beiden Gleichungen in Fig. 1 beschrieben werden.[1] Das Betriebsverhalten des

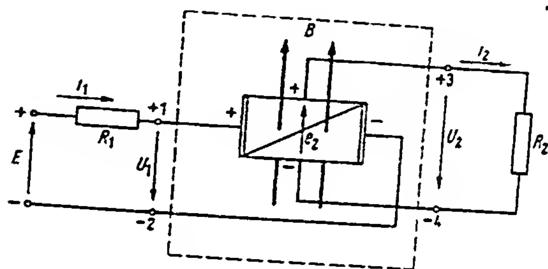

$$u_1 = R_{1L}\, i_1 + K_0 B\, i_2$$

$$u_2 = K_0 B\, i_1 - R_{2L}\, i_2$$

FIG. 1. Hallgenerator als Vierpol.

Hallgenerators wird erschöpfend durch die drei Betriebsgrößen des Vierpoles, nämlich den primären bzw. sekundären Leerlaufwiderstand R_{1L} bzw. R_{2L} und durch den Kernwiderstand K_0B. festgelegt. Bei der Beschreibung der Eigenschaften der Hallgeneratoren kann man sich also im wesentlichen auf eine Diskussion dieser drei Betriebsgrößen beschränken.

Mit dem Halleffekt ist stets eine zweite, bei der technischen Ausnützung meistens störende Erscheinung verknüpft, nämlich die Magnetfeldabhängigkeit der Leerlaufwiderstände R_{1L} und R_{2L}, die insbesondere bei Materialien mit hoher Trägerbeweglichkeit wie z.B. bei Indium-Antimonid und Indium-Arsenid besonders in Erscheinung tritt.[2, 3]

Beim sekundären Leerlauf, d.h. $i_2 = 0$, folgt aus der zweiten Gleichung in Fig. 1 die bekannte Beziehung für den Halleffekt $u_{20} = K_0 i_1 B$. Wenn die betrachtete Halbleiterplatte die Form eines sehr langen (theoretisch unendlich langen) Streifens aufweist, ist K_0 mit der bekannten Beziehung $K_0 = R_h/d$ (Hallkonstante/Plattendicke) identisch. Bei endlicher Streifenlänge, also bei einer Rechteckplatte gemäß Fig. 1 bzw. Fig. 2, hängt dagegen K_0 vom

Magnetfeld ab. *Exakte Proportionalität* zwischen Hallspannung und Magnetfeld liegt also nur im Sonderfall des unendlich langen Streifens vor, bei der Rechteckplatte treten dagegen Abweichungen von der Proportionalität auf [4, 5, 6]. Bei vielen Anwendungen [7] wird eine möglichst gute Proportionalität zwischen Hallspannung und Magnetfeld gefordert. Deshalb müssen alle jene Effekte, die zu einer Abweichung von der Proportionalität führen, quantitativ faßbar sein, damit eine befriedigende Aussage über die Abweichungen von der Proportionalität bei den verschiedenen Betriebsbedingungen des Hallgenerators gemacht werden kann. Eine erschöpfende Vierpol-Theorie des Hallgenerators liegt also erst dann vor, wenn die Feldabhängigkeit der Betriebsgrößen R_{1L}, R_{2L} bzw. $K_0 B$ und ihre Abhängigkeit von den geometrischen Abmessungen der Halbleiterplatte übersehen werden kann.

Fig. 2 zeigt die praktische Ausführung der Halbleiterplatte eines Hallgenerators. Die Eigenschaften der Betriebsgrößen R_{1L}, R_{2L} und $K_0 B$ werden maßgeblich durch das Seitenverhältnis a/b der Rechteckplatte

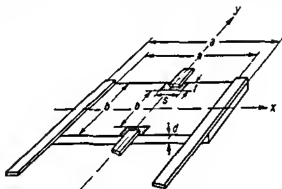

Fig. 2. Aufbau des elektrischen Systems eines Hallgenerators

durch die relative Breite s/a der Hallelektroden und durch die Dicke d der Rechteckplatte bestimmt. Die Betriebsgrößen können formal durch die Beziehungen (1), (2) und (3) in Fig. 3 dargestellt werden; dabei ist es zweckmäßig, die Leerlaufwiderstände auf den Wert R_{1L} (0) bzw. R_{2L} (0) beim Feld $B = 0$ zu beziehen. In den Beziehungen für die relativen Leerlaufwiderstände und für den Kernwiderstand treten jeweils zwei Faktoren auf: der erste Faktor, nämlich der relative spezifische Widerstand $\rho(B)/\rho(0)$ bzw. die Hallkonstante R_h, bringt die Abhängigkeit der Betriebsgrößen von den Materialeigenschaften zum Ausdruck, während der zweite Faktor G_s, G_h bzw. H die Abhängigkeit der Betriebsgrößen von den geometrischen Abmessungen und vom magnetischen Feld angibt. G_s und G_h werden deshalb als Geometriefunktionen des Widerstandseffektes bezeichnet; H wird Geometriefunktion des Halleffektes genannt.

Die Abhängigkeit der Betriebsgrößen von den Materialeigenschaften kann leicht überblickt werden, denn $\rho(B)/\rho(0)$ und R_h kann für ein vorgegebenes Material einfach durch Messung bestimmt werden [8–13]. Der Einfluß der geometrischen Abmessungen ist indessen nur dann vollkommen zu

übersehen, wenn die Berechnung der Geometriefunktionen gelingt. Diese Aufgabe führt auf ein Problem der Potentialtheorie mit gemischten Randbedingungen, das in Fig. 4 oben durch die Äquipotentiallinien und Feldlinien angedeutet ist. Ansätze zur Lösung dieses Problems liegen im

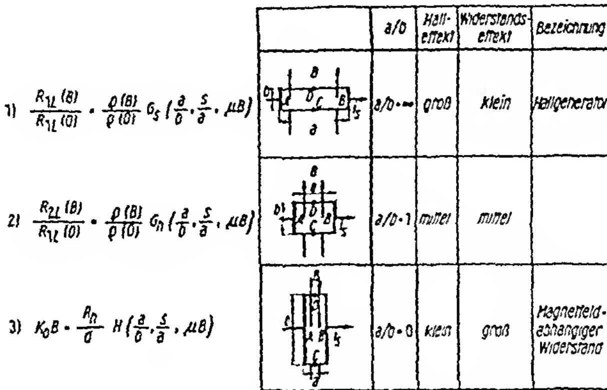

Fig. 3. Die Vierpolkonstanten des Hallgenerators.

Schrifttum vor, [14, 15] desgleichen gewisse Näherungslösungen.[15, 16] Die exakte und vollständige Lösung dieses Problems für den Sonderfall punktförmiger Hallelektroden wurde von F. Kuhrt und H. J. Lippmann angegeben.[4, 5, 6]

Fig. 4 zeigt die Ergebnisse für punktförmige Hallelektroden. Links unten ist die Feldabhängigkeit des Kernwiderstandes K_0B, also die Leerlauf-

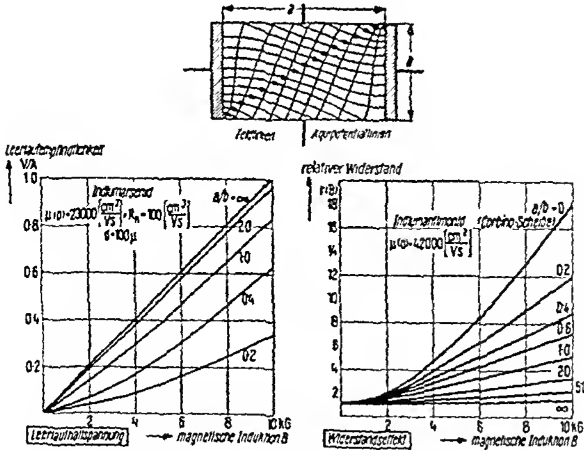

Fig. 4. Galvanomagnetische Effekte (theoretisch).

hallspannung pro Steuerstromeinheit, in Abhängigkeit vom Magnetfeld B für verschiedene Seitenverhältnisse a/b aufgetragen. Rechts unten ist der relative Widerstand $r(B) = R_{1L}(B)/R_{1L}(0)$ in Abhängigkeit vom Magnetfeld B für verschiedene Seitenverhältnisse a/b dargestellt. Die linke Kurvenschar wurde für Indium-Arsenid, die rechte für Indium-Antimonid errechnet. Aus den Kurvenscharen erkennt man, daß die bei einer Rechteckplatte

erzielbare Hallspannung mit dem Seitenverhältnis a/b abnimmt, die Magnetfeldabhängigkeit des Widerstandes dagegen anwächst. Diese Verhältnisse sind in Fig. 3 anschaulich zusammengestellt und zeigen, daß für Hallgeneratoren langgestreckte Platten, für magnetfeldabhängige Widerstände dagegen möglichst kurze Platten günstig sind.

Halleffekt und Widerstandseffekt haben dieselbe physikalische Ursache und treten stets gleichzeitig auf; beide Erscheinungen werden deshalb häufig unter der übergeordneten Bezeichnung "Galvanomagnetische Effekte" zusammengefaßt. Einen Halbleiterkörper, bei dem die galvanomagnetischen Effekte ausgenutzt werden, bezeichnet man häufig als "Galvanomagnetisches Element". Durch die geometrische Formgebung der Rechteckplatte kann nach Fig. 3 erreicht werden, daß einer der beiden galvanomagnetischen Effekte besonders stark hervortritt; man spricht dann von einem "Hallgenerator" bzw. von einem "magnetisch steuerbaren Widerstand". Hallgeneratoren bzw. magnetisch steuerbare Widerstände sind also galvanomagnetische Elemente mit besonders hoher Hallspannung bzw. hohem Widerstandseffekt.

Die Lösung des Potentialproblems bei einer von Null verschiedenen relativen Breite s/a der Hallelektroden ist noch nicht abgeschlossen, so daß im Augenblick nur experimentell ermittelte Angaben vorliegen. Fig. 5

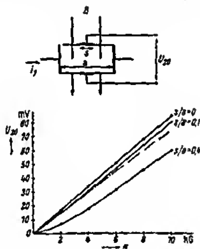

FIG. 5. *Hallgenerator-Leerlaufkennlinien in Abhängigkeit von Breite s/a der Hallelektroden.*

zeigt den Einfluß der Elektrodenverbreiterung bei einer Rechteckplatte mit dem Seitenverhältnis $a/b = 2$ für Indiumarsenid der Hallkonstanten 120 cm³/As [17].

Aus den Vierpolgleichungen in Fig. 1 kann die Hallspannung u_2 am Abschlußwiderstand bei beliebigen Betriebsbedingungen des Hallgenerators berechnet werden. In das Ergebnis gehen die drei Vierpolbetriebsgrößen (R_{1L}, R_{2L} und K_0B) ein, deren Feldabhängigkeit gewisse Abweichungen von der Proportionalität zwischen Hallspannung und Magnetfeld (Linearitätsabweichungen) zur Folge hat. Bei allen Anwendungen der Hallgeneratoren, bei denen auf gute Proportionalität Wert gelegt wird, müssen deshalb Maßnahmen getroffen werden, die diese Linearitätsabweichungen auf ein Mindestmaß beschränken.

Bei der Belastung eines Hallgenerators mit dem Aussenwiderstand R_a wird die Leerlaufhallspannung $u_{20} = K_0 i_1 B$ im Verhältnis Innen- zu Aussenwiderstand aufgeteilt, so daß nur der Bruchteil u_2 als nutzbare Hallspannung zur Verfügung steht. Für u_2 liest man unmittelbar die Beziehung in Fig. 6 ab. u_2 ist demnach zwar dem Produkt $i_1 B$ proportional, darüber hinaus aber

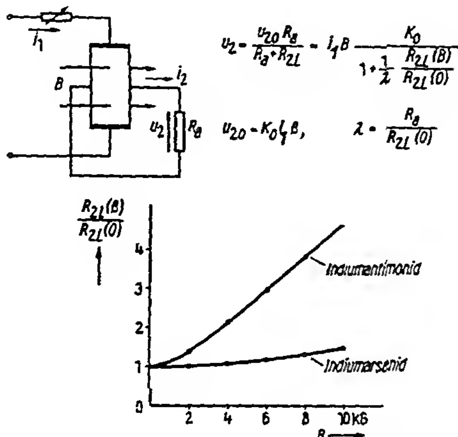

FIG. 6. Einfluss der Magnetfeldabhängigkeit des Innenwiderstandes auf die belastete Hallspannung.

noch mit einem Faktor behaftet, dessen Feldabhängigkeit durch K_0 und R_{2L} bestimmt wird. Dieser Faktor hängt außerdem noch von der Belastung ab, die durch das Anpassungsverhältnis $\lambda = R_a/R_{2L}$ (0) beschrieben wird. Die Feldabhängigkeit des Störfaktors wird somit durch die drei Parameter a/b, s/a und λ festgelegt. Durch geeignete Wahl dieser drei Parameter kann—zumindest in einem bestimmten Feldintervall, etwa $B = 0$ bis $B = B_m$ —die Feldabhängigkeit des Faktors zu einem Minimum gemacht werden [17] ; Hallspannung und Magnetfeld werden dann weitgehend proportional zueinander. Bei einem vorgegebenen Hallgenerator, also bei festliegenden Parametern a/b und s/a, liegen diese günstigsten Verhältnisse somit nur bei einer bestimmten Anpassung, die als " lineare Anpassung " bezeichnet wird, vor ; d. h. der Hallgenerator muß stets mit einem bestimmten Abschlußwiderstand betrieben werden, wenn bestmögliche Proportionalität zwischen Hallspannung und Magnetfeld erreicht werden soll. Durch Reihen-bzw. Parallelschaltung geeigneter Widerstände kann diese Bedingung in der Praxis immer erfüllt werden.

Die Abhängigkeit der Hallspannung u_2 vom Magnetfeld B ist in Fig. 7 schematisch dargestellt ; sie kann in dem Feldbereich von $B = 0$ bis $B = B_m$ durch eine Ursprungsgerade derart angenähert werden, daß die positiven und negativen Maximalabweichungen ϵ_{max} einander gleich sind. Dem Gebrauche der Meßinstrumententechnik folgend, wird die Maximalabweichung ϵ_{max} auf die Hallspannung u_{2m} am Bereichsende B_m bezogen und als Fehler $F = \epsilon_{max}/u_{2m}$ des Hallgenerators bezeichnet. Dieser Fehler hängt nach Fig. 7 rechts vom Abschlußwiderstand, also von der Anpassung λ ab und besitzt bei der bereits oben erwähnten günstigsten linearen Anpassung $\lambda = \lambda_{lin}$ sein Minimum.[1] Der Verlauf in der Umgebung des Minimums ist

flach so daß eine besonders sorgfaltige Anpassung nicht erforderlich ist Die Fehlerkurve in Fig 7 gilt fur einen handelsubblichen Hallgenerator, der bei 10 000 G und maximalem Steuerstrom eine Leerlaufspannung von ca 1 0 V abgibt , der Fehler betragt dabei weniger als 1% Mit kleiner werden dem Linearisierungsbereich nimmt auch der Fehler ab , in einem Bereich von O bis 2000 G kann der Linearisierungsfehler z B bereits kleiner als 2‰ gehalten werden

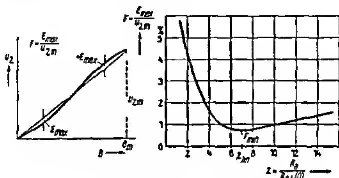

Fig 7 Linearisierungsfaktor eines Hallgenerators

Zum Schutze gegen mechanische Zerstorungen muß das dunne Halbleiterplattchen in einem Schutzmantel untergebracht werden der aus unmagnetischem Material z B Gießharz Sinterkeramik usw oder auch aus ferromagnetischem Material z B Ferriten bestehen kann die Dicke des Schutzmantels muß dabei ein Vielfaches der eigentlichen Halbleiterschicht betragen damit vor allem gegenuber Biegespannungen hinreichend Schutz gewahrt wird

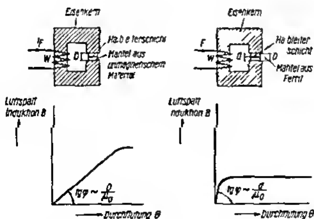

Fig 8 Hallgeneratoren mit unmagnetischem und magnetischem Mantel
Gegenuberstellung

Fig 8 zeigt zwei Eisenkerne deren Luftspaltinduktion bei geeigneter Materialauswahl und Dimensionierung proportional zum Erregerstrom der Feldwicklung verandert werden kann Der Luftspalt des linken Eisenkernes enthalt einen Hallgenerator mit unmagnetischem der Luftspalt des rechten Eisenkernes einen Hallgenerator mit magnetischem Mantel Der

Vergleich beider Anordnungen zeigt, daß die Ferritplatten eine erhebliche Verkleinerung des wirksamen Luftspaltes und damit eine entsprechende Verringerung der Durchflutung bzw. der zum Aufbau des Luftspaltfeldes erforderlichen Wirkleistung zur Folge haben. Diese Vorteile gelten jedoch nur bis etwa 2000, höchstens 3500 G, denn dann gehen die Ferritplatten in Sättigung. Wesentlich höhere Hallspannungen, allerdings bei beträchtlich größeren Steuerleistungen, werden mit Hallgeneratoren aus unmagnetischem Mantel erreicht, da bei geeigneter Dimensionierung des Eisenkernes und Verwendung von Eisen mit hoher Sättigung Luftspaltinduktionen bis 15,000 G und mehr erzeugt werden können.

Man kann die am Abschlußwiderstand R_a abgegebene nutzbare Halleistung N_a zur Eingangsleistung N_e ins Verhältnis setzen. Man erhält die zwei Formeln in Fig. 9.

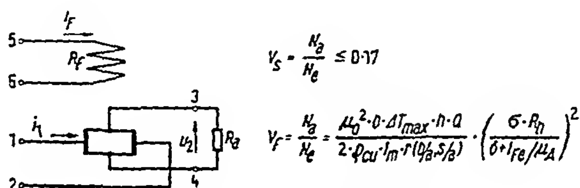

Einbettung der Halbleiterschicht in:		
magnetisch inaktive Vergußmasse	Ferrit	
δ = 1mm V_F = 0·02 $N_{a\,max}$ = 100 mW	δ = 0·3mm V_F = 0·12 $N_{a\,max}$ = 10 mW	δ = 0·02mm V_F = 10 $N_{a\,max}$ = 10 mW

Fig. 9. Hallgenerator als Verstärker.

Bei der ersten Formel wird die den Klemmen 1,2 zugeführte Leistung als Eingangsleistung betrachtet; man kann theoretisch zeigen, daß dieses Leistungsverhältnis V_s stets kleiner als 0·17 sein muß und daß dieser Wert asypmtotisch erreicht wird, wenn das Produkt Trägerbeweglichkeit mal Magnetfeld gegen Unendlich geht.[1] Bei der zweiten Formel wird die den Klemmen 5,6 zugeführte Leistung als Eingangsleistung betrachtet; unter der Voraussetzung, daß für die Erwärmung der Halbleiterplatte eine Höchstgrenze angegeben ist, erhält man für V_F die in Fig. 9 angegebene Beziehung.[18, 19] Bei geeigneter Dimensionierung und Materialauswahl wird dieser Ausdruck größer als 1, d. h. der Hallgenerator wirkt als Leistungsverstärker. Die Leistungsverstärkung nimmt, wie aus dem letzten quadratischen Glied der Formel zu erkennen ist, mit dem Quadrat der Trägerbeweglichkeit zu und wächst außerdem umgekehrt proportional mit dem Quadrat der Luftspalthöhe an. Die Tabelle darunter zeigt den Faktor V_F für verschiedene effektive magnetische Luftspalte.

Bei der Anwendung der Hallgeneratoren kann man zwei Fälle unterscheiden:

(a) Das magnetische Steuerfeld ist irgendwie fest vorgegeben (Fig. 10 unten).

(b) Das Magnetfeld, z. B. im Luftspalt des Eisenkernes, kann durch eine

elektrische Große namlich durch den Erregerstrom der zugehorigen Wicklung gesteuert werden

Bei jedem dieser beiden Anwendungsprinzipien konnen Hallgeneratoren sowohl mit magnetischem als auch mit unmagnetischem Mantel versehen werden Man erhalt dann die in Fig 10 dargestellten vier Anwendungs prinzipien der Hallgeneratoren Jedes dieser Verfahren besitzt ganz

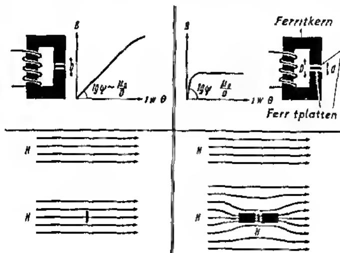

Fig 10

bestimmte charakteristische Eigenschaften so daß man bei der Aufgabe stellung im allgemeinen bereits festlegen kann welches dieser vier Grundver fahren zur Losung der Aufgabe in Frage kommen wird

1 Hallgeneratoren mit unmagnetischem Mantel im Luftspaltfeld eines Eisenkernes Anwendungsbereich sind Aufgaben bei denen hinreichend Steuerleistung zur Erzeugung des Luftspaltfeldes zur Verfugung steht große Hallspannung und große Halleistungen gefordert werden z B Messung hoher Gleichstrome [20, 21] Messung von Gleichstromleistungen und Leistungsimpulsen [7] Drehmomentenanzeige [22] elektrische Darstellung des Produktes Ankerstrom mal Drehzahl bei großen Walzmotoren usw

2 Hallgeneratoren mit magnetischem Mantel im Luftspaltfeld eines Eisenkernes Anwendungsbereich sind Aufgaben bei denen nur gering fugige Steuerleistungen zur Erzeugung des Magnetfeldes zur Verfugung stehen z B Durchfuhrung von Rechenoperationen wie Multiplizieren [3] Dividieren usw Modulator [7] Speicherelement das beliebig oft abgefragt werden kann usw

3 Der Hallgenerator mit magnetischem Mantel in einem vorgegebenen Magnetfeld Der Anwendungsbereich erstreckt sich auf Aufgaben bei denen das Ursprungsfeld durch den Hallgenerator nicht verzerrt werden darf und Proportionalitat zwischen Magnetfeld und Hallspannung gefordert wird z B Messung von Streufeldern in Maschinen [7] [23] Messung von Luftspalt feldern Ausmessung der Magnete von Beschleunigermaschinen Messung der Tangentialkomponente [24] in Eisen usw

4 Der Hallgenerator mit ferromagnetischem Mantel in einem vorge gebenen Magnetfeld Der Anwendungsbereich erstreckt sich auf Aufgaben bei denen das Ursprungsfeld durch die Ferritplatten oder durch Polschuhe

die zur Verstärkung der magnetischen Wirkung der Ferritplatten angebracht sind, verzerrt werden darf und eine Proportionalität zwischen Ursprungsfeld und Hallspannung nicht unbedingt gefordert ist. Durch die Bündelwirkung im Luftspalt sind kleinen Ursprungsfeldern bereits beträchtliche Luftspaltfelder, also beträchtliche Hallspannungen zugeordnet, so daß diese Anordnung insbesondere dann am Platze ist, wenn bereits kleinste Magnetfelder noch praktisch verwertbare Hallspannungen hervorrufen sollen.[25] Mit solchen Anordnungen ist es z. B. möglich, Magnetfeldänderungen von einigen Gamma anzuzeigen.

Literatur

1. Kuhrt, F. u. Hartel, W. Der Hallgenerator als Vierpol, *Arch. Elektrotech.* 43, 1, 1–15 (1957).
2. Welker, H. Über neue halbleitende Verbindungen I *Z. Naturf.* 7a, 744–9 (1952).
3. Welker, H. Über neue halbleitende Verbindungen II, *Z. Naturf.* 8a, 248–51 (1953).
4. Lippmann, H. J. u. Kuhrt, F. Einfluß der Geometrie auf Halleffekt und magnetischen Widerstandseffekt bei rechteckförmigen Halbleiterproben, *Naturwissenschaften* 7, 156–7 (1958).
5. Lippmann, H. J. u. Kuhrt, F. Der Geometrieeinfluß auf den transversalen magnetischen Widerstandseffekt bei rechteckförmigen Halbleiterplatten, *Z. Naturf.* 13a/6 462–74 (1958).
6. Lippmann, H. J. u. Kuhrt, F. Der Geometrieeinfluß auf den Halleffekt bei rechteckförmigen Halbleiterplatten. *Z. Naturf.* 13a/6 474–83 (1958).
7. Hartel, W. Anwendungen der Hallgeneratoren, *Siemens-Z.* 28, 376–84 (1954).
8. Weiß, H. Die magnetische Widerstandsänderung in InAs, *Z. Naturf.* 12a, 1, 80 (1957).
9. Weiß, H. u. Welker, H. Zur transversalen magnetischen Widerstandsänderung von InSb, *Z. Phys.* 138, 322 (1954).
10. Weiß, H. Über die elektrischen Eigenschaften von InSb, *Z. Naturf.* 8a, 463–9 (1953).
11. Madelung. O. u. Weiß, H. Die elektrischen Eigenschaften von InSb II, *Z. Naturf.* 9a, 527–34 (1954).
12. Folberth, O. G., Grimm, R. u. Weiß, H. Über die elektrischen Eigenschaften von InAs, *Z. Naturf.* 8a, 826 (1953).
13. Folberth, O. G., Madelung, O. u. Weiß, H. Die elektrischen Eigenschaften von InAs II, *Z. Naturf.* 9a, 954–8 (1954).
14. Wick, R. F. Solution of the field problem of the germanium gyrator, *J. appl. Phys.* 25, 741–56 (1954).
15. Isenberg, J., Russell, B. R. u. Greene, R. F. Improved method for measuring hall coefficients, *Rev. sci. Instrum.* 19, 685–8 (1948).
16. Volger, J. Note on the hall potential across an inhomogeneous conductor, *Phys. Rev.* 79, 1023–4 (1950).
17. Kuhrt, F. Eigenschaften der Hallgeneratoren, *Siemens-Z.* 28, 370–6 (1954).
18. Weiß, H. Der rückgekoppelte Hallgenerator, *Z. Naturf.* 11a, 684–8 (1956)
19. Kuhrt, F. Der Hallgenerator als Leistungsverstärker und Schwingungserzeuger, *Elektrotech. Z.* 78, 10, 342–4 (1957).
20. Kuhrt, F. u. Maaz, K. Messung hoher Gleichströme mit Hallgeneratoren, *Elektrotech. Z.* 77, A14, 487–90.
21. Maaz, K. u. Schmid, R. Hochstromjoche mit Hallgeneratoren, *Elektrotech. Z.* 78, 20, 734–6 (1957).

22. Kuhrt, F. u Braunersreuther, E. Drehmomentmessung an einem Gleichstrommotor mit Hilfe des Halleffektes, *Siemens Z.* 28, 7, 299–302 (1954).
23 Kuhrt, F. u. Braunersreuther, E. Messung des Feldverlaufes im Luftspalt eines Gleichstrommotors mit Hilfe des Halleffektes, *Elektrotech Z.* 77, 578–81 (1956)
24 Kuhrt, F. u. Hartel, W. Der Eigenfeldfehler bei der Messung der Tangentialfeldstarke in Eisen mittels des Halleffektes, *Arch. Elektrotech.* 42, 7, 398–409 (1956).
25. Hieronymus, H. u Weiß, H. Uber die Messung kleinster magnetischer Felder mit Hallgeneratoren, *Siemens Z.* 31, 8, 404–9 (1957).

The Properties and Applications of p-type InSb

C. HILSUM

Services Electronics Research Laboratory, Baldock, Herts

1. Introduction

Though much interest has been expressed recently in the properties of indium antimonide, little work has been done on material containing an excess of holes at room temperature. Because the mobility ratio is large, such material will have a negative Hall coefficient unless there are several hundred times more holes than electrons. The determination of the carrier mobilities and concentrations becomes complicated, since measurement of Hall constant R_H and resistivity ρ_0 is insufficient to determine the four unknown parameters. It has been shown [1] that if one measures in addition the variation of R_H and ρ_0 in a magnetic field, it is possible to derive the electron and hole concentrations n, p, the electron mobility μ and the mobility ratio b. In this paper the properties of p-type InSb are discussed in more detail, and some applications of the material are described.

2. Hall Constant, Resistivity and Lifetime

The measurements of electrical properties described by Hilsum and Barrie [1] indicated that the important scattering mechanisms for electrons in InSb are polar scattering, electron-hole scattering and ionized impurity scattering : these combine to give the dependence of mobility on impurity concentration shown in Fig. 1. At a given impurity concentration the mobility in n-type material is higher than in p-type because there is less electron-hole scattering. For the hole mobility, which is predicted less accurately by the theory, the dominant scattering mechanisms are assumed to be acoustic scattering and ionized impurity scattering. We observe a gradual decrease from 750 cm²/volt. sec. for intrinsic material to about 500 cm²/volt. sec. for material of zero Hall coefficient.

R_H and ρ_0 are given as a function of impurity concentration in Fig. 2. The impurity content is expressed as the ratio of the intrinsic concentration n_i to the hole concentration, and the left-hand axis represents intrinsic material. The Hall coefficient rises from the intrinsic value of under 400 cm³/coulomb to a maximum of 950 cm³/coulomb when p equals $6{\cdot}5 \times 10^{16}$ cm^{-3}, and then decreases, changing sign when p is greater than 3×10^{17} cm^{-3}. The resistivity of p-type material is markedly greater than that of intrinsic, a point to note, since specimens made from high mobility compounds are generally of inconveniently low resistance.

Carrier lifetime in InSb is so short that the only accurate method of measuring it at room temperature is by means of the photoconductive and photoelectromagnetic effects. For p-type specimens it is necessary to deter-

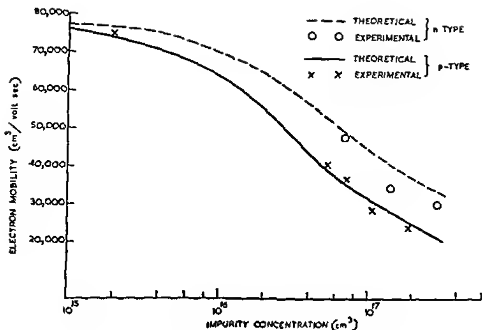

Fig 1 Variation of electron mobility with impurity content

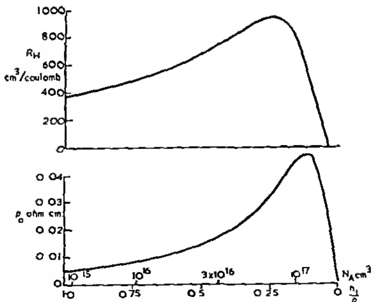

Fig 2 Hall constant and resistivity as a function of hole concentration

mine the mobilities first. Some typical results are given in Fig. 3. The theoretical curve is obtained by combining radiative recombination with recombination via traps with a trap density of about 10^{14} cm^{-3} at a level half-way between the conduction and valence bands.

3. Applications

In three fields where it has been shown that devices made from InSb have practical applications, the use of *p*-type material gives some advantages. It can be used in photocells, magnetoresistance devices and Hall effect applications.

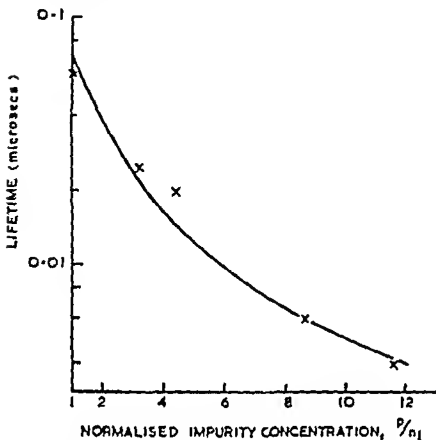

Fig. 3. Dependence of lifetime on impurity concentration.
X = experiment ; —— = theory.

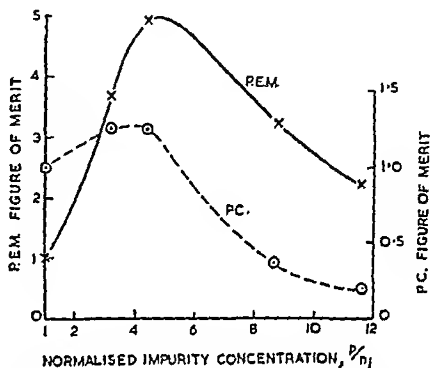

Fig. 4. P.E.M. and P.C. figures of merit as function of impurity concentration.

(A) Photocells

Since InSb has an energy gap smaller than 0·2 eV, photocells made from it have a spectral response at room temperature out to beyond 7μ ; several laboratories have reported on InSb photocells,[2, 3, 4] and uncooled photoconductive (P.C.) and photoelectromagnetic (P.E.M.) cells have been described. A cell made from *p*-type material will obviously give a shorter response time and, as shown in Fig. 4, for P.E.M. cells a considerable increase in sensitivity is also obtained. A small improvement is shown for P.C. cells. A full account of these measurements will be given elsewhere.

(B) Magnetoresistance devices

A specimen of intrinsic InSb with a length more than three times its width shows a 60 per cent. increase in resistance in a magnetic field of 10,000 gauss ; material with 5×10^{16} acceptors per cm^3 shows an effect three times as large. In Fig. 5, the magnetoresistance effects for four impurity concentrations are illustrated. Since the resistivity of *p*-type material is up to ten times as large as intrinsic, the absolute resistance change is many times greater. But it must not be forgotten that in most applications the specimen is shaped to give the largest possible resistance change, i.e. as a Corbino disc, or with a length smaller than the width. These structures are far less effective for *p*-type specimens (Fig. 6). The largest fractional change now

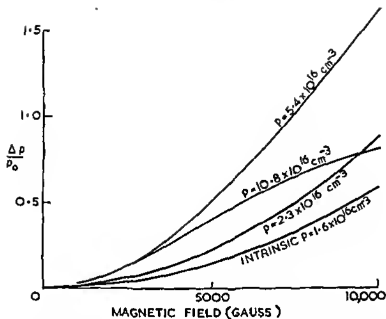

FIG 5 Magnetoresistance of specimens of various impurity concentrations

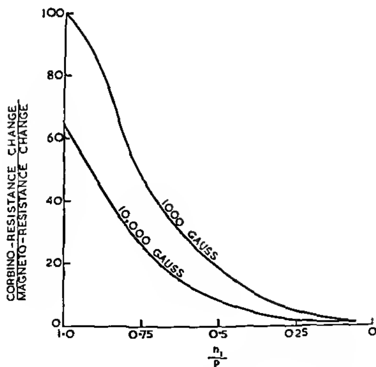

FIG 6 The gain in using Corbino disc specimens as a function of impurity concentration

occurs for a disc made of intrinsic material, which increases in resistance almost 40 times in a field of 10,000 gauss. A *p*-type specimen (4×10^{16} acceptors per c.c.) increases eight times. A square specimen is sometimes used where the disc shape is inconvenient, and here there is little difference in the relative change for various impurity concentrations; the absolute change is of course larger for the *p*-type specimens.

A typical application of the magnetoresistance effect is in the displacement transducer.[5] A small permanent magnet gives a strong localized field in which an InSb specimen is supported (Fig. 7a): the specimen is a com-

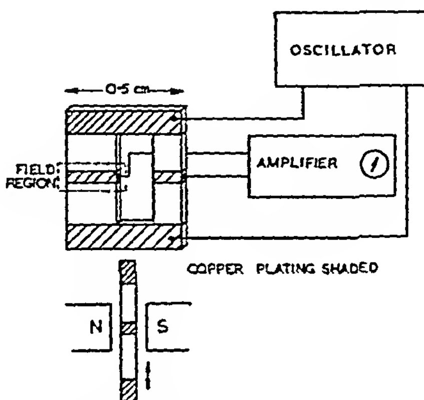

FIG. 7a. A bridge specimen for use in a displacement meter.

plete bridge network and when the left-hand side is symmetrical in the magnetic field the bridge is balanced. A vertical movement relative to the magnet causes one arm of the bridge to increase in resistance, and the other to decrease. The system works equally well with D.C. or A.C. drive and without amplification an output of 1 mV is obtained for a motion of 20 microns; with a simple transistor amplifier connected across the bridge a motion of 10 Å can be detected. Some pains must be taken in the mechanical design to achieve this performance and the complete instrument* is shown in Fig. 7b. The present performance does not yet approach the theoretical sensitivity limit, for with a response time of one second a signal equal to the inherent noise in the bridge is given by a movement of less than 0·1 Å.

The advantage in using *p*-type material here comes from its higher resistivity. The individual arms can be made with a resistance of 5–10 ohms, and there is little loss of sensitivity due to contact resistances.

(C) HALL EFFECT APPLICATIONS

Several authors have suggested using the Hall effect for multipliers,[6] gaussmeters,[7] compasses,[8] amplifiers.[9] etc. Here we deal with its use in a magnetometer. It may be shown theoretically that indium antimonide is the most suitable material for detecting very small magnetic fields, because it has the highest electron mobility. Other points which must also be considered are contact rectification and temperature stability. It is apparent that the best device will have ohmic contacts and InSb is satisfactory in this

* This instrument was designed by R. D. Knight and will be described fully in a subsequent publication.

Fig 7b The displacement transducer

Fig 8 A Hall effect unit compared in size with a transistor

respect. There are two results of a change of temperature in a Hall-effect device : the sensitivity changes, and a calibration curve is therefore necessary. A more important effect for this application is the zero drift. We have found that the best stability is obtained by constructing the unit so that there is a negligible Hall voltage output when there is no magnetic field, and using material with temperature independent R_H or R_H/ρ_0 depending on the method of driving current through the unit ; p-type InSb may be produced with R_H a maximum near the operating temperature, and over an operating range of 20 centigrade degrees, R_H varies by $\pm$ 1·5 per cent. Material of rather smaller acceptor concentration gives a fairly constant R_H/ρ_0, the Hall mobility. This is constant to $\pm$ 1 per cent. over the same working range.

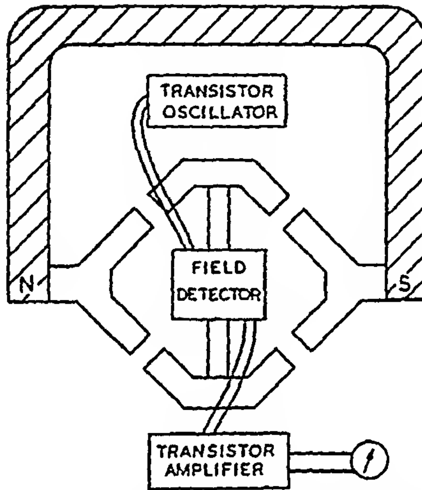

FIG. 9. The use of an InSb Hall effect unit in a susceptibility meter.

The voltage sensitivity of Hall units is proportional to $R_H/\sqrt{\rho_0}$ and this is larger for p-type InSb than for either intrinsic InSb or the impure InAs often used.

A versatile Hall unit is illustrated in Fig. 8. When $\frac{1}{4}$-in. diameter Permalloy rods 4 in. long are attached to the unit, magnetic fields of 10^{-5} gauss may be detected. The unit may be considered as the magnetic analogue of the galvanometer. If we construct the analogue of a Wheatstone bridge, with a permanent magnet driving flux through four equal reluctances (Fig. 9), the unit provides a means of measuring small changes in reluctance.[10] When a material of permeability slightly different from unity is placed in one gap, the bridge becomes unbalanced and flux passes through the detector. Since fields in each gap of 1000 gauss may be obtained without difficulty the instrument will measure susceptibilities approaching 10^{-7} c.g.s. units. The assembly of Fig. 9 is thus a portable susceptibility meter with a sensitivity approaching that of the conventional balances.

ACKNOWLEDGMENT

Acknowledgment is made to the Admiralty for permission to publish.

REFERENCES

1 Hilsum C and Barrie R *Proc phys Soc Lond* **71**, 676 (1958)
2 Mitchell G R Goldberg A E and Kurnick S W *Phys Rev* **97**, 239 (1955)
3 Avery D G Goodwin D W and Rennie A E *J sci Instrum* **34** 394 (1957)
4 Hilsum C and Ross I M *Nature Lond* **179**, 146 (1957)
5 Ross I M and Saker E W *Nature Lond* **178**, 1196 (1956)
6 Kuhrt F *Siemens Z* **28**, 370 (1954)
7 Saker E W Cunnell F A and Edmond J T *Brit J appl Phys* **6** 217 (1955)
8 Ross I M Saker E W and Thompson N A C *J sci Instrum* **34** 479 (1957)
9 Ross I M and Thompson N A C *Nature Lond* **175**, 518 (1955)
10 Hilsum C and Rose Innes A C *Nature Lond* **182** 1082 (1958)

Strahlungsnachweis mit III-V-Verbindungen

R. GREMMELMAIER

Siemens-Schuckertwerke A.G., Erlangen

Zu den III-V-Verbindungen gehören Halbleiter, deren elektrische Eigenschaften sich zum Teil sehr stark voneinander unterscheiden. Z.B. reicht die Breite der verbotenen Zone von 0·25 eV beim InSb bis zu einigen eV bei den Nitriden. Auch der Stand unserer Kenntnisse über die einzelnen Verbindungen ist recht unterschiedlich. Während einige Verbindungen schon weitgehend untersucht und ihre Eigenschaften bekannt sind, weiß man über andere noch verhältnismäßig wenig. Das hat zu einem guten Teil präparative Gründe. Einen Teil der Verbindungen kann man mehr oder weniger leicht in Form von Einkristallen erhalten, bei anderen ist es schon schwierig, sie überhaupt in kristalliner Form herzustellen. Auf Grund dieser Unterschiede ist es für unsere Betrachtung zweckmäßig, die III-V-Verbindungen zu drei Gruppen zusammenzufassen.

Zur ersten Gruppe können wir die Verbindungen mit kleiner Breite der verbotenen Zone rechnen : InSb, InAs und GaSb, zur zweiten Gruppe die dem Silizium ähnlichen Verbindungen InP, GaAs und AlSb und zur dritten Gruppe das GaP und die übrigen III-V-Verbindungen mit großer Breite der verbotenen Zone. Die Eigenschaften der Verbindungen der ersten beiden Gruppen sind schon weitgehend untersucht, und es liegen auch eine ganze Reihe von Arbeiten über die Verwendung dieser Verbindungen zum Strahlungsnachweis vor. Über die dritte Gruppe sind bisher nur wenige Arbeiten erschienen.

Im folgenden möchte ich besonders auf einige Messungen an den Verbindungen der zweiten Gruppe dieser Einteilung, vor allem an InP und GaAs eingehen.

Unter Strahlungsnachweis soll die Verwendung der Halbleiter als Detektoren für Lichtstrahlung und jede Art von ionisierender und korpuskularer Strahlung verstanden werden. Zum Nachweis der Strahlung kann die Photoleitung, der photoelektromagnetische Effekt oder der Photoeffekt an Sperrschichten verwendet werden. Photoeffekt, Photoleitung usw. sind dabei im allgemeinen Sinne zu verstehen. Die entsprechenden Effekte treten in gleichen Weise wie bei Lichtstrahlung auch bei ionisierender Strahlung, also z. B. ß-Strahlen, α-Strahlen auf. Wesentlich ist nur, daß die Strahlung imstande ist, im Halbleiter in Primär-oder Sekundärprozessen zusätzliche freie Ladungsträger zu erzeugen. Die Zahl der pro Zeiteinheit erzeugten Ladungsträger und die örtliche Verteilung der Erzeugung hängt zwar von der Strahlenart, Strahlungsintensität und von den Absorbtionsverhältnissen im Halbleiter ab, bei einer gegebenen Erzeugungsrate hängt jedoch die Größe des Photoeffektes, der Photoleitung usw. nur noch von den elektrischen Eigenschaften des Halbleiters ab. Es muß hier allerdings hinzugefügt werden, daß durch energiereiche Strahlung in dem Halbleiter Gitterstörungen erzeugt werden können, die ihrerseits

die elektrischen Eigenschaften des Halbleiters und damit die Größe des Photoeffektes beeinflussen.

Zur dritten Gruppe läßt sich in diesem Zusammenhang wenig sagen. An GaP und AlN [1] wurden Photoleitungen und Photoeffekt an Sperrschichten beobachtet, soweit mir bekannt ist aber noch nicht quantitativ untersucht. Die beobachteten Effekte sind bisher noch sehr klein. Den Untersuchungen stehen—besonders bei den Nitriden und Boriden—verhältnismäßig große technologische Schwierigkeiten bei der Herstellung der Stoffe in kristalliner Form entgegen.

Anders liegen die Verhältnisse bei den Verbindungen der ersten Gruppe. Auf Grund der Lage der Absorptionskante ergibt sich für die Verbindungen InSb und InAs eine wichtige Anwendungsmöglichkeit als Detektoren für Ultrarotstrahlung. Ich möchte hier auf die eingehenden Arbeiten hinweisen, die Photoeffekte in InSb und InAs behandeln.[2] InSb ist bei Zimmertemperatur als Detektor für Strahlung bis zu nahezu 7,5 μ geeignet, InAs bis zu Wellenlängen von ungefähr 4 μ. Aus beiden Verbindungen lassen sich Detektoren auf der Basis des photoelektromagnetischen Effektes, Detektoren auf der Basis der Photoleitung und p-n-Photoelemente herstellen.

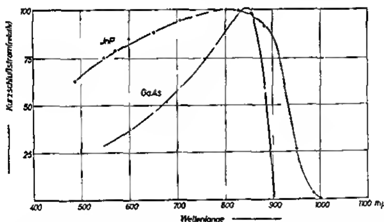

Fig. 1. Spektrale Empfindlichkeit eines GaAs- und eines InP-Photoelementes. Kurzschlußstrom in Abhängigkeit von der Wellenlänge bei gleicher einfallender Strahlungsleistung. (Kurzschlußstrom in relativem Maßstab.)

Die Verbindungen der zweiten Gruppe InP, GaAs und AlSb haben das Maximum ihrer spektralen Empfindlichkeit im nahen Ultrarot bzw. Rot. Fig. 1 zeigt die spektrale Empfindlichkeit eines GaAs- und eines InP-p-n-Photoelementes. Das GaAs-Element wurde im Diffusionsverfahren hergestellt, das InP-Element stellte Herr Dr. Henkel im Legierungsverfahren her. Die Fläche des GaAs-Elementes beträgt ungefähr 1 cm², die des InP-Elementes ungefähr 0,2 cm². Die Messungen führte ebenfalls Herr Dr. Henkel durch. Die in Fig. 1 wiedergegebenen Ergebnisse wurden mit einem Monochromator gewonnen. Die absolute Empfindlichkeit erhält man besser aus Messungen mit Filtern und einem geeichten Thermoelement. Die Ergebnisse einer solchen Messung sind in Fig. 2 wiedergegeben. Hier ist die Zahl der im Kurzschlußfall über den p-n-Übergang fließenden Ladungsträger bezogen auf die Zahl der auf das Photoelement auffallenden Licht-

quanten aufgetragen gegen die Wellenlänge. Da ungefähr 30% des auffallenden Lichtes reflektiert werden, ist die Zahl der Ladungsträger bezogen auf die Zahl der absorbierten Quanten entsprechend höher. Im Maximum erhält man für das GaAs-Element rund 0·8 und für das InP-Element rund 0·6 Landungsträger pro absorbiertes Quant. Der Abfall der Empfindlichkeit zu kürzeren Wellenlängen bei dem GaAs-Element rührt

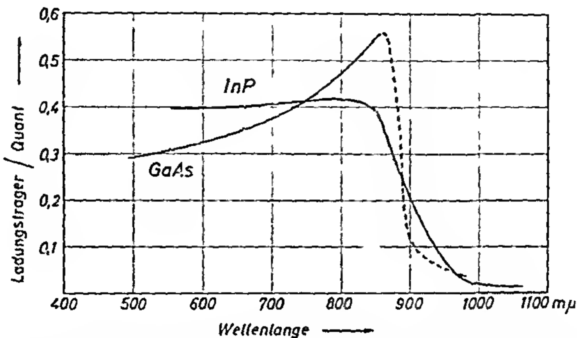

FIG. 2. Spektrale Empfindlichkeit eines GaAs- und eines InP-Photoelementes. Zahl der im Kurzschlußfall pro auftreffendem Quant über den *p-n*-Übergang fließenden Ladungsträger in Abhängigkeit von der Wellenlänge.

daher, daß der Abstand des *p-n*-Übergenges von der Oberfläche ungefähr gleich der Diffusionslänge der Elektronen ist, nämlich einige μ. D.h. da das kurzwellige Licht nicht sehr tief eindringt, erreichen nicht mehr alle erzeugten Elektronen den *p-n*-Übergang. Beim InP-Element ist der Abstand zwischen Oberfläche und *p-n*-Übergang geringer als beim GaAs-Element, die Diffusionslänge etwas größer, so daß die Empfindlichkeit zu kurzen Wellen nicht wesentlich absinkt. Daß die Kurve nicht den Wert 1 erreicht (unter Berüchsichtigung der Reflexion) liegt daran, daß das Element inhomogen ist, daß also nicht die ganze Fläche des Elementes wirksam ist. Man kann aus den Kurven entnehmen, daß sich GaAs- und InP-*p-n*-Photoelemente sehr gut für den sichtbaren Spektralbereich eignen. Bemerkenswert ist die relativ hohe Photospannung, die sich vor allem mit GaAs-Photoelementen erzielen läßt. Gute Exemplare liefern im Sonnenlicht bis zu 0·9 V Leerlaufspannung.

Photoelemente aus GaAs und InP können außerdem zum Nachweis ionisierender Strahlung verwendet werden. Hier ist allerdings die Diffusionslänge der Minoritätsträger wegen der teilweise sehr großen Eindringtiefe der Strahlung von noch größerer Bedeutung als bei der Verwendung zum Nachweis von Licht. Der Kurzschlußstrom über einem *p-n*-Übergang wird von den Ladungsträgern getragen, die, grob gesagt, innerhalb einer Diffusionslänge beiderseits des *p-n*-Überganges erzeugt werden. Solange die mittlere Eindringtiefe der Strahlung kleiner als die Diffusionslänge ist, kann man erreichen, daß nahezu alle erzeugten Ladungsträger zum Kurzschlußstrom beitragen. Ist die mittlere Eindringtiefe der Strahlung dagegen sehr groß, dann ist der Kurzschlußstrom proportional der Diffusionslänge. Hier bietet sich übrigens eine Möglichkeit, die Diffusionslänge bei Bestrahlung mit durchdringender Strahlung (z. B. γ-Strahlen

einer Co^{60} Quelle) zu messen[3]. Da für γ-Strahlen alle erforderlichen Daten bekannt sind, kann man die Zahl der pro Zeit und Raumeinheit erzeugten Ladungsträger berechnen und man erhält aus dem Kurzschlußstrom unmittelbar die Diffusionslänge. An GaAs p-n-Übergängen konnten wir auf diese Weise Diffusionslängen der Elektronen von einigen μ bis zu maximal ungefähr 10 μ messen, an InP-Übergängen in Einzelfällen bis zu maximal 150 μ. Diese Diffusionslängen entsprechen einer Lebensdauer von 10^{-8} sec in GaAs und ungefähr 10^{-6} sec in InP. Der Wert für die Diffusionslänge und Lebensdauer in InP ist in guter Übereinstimmung mit dem Wert, den Reynolds und Mitarbeiter bei ihren Untersuchungen an InP abgeschätzt haben[4].

Infolge der größeren Diffusionslängen in InP ist die Empfindlichkeit der untersuchten InP-Photoelemente gegenüber durchdringender Strahlung (z. B. γ-Strahlung von ungefähr 1 MeV) bis zu 10 mal größer als die der GaAs-Photoelemente. Als Maß für die Empfindlichkeit kann folgende Angabe dienen. Bei einer Bestrahlung mit 10^7 γ-Quanten pro sec einer Co^{60}-Quelle (Energie 1,17 bzw. 1,33 MeV) erhält man z. B. in einem InP-Element einen Kurzschlußstrom von ungefähr 10^{-9} A. InP- und GaAs-Photoelemente eignen sich daher vor allem zum Nachwies und zur Messung größerer Strahlungsintensitäten. Bei der Messung weicher Röntgen- oder Elektronenstrahlen, wie sie von Pfister[5] mit GaAs-Photoelementen durchgeführt wurde, ist besonders günstig, daß die Overfläche der Elemente nicht geschützt werden braucht. An normaler Atmosphäre ändern sich nämlich die Eigenschaften der GaAs-Photoelemente über Monate nicht merklich. (Die längste Beobachtungsreihe ging bisher über ein Jahr.)

Mit InP-Photoelementen lassen sich neben ionisierender Strahlung auch thermische Neutronen nachweisen[6]. In einem Neutronenfluß wird das Indium aktiviert, es entsteht radioaktives Indium. Das Indium zerfällt unter β-Strahlung und die durch die β-Strahlung in InP erzeugten Ladungsträger liefern den Photostrom. Wenn man das Element aus dem Neutronenstrom nimmt, klingt die Photospannung mit der Aktivität des Indiums ab.

In AlSb scheint die Lebensdauer der Ladungsträger noch wesentlich kleiner zu sein als in GaAs. Im allgemeinen ist daher auch der an AlSb p-n-Übergängen beobachtete Photoeffekt viel kleiner als der an GaAs p-n-Übergängen beobachtete. Über Photospannungen bis 0,6 V an AlSb p-n-Übergängen berichten Genser und Allred[7] und Abrahám berichtet über Photoleitung und Photoeffekt in polykristallinem AlSb[8].

Zum Schluß noch eine Bemerkung zum GaAs. Die oben erwähnten Messungen wurden mit GaAs p-n-Photoelementen durchgeführt. GaAs kann jedoch auch als Photoleiter verwendet werden. Beim Herstellen von GaAs-Einkristallen erhält man mitunter große Bereiche, deren Widerstand nahe an den Eigenleitungswiderstand des GaAs herankommt. Der Widerstand dieser Kristalle liegt bei 10^6–10^7 Ω an, während der Eigenleitungswiderstand bei 10^8–10^9 Ω an liegen dürfte. Der hohe Widerstand kommt offenbar durch Störstellenkompensation zustande. Diese Kristalle zeigen eine sehr gute Photoleitung. Fig. 3 zeigt den Photostrom durch ein GaAs-Plättchen in Abhängigkeit von der Beleuchtungsstärke. Das Plättchen ist ungefähr 0,1 mm dick und 1,5 mm breit. Die Elektroden sind auf der Oberfläche im Abstand von ungefähr 1 mm angebracht. Die beleuchtete Fläche beträgt also ungefähr 1,5 mm². Der Dunkelwiderstand liegt bei

$10^9\ \Omega$, d.h. der Dunkelstrom liegt um zwei Zehnerpotenzen unter dem Photostrom, der bei einer Beleuchtungsstärke von 100 Lux fließt. Das Maximum der spektralen Empfindlichkeit liegt wie bei den Photoelementen zwischen 850 und 900 mμ. Bei den bisher untersuchten hochohmigen GaAs-Proben wurden Anstiegs—bzw. Abklingzeiten von mehreren Sekunden beobachtet. Die Messungen an diesen Proben sind allerdings noch nicht

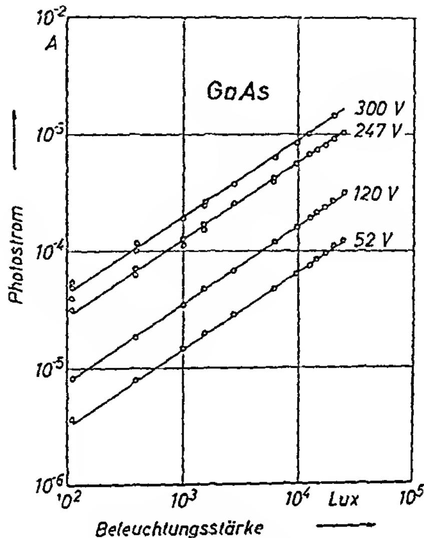

Fig. 3. Photoleitung in hochohmigem GaAs. Photostrom in Abhängigkeit von der Beleuchtungsstärke bei verschiedenen Spannungen.

abgeschlossen, sodaß sich über die Lebensdauer der Ladungsträger und die Spannungsabhängigkeit und Temperaturabhängigkeit des Stromes noch nichts endgültiges sagen läßt. Die Abhängigkeit des Photostromes von der Beleuchtungsstärke zeigt, daß die Lebensdauer in dem gemessenen Bereich mit der Lichtintensität abnimmt.

Literatur

1. Lagrenaudie, J. *J. Chim. phys.* **53**, 222 (1955).
2. Tauc, J. and Abraham, A. *Czech. J. Phys.* **4**, 478 (1954).

   Avery, D. G., Goodwin, D. W., Moss, T. S. and Lawson, W. D. *Proc. phys. Soc. Lond.* B **67**, 761 (1954).

   Talley, R. M. and Enright, D. P. *Phys. Rev.* **95**, 1092 (1954).

   Mitchell, G. R., Goldberg, A. E. and Kurnick, S. W. *Phys. Rev.* **97**, 239 (1955).

   Kurnick, S. W. and Zitter, R. N. *J. appl. Phys.* **27**, 278 (1956).

   Hilsum, C. and Ross, I. M. *Nature, Lond.* **179**, 146 (1957).

   Avery, D. G., Goodwin, D. W. and Rennie, A. E. *J. sci. Instrum.* **34**, 394 (1957).

   Goodwin, D. W. *J. sci. Instrum.* **34**, 367 (1957).

   Hilsum, C. *Proc. phys. Soc. Lond.* B **70**, 1011 (1957).

   Dixon, J. R. *Phys. Rev.* **107**, 374 (1957).

3 Gremmelmaier, R *Phys Verh*, *Mosbach* **8**, 196 (1957), *Proc Inst Radio Engrs, N Y* 46 1045 (1958)
4 Reynolds, W N, Lilburne M T and Dell, R M *Proc phys Soc Lond* **71**, 416 (1958)
5 Pfister, H *Z Naturf* 11a, 434 (1956) *Z Naturf* 12a, 217 (1957)
6 Gremmelmaier, R and Welker, H *Z Naturf* 11a, 420 (1956)
7 Genser, M and Allred W P *Bull Amer phys Soc* 1/6, F3 (1956)
8 Abraham, A *Czech J Phys* **6**, 624 (1956)

Electroluminescence at Grain Boundaries in Gallium Phosphide

G. F. ALFREY, C. S. WIGGINS

Electron Physics Department, University of Birmingham

THE electroluminescence of gallium phosphide has been studied with direct current excitation. A few volts applied to the crystal is sufficient to produce some electroluminescence. For greater light intensity it is necessary to use a pulsing technique to avoid overheating the crystal, since its impedance falls rapidly with increasing current. At high currents low-resistance contacts are desirable, and these are made with indium.

A microphotograph of the electroluminescence of an irregular polycrystal is shown in Fig. 1, for current flow from left to right. It is observed to consist of a pattern of narrow lines, as reported earlier [1]; these are chiefly

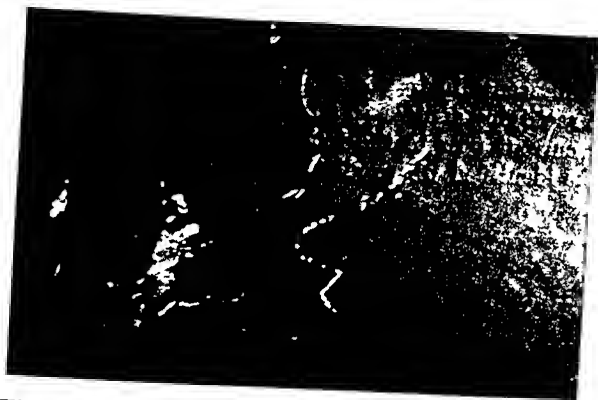

FIG. 1. Electroluminescence from an irregular gallium phosphide polycrystal. Current flowing from left to right. (×16 approx.)

in the surfaces, and those in the lower surface are out of focus. Fig. 2 was made under the same conditions except for reversal of the current, and some changes in the pattern are noticeable. That the electroluminescence occurs at grain boundaries is shown when the surface is lightly etched. Fig. 3 is a double exposure of a thinner, more regular polycrystal, once to show the grain boundaries by external illumination, and the second by electroluminescent light alone, so that the sources can be identified. At higher currents the electroluminescence tends to grow throughout the boundary inside the crystal, forming a sheet joining the lines in the upper and lower surfaces. To show this more clearly, Fig. 4 shows the same crystal, only exposed to electroluminescent light. It will be observed that not all of the boundaries are electroluminescent, though some others are for different electrode

positions Voltage probing experiments show that almost all the voltage drop occurs at grain boundaries and that the impedance across a boundary is non linear Since the electroluminescence at a boundary is proportional to the current these changes in the electroluminescence pattern in a typical specimen in which the grain boundaries represent a complicated network of impedances in series and parallel are to be expected

FIG 2 Polarity reversed Current flow from right to left (×16 approx)

Electroluminescence in GaP is observed not only at a grain boundary but also at a rectifying contact to a single grain In this case light is only observed for current flow in the forward direction and the electroluminescence can be identified with radiative recombination of minority carriers

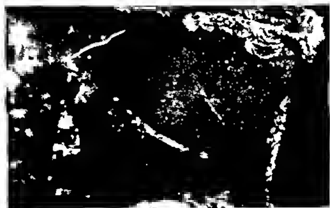

FIG 3 Double exposure of a thinner more regular gallium phosphide polycrystal (a) by electroluminescence (b) with external illumination (× 15 approx)

injected at the contact Preliminary studies of the spectral composition of the light emitted at a grain boundary indicate that it is produced by the same process

Thus a high field region is not sufficient to give electroluminescence and minority carrier injection must take place at a grain boundary this could

occur if there was a region of *n*-type gallium phosphide between the *p*-type grains. For a given direction of current flow across the boundary, one *p-n* junction would be in the forward direction, giving injection of minority carriers, and the other would be in the blocking direction, and would give the voltage barrier observed by probing.

Fig. 4. As Fig. 3, with electroluminescence alone. (× 15 approx.)

This interpretation is supported by the current-voltage characteristics of a boundary. With about 10 volts applied to a boundary, a large increase of current occurs, which corresponds to " punch-through " of the *n* region At higher voltages, the current increases less rapidly with voltage, and seems to be space charge limited.

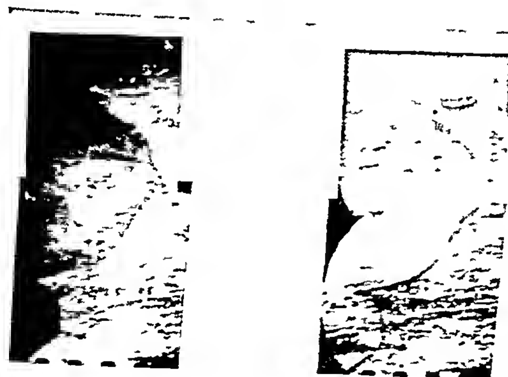

Fig. 5. Scanning electron micrograph of part of central light source in Fig. 1 for current flow in both directions. (× 40 approx.)

The voltage barriers at a grain boundary can also be investigated by a scanning electron microscope technique developed by Oatley and Everhart,[2] in which contrast is very sensitive to small changes in surface potential. Dr. Everhart has kindly examined a gallium phosphide specimen in this way. The line of one boundary is shown in Fig. 5, for current flow in both directions. The abrupt change in voltage on crossing the boundary is clearly seen ; in

the absence of a potential difference across the boundary it is quite invisible under the microscope The boundary under examination is one shown in Fig 1, running from the top edge of that figure in the centre The shape of the boundary on Figs 1 and 5 does not correspond exactly due to fore shortening effects in the electron micrograph In Fig 6 two pictures of the boundary under higher magnification are shown again for opposite directions

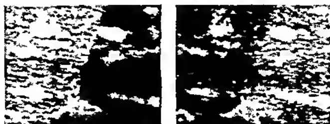

Fig 6 Portion of boundary in Fig 5 at higher magnification to show shift as current is reversed (× 4000 approx)

of current , here the position of the boundary can be defined with respect to fixed features of surface topography and a shift of the boundary on reversal of the current can be seen this would correspond to the thickness of the n region in the model discussed above and a value of $\frac{1}{4}\,\mu$ can be deduced from Fig 6 with little variation along the boundary

This relatively thick n region is thought to arise from the segregation of donor impurity at the grain boundary It is hoped that further investigations of electroluminescence at grain boundaries will provide a means of studying this segregation

We wish to thank Professor Welker for supplying the gallium phosphide specimens and Dr D B Holt for his collaboration in the earlier stages of this work

References

1 Holt, D B Alfrey G F and Wiggins C S *Nature Lond* **181**, 109 (1958)
2 Oatley, C W and Everhart T F *J Electronics* **3** 568 (1957)

Some Observations on the Electrical Properties of Indium Antimonide at Low Temperatures

E. H. PUTLEY

Royal Radar Establishment, Great Malvern

THIS paper describes briefly some of the properties of InSb prepared at R.R.E.; p- and n-type material has been prepared with carrier concentrations down to 5×10^{13}/c.c. Estimates of the total impurity concentration based on analyses of the variation of mobility (n-type) and carrier concentration (p-type) with temperature indicate total concentrations down to about 5×10^{14}/c.c.

The first Figure shows the behaviour of some of the best n-type material in the intrinsic range. From these results the intrinsic carrier concentration was found to vary with temperature as

$$n_i = 5{\cdot}70 \times 10^{14}\, T^{3/2} \exp - \frac{0{\cdot}125}{kT} \quad (\pm 10 \text{ per cent.}) \tag{1}$$

valid between 300° K and 180° K.

Figs. 2 and 3 show the conductivity and Hall coefficient for a number of p-type specimens from 20° K upwards. The most striking feature of these results is that two impurity levels are present. The shallower one, at about 0·0075 eV above the valence band, corresponds with that reported earlier by a number of workers (Fritzsche and Lark-Horovitz, 1955[3]; Hrostowski *et al.* 1955[4]) and is believed to be associated with the presence of zinc. The deeper one appeared in material from which the source of the shallow level was removed and which was then subject to an annealing process. This level is at about 0·02 eV, but the type of impurity responsible for it has not yet been identified.

An analysis of the data for the material containing the shallower level showed that the variation of hole concentration with temperature could be accounted for by the expression

$$\frac{p(p + N_D)}{N_A - N_D - p} = \frac{(2m^*kT)^{3/2}}{h^3} \exp \frac{-E_A}{kT} \tag{2}$$

Taking $m^* = 0{\cdot}18\, m$ and $E_A = 0{\cdot}0075$ eV, values of N_A and N_D were calculated for a number of specimens. Table 1 shows the results obtained

TABLE 1. Concentration of impurity centres and scattering centres (cm^{-3})

Specimens	N_A–N_D	N_A	N_D	N_I
C19/1	$10{\cdot}0 \times 10^{14}$	$16{\cdot}1 \times 10^{14}$	$6{\cdot}1 \times 10^{14}$	$4{\cdot}5 \times 10^{14}$
C19/5	5·75	11·5	5·8	2·9
C19/7	4·69	10·6	5·9	3·8
C19/11	1·55	12·5	11·0	3·3
C19/2	0·57	18·1	11·5	8·0

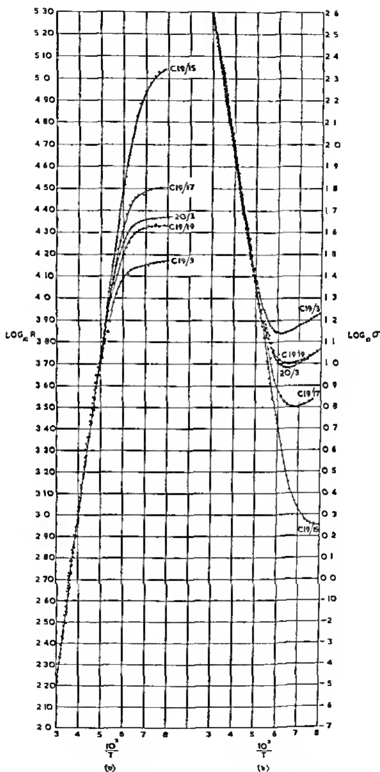

FIG. 1. (*a*) Intrinsic Hall coefficient (*b*) Intrinsic conductivity.

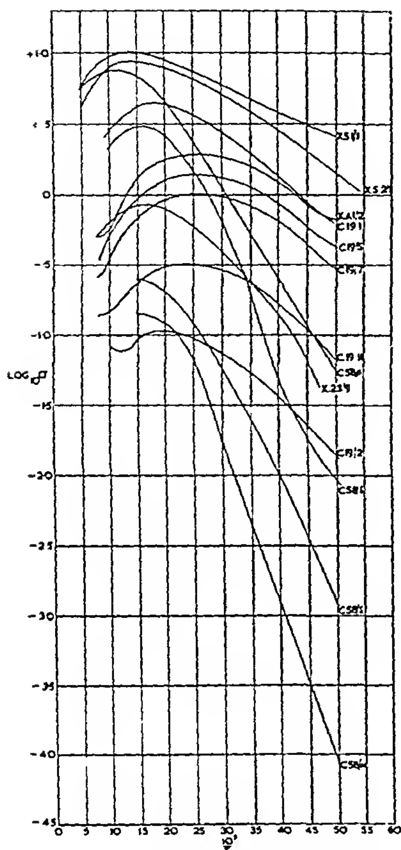

Fig. 2. Conductivity of p-type InSb.

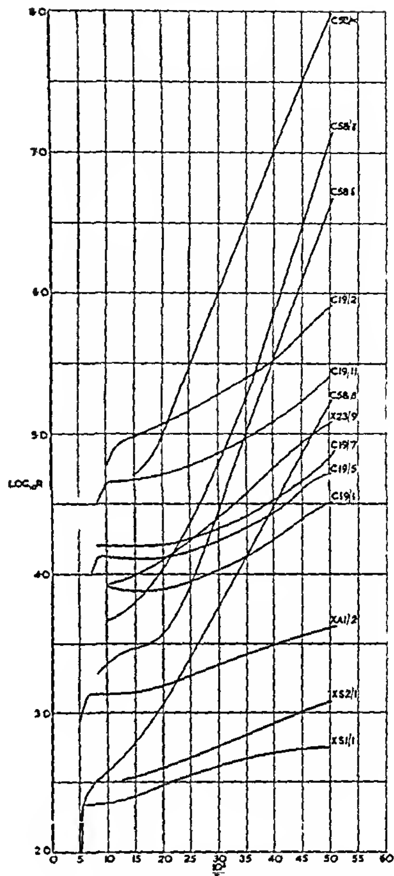

Fig. 3. Hall coefficient for p-type InSb.

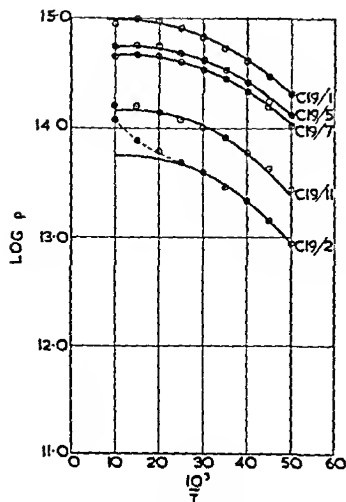

Fig. 4. Hole concentration in p-type specimens of InSb. C19.

○ Experimental points curves calculated from

$$\frac{p(p+N_D)}{N_A-N_D-p}=\frac{(2\pi m^*kT)^{3/2}}{h^3}\,\text{Exp.}-\frac{E_A}{kT}$$